Ph.D

Thesis

SYNTHESIS AND CHARACTERIZATION OF BARIUM ZINC TANTALATE CERAMICS FOR MICROWAVE APPLICATIONS

A THESIS

Submitted

in the partial fulfillment of the requirements for

the award of the degree of

DOCTOR OF PHILOSOPHY

In

MATERIALS ENGINEERING

By

SWATHI. M

[Reg. No. 12ETPM01]

SCHOOL OF ENGINEERING SCIENCES AND TECHNOLOGY

UNIVERSITY OF HYDERABAD

HYDERABAD-500046

INDIA

AUGUST

2017

Dedicated to my Parents

Mr. A. Manivannan

and

Mrs. Kothai Manivannan

DECLARATION

I hereby declare that the matter embodied in this thesis entitled, "**SYNTHESIS AND CHARACTERIZATION OF BARIUM ZINC TANTALATE CERAMICS FOR MICROWAVE APPLICATIONS**" submitted to University of Hyderabad for the award of **Doctor of Philosophy** in **Materials Engineering** is a record of original research work carried out by me under the supervision of **Dr.Dibakar Das,** Professor, School of Engineering Sciences and Technology, University of Hyderabad. To the best of my knowledge, this work is not submitted for any degree in any University or Institute.

(SWATHI . M)

Place: Hyderabad
Date:

CERTIFICATE

This is certified that the thesis entitled **"Synthesis and Characterization of Barium Zinc Tantalate Ceramics for Microwave Applications"** submitted by **Swathi. M** bearing registration number **12ETPM01** in partial fulfilment of the requirements for award of **Doctor of Philosophy** in the **School of Engineering Sciences and Technology** is a bonafide work carried out by her under my supervision and guidance.

This thesis is free from plagiarism and has not been submitted previously in part or in full to this or any other University or Institution for award of any degree or diploma.

Parts of this thesis have been:

A. Published in the following publications:

1. "Effect of colloidal processing on densification and dielectric properties of $Ba(Zn_{1/3}Ta_{2/3})O_3$ Ceramics", Swathi Manivannan, Andrews Joseph, P.K Sharma, K.C. James Raju, Dibakar Das, ***Ceramics International (2017), 10.1016/j.ceramint.2017.06.147***
2. "Effect of microwave and conventional sintering on densification, microstructure and dielectric properties of BZT–xCr_2O_3 ceramics", Swathi Manivannan, Andrews Joseph, P.K. Sharma, K.C. James Raju, Dibakar Das, ***Ceramics International (2015), 10.1016/j.ceramint.2015.05.035***
3. "Investigation of brazing of $Ba(Zn_{0.33}Ta_{0.67})O_3$ ceramic with Ti6Al4V alloy", Suresh Beera, Swathi Manivannan, Amit kumar Singh, Pramod Kumar Sharma, G Madhusudan Reddy, Dibakar Das, ***Ceramics International (2015), 10.1016/j.ceramint.2016.02.006***
4. "Effect of Flux Addition on Mechanical and Microwave Dielectric Properties of Barium Zinc Tantalate Ceramics", Swathi Manivannan, V. S. Surya Chandra, P. K. Sharma, K. C. James Raju, Dibakar Das, ***Trans. Ind. Ceram. Soc., (2014), 10.1080/0371750X.2014.922419***

B. Presented in the following conferences:

1. "Effect of Additives on Densification and Thermal Conductivity of Barium Zinc Tantalate Ceramics", Swathi Manivannan, P.Kumar Sharma, Tanjore V. Jayaraman, Dibakar Das, ***oral presentation in Characterization of Minerals, Metals, and Materials Symposium, 2016 TMS Annual Meeting & Exhibition, Nashville, Tennessee, USA***

2. "Densification behavior and dielectric properties of gel cast Barium Zinc Tantalate ceramics", Swathi Manivannan, P.Kumar Sharma, Dibakar Das, ***oral presentation in Characterization of Minerals, Metals, and Materials Symposium, 2016 TMS Annual Meeting & Exhibition, Nashville, Tennessee, USA***
3. "Structure and Microwave Dielectric Properties correlation in $Ba_{1-x}La_x(Zn_{(1+x-2y)/3}Ta_{(2-x-y)/3}Ga_y)O_3$ Ceramics", Swathi Manivannan, Santhosh Kumar Gunapu, Pramod Kumar Sharma, K.C James Raju, Dibakar Das, ***Characterization of Minerals, Metals, and Materials Symposium, 2015 TMS Annual Meeting & Exhibition, Orlando, Florida, USA***
4. "Effect of Processing parameters on structural and microwave dielectric properties of Barium Zinc Tantalate Ceramics", Swathi Manivannan, D V Santhosh Kumar Gunapu , K. C. James Raju, P.K Sharma, Dibakar Das, ***Poster ID – EC28, presented in ICAFM – 2014, Trivandrum***

Further the student has passed the following courses towards fulfillment of coursework requirements for Ph.D.

Course Code	**Name**	**Credits**	**Pass/Fail**
MT601	Research Methodology	4	Pass
MT801	Thermodynamics and Phase Equilibria	4	Pass
MT802	Characterization of Materials	4	Pass
MT803	Advanced Engineering Mathematics	4	Pass
MT804	Seminar	2	Pass
MT805	Mechanical Behavior of Materials /Selection of Materials	4	Pass
MT806	Concepts of Materials Science	4	Pass
MT807	Materials Processing & Characterization Laboratory	4	Pass
MT808	Dislocation & Plasticity	2	Pass

Supervisor **Dean of School**

CONTENTS

ACKNOWLEDGEMENTS

The work presented in the thesis wouldn't have been possible without my close association with many people who were always there when I needed them the most. I take this opportunity to acknowledge them and express my sincere gratitude for being instrumental in this pivotal period of research life.

First and foremost, I would like to express my sincere gratitude to my guide **Dr. Dibakar Das**, for motivating and inspiring every bit of me towards new possibilities in life. I truly enjoyed working in research environment that stimulates original thinking and initiative. I would like to thank my supervisor for introducing the present topic of dielectrics and for his skillful guidance through serendipitous observation, stoic patience and innovative ideas throughout my research work.

I am also very thankful to Dean of SEST **Prof. Ghanashyam Krishna**, Former dean **Prof. R. Singh and Prof. M. Sundararaman** and all other faculties in department for providing me the facilities and the guidance to carry out my research work. In particular I would like to record my gratitude to **Dr. Pradip Paik (SEST) and Dr. Surajit Dhara (SOP)** for their constant encouragement and support during the doctoral committee meetings.

I would like to acknowledge the (funding body) **BRFST** (sanction number BRFST/NFP/2012/Aug/N/11) for providing the fellowship and facilities for the project. My special words of thanks to Dr. Pramod Sharma, for always being so kind, helpful and motivating. I would like to acknowledge Dr. Kiran kumar K Ambulkar and Pramod R Parmar for their efforts in materializing the project for successful application.

I would like to extend my sincere gratitude to Prof. K.C James Raju for his support during the course of my research work. I would like to thank Surya Chandra (SOP), Santhosh Kumar Gunapu (SOP) and Andrews Joseph (SOP) for offering me help to in dielectric properties measurement.

I would like to acknowledge all the teachers I learnt from since my childhood, I would not have been here without their guidance, blessing and support. My special thanks to Dr. Roy Johnson, Centre for Ceramic Processing, ARCI, for being role model for me. I feel privileged to be his student once, a feeling that every student of his will second.

My acknowledgement will never be complete without the special mention to all my lab mates who have taught me the lab culture and have lived by example to make me understand the hard facts of life. I would sincerely like to thank all my lab mates Paul Praveen, Vinitha, Suresh Beera, Chandrakala, Jaishree, Srinivas Indla, Ummen Sabu, Mohd Qasim, Kushi, Mahesh and other research scholars in SEST for providing a joyful environment in the lab and helping me in all ways. The work done with them as a co-worker has taught me how a person can succeed in achieving what seems impossible to begin with. My special words of gratitude to Rajkumar, Koushi kumar, Bhuvaneswari, Vijayalakshmi, Aneela, Varalakshmi, Vinoth and Johny Varghese for all their personal and professional help that they have extended to me throughout the course of work.

I would like to thank project students Ganapathy, Nandhini, Amruth and Shiva for helping and in being part of my research work.

I would also like to thank the technicians and non-teaching staff of SEST Mallesh anna, Padma madam, Venu anna Venkat anna, Kranti madam and Malathy madam.

I would like to thank all my department friends for their moral support and motivation, which drives me to give my best.

Finally I would like to thank my parents **Kothai and Manivannan, Madhan Kumar** (husband) for their constant trust, support and encouragement. Finally, I would like to acknowledge my daughter Tharunika who means the world to me. I extend my respect to my in-laws and all elders to me in the family. I consider myself the luckiest in the world to have such a supportive family, standing behind me with their love and support.

List of figures

List of tables

Abbreviations

BZT	$Ba(Zn_{1/3}Ta_{2/3})O_3$
XRD	X-Ray Diffraction
SEM	Scanning Electron Microscopy
FESEM	Field Emission Scanning Electron Microscopy
DR	Dielectric Resonator
RF	Radio Frequency
LHCD	Low Hybrid Current Drive
SST	Steady State Tokamak
MLCC	Multi Layer Ceramic Capacitor

This thesis describes the research work on the synthesis and investigation of the structural and microwave dielectric properties of **$Ba(Zn_{1/3}Ta_{2/3})O_3$ (BZT)** ceramics for the following applications as

- Ceramic window sections to be used in high power microwave windows in fusion systems
- Microwave dielectric resonator to be used in communication devices

The ceramic material to be used as dielectric resonator in communication devices or as microwave window in fusion reactor is expected to have very high density, uniform microstructure, excellent microwave dielectric properties, good thermal conductivity and thermal stability. BZT ceramics are extremely useful for applications as microwave window section in fusion reactors, in particular. The window has to offer an ultrahigh vacuum tight sealing as well as to deliver (transmit) the high power microwave into the reactor to sustain the fusion plasma. The thesis is divided into eight chapters and summarized as follows,

Chapter 1

In this chapter, a general introduction about 'Microwave dielectric ceramics', which includes basics on Dielectric resonators (DR) and RF window, have been presented. Desirable material properties for applications as DRs and window section have been listed. Brief introduction on $A(B_{1/3}B'_{2/3})O_3$ class of perovskites have been presented. The procedure followed for measurement of microwave dielectric properties (Quality Factor ($Q\times f$), Dielectric constant (ε_r) and Temperature coefficient resonant of frequency (τ_f)) have been summarized in this chapter.

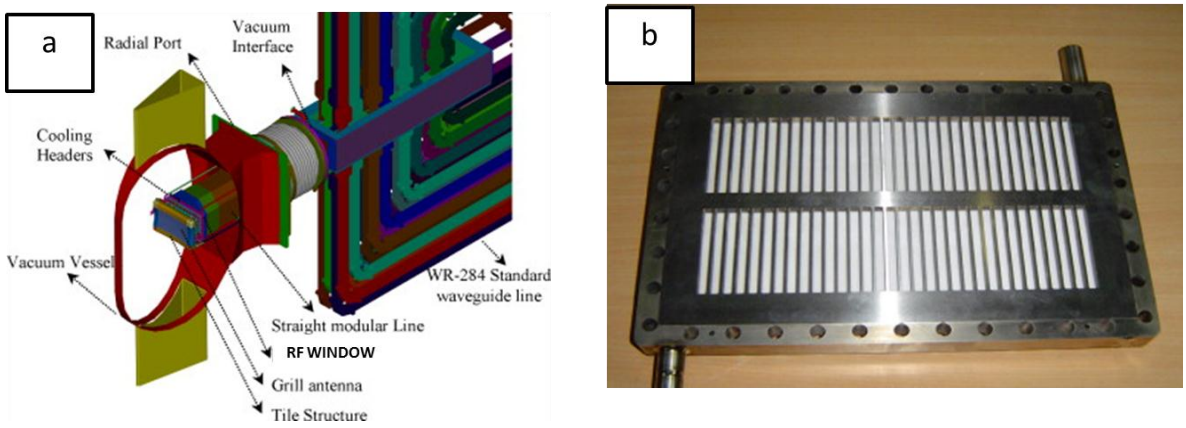

Fig 1 (a) Schematic view of In-vessel LHCD system on SST 1 Tokamak (b) RF window with single titanium frame and 64 slots with ceramics components

Microwave dielectric ceramics have influenced the wireless technology with a wide range of applications including satellite broad casting, global positioning systems, personal communication devices, etc.,. DRs form a crucial module in microwave circuits due to its ability to sustain a standing

electromagnetic radiation within it. DRs are capable of confining the EM radiation and hence find applications in antennas, filters and oscillators [1,2].

Many aspiring energy projects have been going on in present days and one of such projects is Tokamak based fusion reactor. Lower Hybrid Current Drive (LHCD) system based on a grill type antenna has in-vessel system (shown in Fig 1(a)) comprising of antenna, RF window and transmission line [3]. RF window (shown in Fig 1(b)), used in the transmission line, acts as a vacuum barrier and transmits the microwave power.

The desirable material properties for application as DR and RF window section include high sintered density, high dielectric constant, low dielectric loss and good thermal stability. The dielectric properties of the ceramic materials are greatly influenced by various intrinsic (crystal structure, symmetry, anharmonicity of lattice vibrations, etc.,) and extrinsic factors (density, microstructure, porosity, defects, etc.,). Hence, studies on processing of ceramics and the effect of various additives on the structure/property have gained more importance. Ceramics with perovskite structure (ABO_3) have dominated the electro ceramics industry. The perovskite structure is one of the most widely studied classes of structures, due to its ability to accommodate extensive range of atomic substitutions and hence offer a robust series of properties. A $(B'_{1/3}\ B''_{2/3})\ O_3$ complex perovskites are the most extensively investigated family in microwave dielectric ceramics. $Ba(Zn_{1/3}Ta_{2/3})O_3$ belongs to $A(B'_{1/3}B''_{2/3})O_3$ class of complex perovskites and has potential for applications in satellite broadcasting at frequencies higher than 10 GHz and as a very high Q dielectric resonator (DR) in mobile phone base stations or combiner filter for PCS applications [4].

Quality factor of the samples were measured by $TE_{01\delta}$ mode dielectric resonator method, using a variable cavity based test fixture manufactured by QWED [5]. The dielectric constant of the material is measured by Hakki and Coleman method modified by Courtney [6, 7]. The shift in resonant frequency is monitored over the temperature range of 25°C – 80°C to calculate temperature coefficient of resonant frequency.

Chapter 2

Chapter 2 focuses on the literature review of the various dielectric materials used for RF window application. The studies on various $A(B'_{1/3}B''_{2/3})O_3$ complex perovskites and effect of processing $Ba(Zn_{1/3}Ta_{2/3})O_3$ (BZT) on microwave dielectric properties have been summarized in this chapter.

High purity Aluminium oxide is considered to be an ideal material for application as RF window. Feasibility of using Beryllium oxide as window section has been tested. Sapphire and Aluminium Nitride window sections suffered from various drawbacks including high dielectric loss and multipacting [8].

Structure and property correlation of A ($B_{1/3}$ $B'_{2/3}$) O_3 complex perovskites have gained sufficient attention and numerous studies were done to tailor different properties by various atomic substitutions. Different compositions of A ($B_{1/3}$ $B'_{2/3}$) O_3 complex perovskites along with microwave dielectric properties and drawbacks involved in selecting and processing of these ceramics have been summarized. Matsumoto et al [9] reported Ba $(Mg_{1/3}Ta_{2/3})O_3$ (BMT) with good dielectric properties ($Q\times f$ – 430000 GHz, ε_r - 24, τ_f - 8ppm/°C). But the disadvantage involved in preparing BMT is that it requires high sintering temperature (1650°C) due to poor sinterability followed by long hours of annealing to establish B site ordering. Solid state synthesis of Ba $(Zn_{1/3}Nb_{2/3})O_3$ was reported by Yue et al ($Q\times f$ - 96000GHz, ε_r - 42, τ_f - 30ppm/°C) [10]. Several authors tailored the dielectric properties (to achieve good thermal stability) of BZN by doping with Co, Ga, Ce, etc. $Ba(Mn_{1/3}Ta_{2/3})O_3$ ceramics also had low loss ($Q\times f$ - 104000 GHz) and high dielectric constant (ε_r - 27). But the system requires special atmosphere during sintering which hampered the commercial exploitation of the material [11]. Ba $(Mg_{1/3}Nb_{2/3})O_3$ (BZN) synthesis by chemical and solid state routes were reported. BMN samples with small Mg deficiency showed better properties ($Q\times f$ - 96000 GHz, ε_r - 32, τ_f - 30ppm/°C). The relatively high τ_f of this system prevents it from practical applications [12].

Barium zinc tantalate $Ba(Zn_{1/3}Ta_{2/3})O_3$ (BZT) is a well-known dielectric ceramics with excellent microwave dielectric properties. The main disadvantage in processing BZT ceramics for such applications is its high processing (sintering) temperature requirement to develop a highly dense material, followed by a high temperature annealing process for prolonged time duration (to obtain the desired crystallographic structure). The major drawback in processing BZT ceramics at high temperatures is the volatilization of low melting Zn from the BZT composition rendering the final product containing lot of defects including the presence of other phases [13]. The problem has been addressed in the prior art in many ways. One such way known is by adding a small amount of other oxides (dopants), such as Al_2O_3, Ga_2O_3, ZrO_2, or TiO_2 to BZT to compensate for the Zn loss from the system [14-18].

Several efforts have also been made to use dopants consisting of similar ions as that of BZT in order to suppress the extended defects arising from other oxides and salts doping in BZT matrix. Nano-sized BZT powder doped with Ga_2O_3, synthesized by wet chemical route and sintered by muffling with calcined BZT powder led to poor densification [19].

In spite of several efforts made to suppress the Zn loss from BZT ceramics, the density and microstructure of the sintered BZT composition (in global scale, with very less magnification) have not been reported in prior arts. Apart from having acceptable microwave dielectric properties, BZT ceramic has to be mechanically robust with minimum level of porosity in the microstructure (with high density as close to the theoretical density as possible) to provide Ultra High Vacuum (UHV) compatibility for RF window application. In order to solve these problems, several other factors also

need to be investigated, based on which the objectives of the current work are listed out in the next chapter.

Chapter 3

Chapter 3 describes the objectives of the present work based on the critical review of the existing literature on synthesis and various doping and their associated problems.

The following objectives were set to develop mechanically robust BZT ceramics with highest density (close to the theoretical density), high dielectric constant, low loss (high quality factor, Q×f), very low and stable temperature coefficient of resonance frequency (τ_f) and high thermal conductivity suitable for high power microwave and millimeter wave device applications. The primary objectives were to

- Study the effect of different process parameters during consolidation and sintering to achieve robust BZT ceramics with high microwave dielectric properties
- Investigate the effect of colloidal processing on the densification and dielectric properties of BZT
- Study the influence of microwave sintering in minimizing zinc volatilization
- Investigate the change in ordering and sinterability of BZT with specific site doping of A site and B site with suitable dopants.

Chapter 4:

In this chapter details of synthesis and processing of pure BZT followed by various characterization techniques carried out in this work are reported in detail

In the present study, BZT ceramics was prepared by conventional solid state reaction. Calcination of the as milled raw powders at 1250°C for 6 hours resulted in complete phase formation which was then characterized by X-ray diffraction (XRD) for its primary crystal structure and composition. The synthesized BZT composition was sintered at different temperatures and densification behavior is studied. Dielectric properties (dielectric constant (ε_r) and unloaded quality factor) were measured by cavity resonator technique by using Vector Network Analyzer (Agilent E8361C) in $TE_{01\delta}$ mode. The temperature coefficient of resonant frequency τ_f is measured by placing the sample in invar cavity and monitoring the shift in the resonant frequency over the temperature range of 25°C – 80°C.

The effect of B_2O_3 flux addition prior to compaction processing on the microstructure, microwave dielectric properties and mechanical properties of BZT ceramics is investigated. A maximum of 97% of the theoretical density was achieved for the samples containing 0.5 wt% B_2O_3 when sintered at a temperature of 1500°C.

The effect of various sintering atmospheres on densification and dielectric properties has been studied. Reaction bed sintering with calcined BZT powder at 1600°C for 2 hours resulted in uniform microstructure with good microwave dielectric properties. Volatilization of zinc is minimized and densification is improved. Effect of peak sintering temperature and dwell time on sintered density of pure BZT during reaction bed sintering has been shown in Fig 2(a).

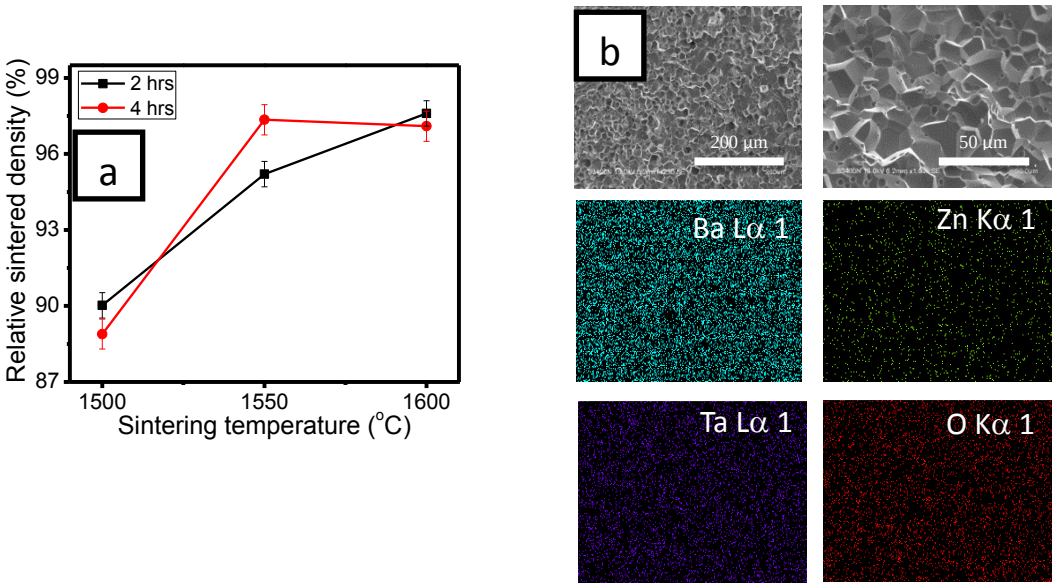

Fig 2 (a) Effect of peak sintering temperature and dwell time on sintered density of pure BZT during reaction bed sintering (b)Microstructure and elemental mapping of sample sintered by reaction bed sintering at 1600°C for 2 hours

98% of theoretical density has been achieved in the sample reaction bed sintered at 1600°C for 2 hours. Dense and uniform microstructure with clear grain boundary is revealed in the fracture surface of sample sintered at 1600°C for 2 hours. Elemental mapping of the sample (Fig 2(b)) reveal that the distribution of zinc is more uniform leading to better densification and good microwave dielectric properties. The crystal structure of reaction bed sintered sample was found to be hexagonal.

Chapter 5

In this chapter, colloidal processing and its effect on densification, microstructure evolution and microwave dielectric properties of BZT have been presented. Three different colloidal processing methods – slip casting, conventional gel casting and gelation using egg albumin have been used to consolidate BZT powders and their densification, microstructure and dielectric behaviors are compared with the samples densified by compaction route.

For microwave window application, large rectangular bars (76mm × 7mm × 3.3mm) with high density, uniform microstructure and good microwave dielectric properties are prerequisites.

Processing of large rectangular slabs of dimensions 55mm × 10mm × 5mm by compaction with the parameters optimized for smaller samples after sintering exhibited both warpage and density gradient.

Slip casting is a well-established shaping technique in which consolidation is effected by capillary suction of micro porous Plaster of Paris (POP) moulds [20]. The concentration of dispersant and solid loading was optimized based on the rheological behavior of slurries to obtain a stable suspension. Linear and volume shrinkage of samples were found to decrease with increase in solid loading due to better particle packing. Maximum sintered density of 96%TD was achieved in sample with maximum solid loading and the sample showed a quality factor (Q×f) of 63900 GHz and ε_r of 28.5.

Use of egg white as an eco-friendly binder for gel casting of ceramics has been adopted in developing low toxic green bodies [21]. Premix containing egg white and water in different proportions were used as a premix to prepare stable suspensions of BZT. Variations of complex viscosity as a function of temperature for suspensions containing different egg white concentrations were studied. Summary of the green density and sintered density and the dielectric properties of sintered samples with different egg white (EW) concentrations have been presented in Table 1.

Table 1 Summary of the green density and sintered density and the dielectric properties of sintered samples with different egg white (EW) concentrations.

DESCRIPTION	RELATIVE GREEN DENSITY (%)	RELATIVE SINTERED DENSITY (%)	Q × f (GHz)	ε_r
25% ovalbumin	50	94	58300	28.1
50% ovalbumin	52	95	59100	28.3
75% ovalbumin	47	93	47200	27.9

Gel casting is recognized as one of the prospective near net shaping process in developing green ceramics with high mechanical strength [22]. The concentrations of monomer, cross-linker and initiator were optimized based on the rheological behavior. The gelation behavior of the slurry was studied by measuring storage modulus (G′) in the oscillatory mode at a frequency of 1 Hz and at a constant strain of 0.5%. Storage modulus of BZT suspensions prepared from premix containing 5 and 10wt.% of MAM and MBAM with optimized initiator concentration were shown in Fig 3(a). Solid loading > 70 wt.% is required to achieve green density > 50% of TD. Sintered density also increases with increase in solid loading and a maximum relative sintered density ~ 98% has been achieved for sample with 88% solid loading (as shown in Fig 3(b)).

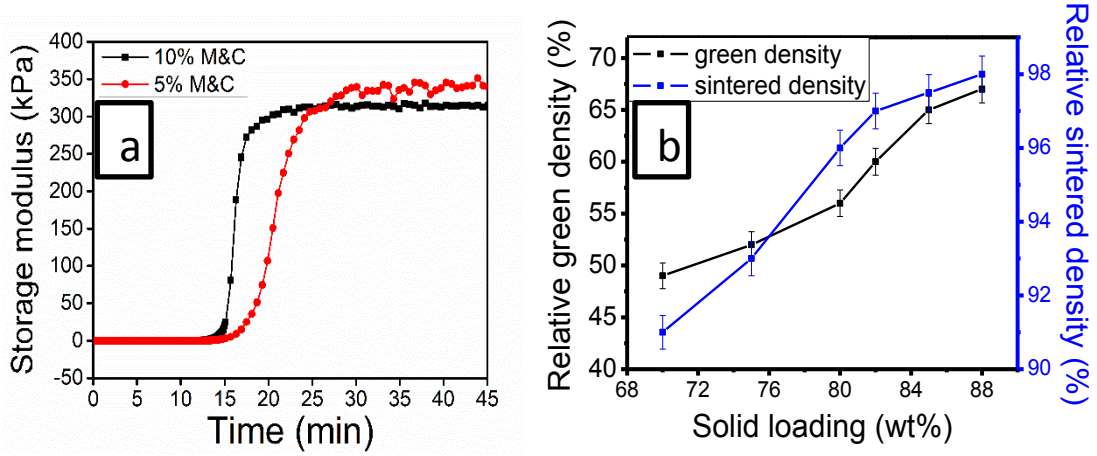

Fig 3 (a) Storage modulus of BZT suspensions prepared from premix containing 5 and 10wt.% of MAM and MBAM with optimized initiator concentration (b)Variation of green and sintered densities as a function of solid loading of the BZT suspensions consolidated by conventional gel casting technique

Shrinkage values remain least for conventional gel cast sample in comparison with slip cast and samples cast with egg white thus enabling near net shaping of BZT. The increase in quality factor and dielectric constant values with increase in solid loading follows the same trend as that of sintered density values. The increase in quality factor is marginal beyond 85% solid loading. Maximum quality factor of 93700 GHz and dielectric constant of 29.5 have been achieved for sample with maximum solid loading containing optimum concentrations of monomer, cross linker and initiator.

Chapter 6

In this chapter, results on microwave sintering of BZT have been presented. Pure BZT did not couple effectively with microwaves and hence various additives, which are known to couple effectively with microwaves, are added to BZT. The variation of density and microstructure with increase in sintering temperature is studied and compared with those obtained by conventional sintering. The effect of these additives on B-site ordering and quality factor of BZT samples are also studied and discussed in this chapter.

Uniaxially compacted pure BZT samples (with green density ~ 55% of TD) after calcination did not respond to microwaves effectively and hence the densification was poor. In the present study few oxides (Cr_2O_3 / Fe_2O_3 / ZrO_2 / MgO) and non-oxide (Si_3N_4 and SiC), which are known to couple effectively with microwaves, were added as secondary phases to BZT. The effect of these additives on densification and crystal structure were primarily studied to select the optimum additive for BZT. Densification behavior of BZT containing different additives for various microwave sintering temperatures is given in Fig 4. Based on the results of density and x-ray diffraction pattern, oxides (Cr_2O_3, Fe_2O_3 and ZrO_2) were chosen as optimum additives for microwave sintering of BZT.

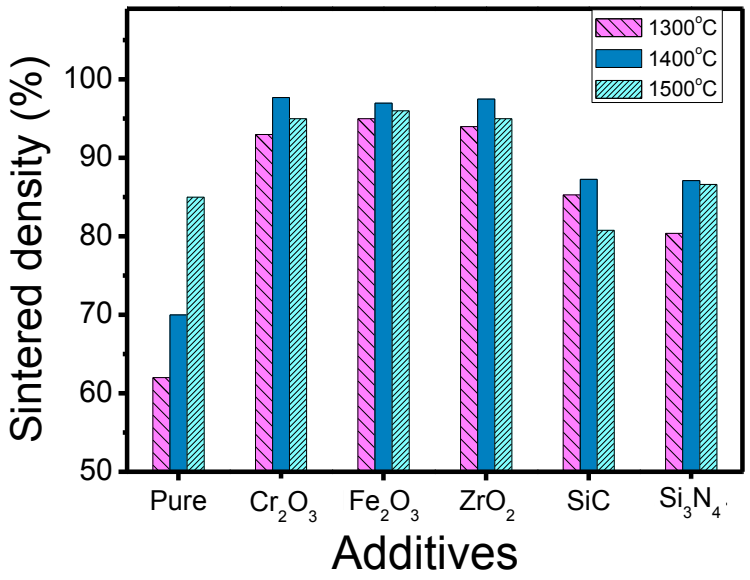

Fig 4 Densification behavior of BZT containing different additives for various microwave sintering temperatures.

Addition of oxide dopants has enhanced the densification and led to higher sintering density of ~97% of TD at a lower sintering temperature of 1400°C using microwave sintering. Processing time to develop a highly dense ceramic has been drastically reduced by microwave sintering. Influence of different concentration of dopants on densification behavior of BZT by microwave sintering has been studied and compared with the samples sintered by conventional sintering. The rate of densification increases rapidly with ZrO_2 addition upto 2mol. % in BZT - $xZrO_2$ samples and with further addition of ZrO_2 (upto 3 mol. %) decrease in the densification rate was observed in microwave sintering (as shown in Fig 5(a)). 98% TD was obtained for sample containing 2 mol% of ZrO_2 in microwave sintering.

Microstructural analysis of the samples was carried out to study the variation of density with increase in concentration of dopant atoms. Microstructures of BZT – $xZrO_2$ (x = 0.5 to 3 mol. %) samples sintered at 1400°C in microwave sintering furnace are shown in Fig 5(b). As the concentration of ZrO_2 is increased, bar shaped grains tend to evolve in the matrix containing small grains. Grain growth is improved for BZT – 2mol% ZrO_2 samples leading to dense microstructure formed from acicular grains with diffused grain boundary.

The sintered samples were characterized for microwave dielectric properties to determine the efficiency of BZT containing dopants for microwave application. The quality factor of perovskite microwave ceramics is known to depend on crystal structure and ordering of B-site ions in the lattice. The crystal structure and ordering of samples sintered using microwaves was studied using X-ray diffraction.

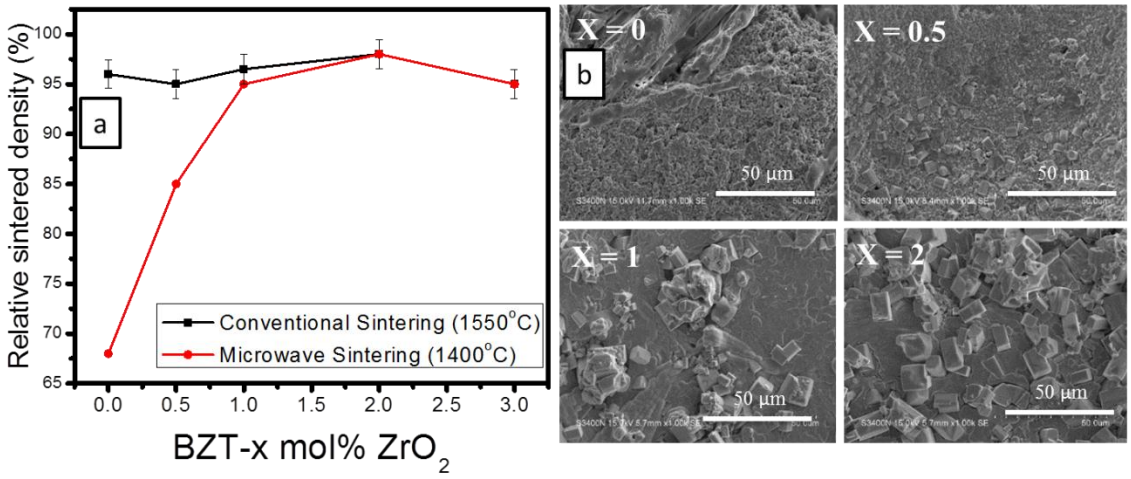

Fig 5 (a) Influence of ZrO_2 content on the sintered densities of BZT – $xZrO_2$ (x = 0 to 3 mol.%) samples 1400°C microwave and 1550°C conventionally sintered (b) Microstructures of BZT – $xZrO_2$ (x = 0 to 2 mol. %) samples microwave sintered at 1400°C

Maximum Q×f value of 137000 GHz has been achieved for annealed BZT – 2 mol% ZrO_2 samples. Lattice parameters, order parameter and crystallite size values for BZT - $xZrO_2$ (x = 0 to 3 mol. %) samples microwave sintered at 1400°C and conventionally sintered at 1550°C are summarized in Table 2.

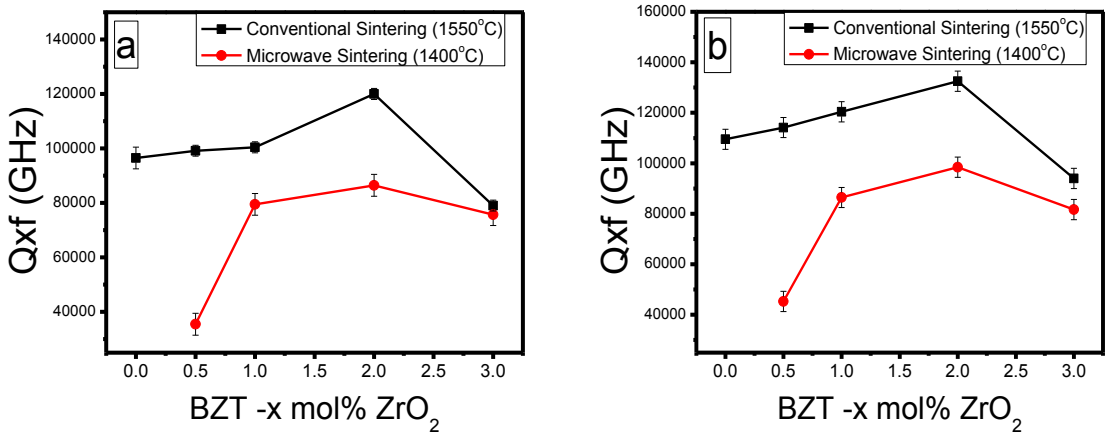

Fig 6 Variation of Quality factor (Q×f) of BZT – $xZrO_2$ (x = 0 to 3 mol. %) samples microwave sintered at 1400°C and conventionally sintered at 1550°C a) before annealing b) after annealing

From the lattice parameter values, it is clearly seen that c/a values decrease with increase in ZrO_2 concentration. The order parameter values were low for BZT - $xZrO_2$ (x < 2 mol%) and ordering is completely lost for samples with ZrO_2 > 2mol%. Crystallite size of conventionally sintered samples was higher than the microwave sintered samples.

Table 2 Lattice parameters, order parameter and crystallite size values for BZT - $xZrO_2$ (x = 0 to 3 mol. %) samples microwave sintered at 1400°C and conventionally sintered at 1550°C

BZT- $xZrO_2$	**Lattice parameters**			**Order parameter**	**Crystallite size**	
	a (Å)	c (Å)	c/a		MW 1400°C	CS 1550°C
0.5	5.77	7.07	1.2237	0.76	26	55
1	5.78	7.08	1.2235	0.69	39	68
2	5.79	7.07	1.2221	--	56	103
3	5.83	7.03	1.2052	--	43	83

Lattice vibrational modes and ordering in the system is studied using Raman spectroscopy. The BZT- $xZrO_2$ (x = 0 to 2 mol. %) samples showed signatures of 1:2 ordering in Raman spectra. For BZT - 3mol% ZrO_2, the peaks corresponding to ordering was not seen as per results from XRD. Also the FWHM of A_{1g}(O) mode was high for BZT - x ZrO_2 (x > 1 mol. %) samples indicating the formation of disordered structure.

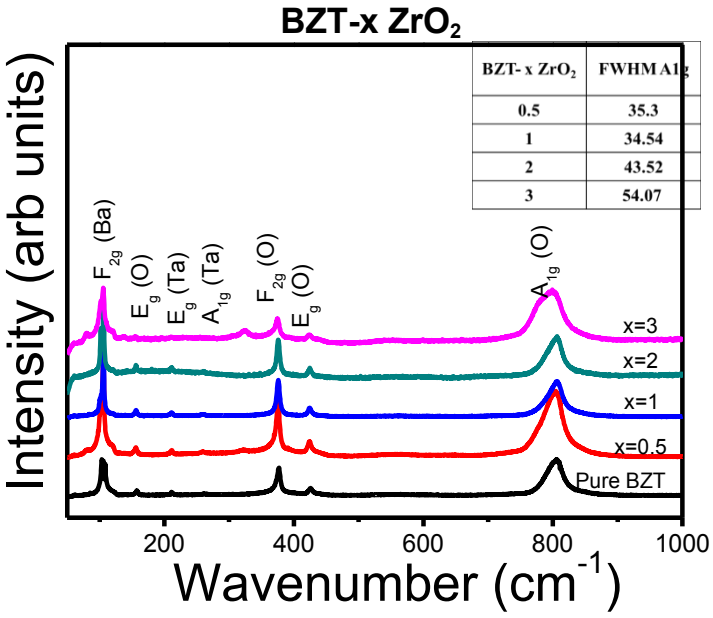

Fig 7 Raman spectra of BZT - $xZrO_2$ (x = 0 to 3 mol. %) sintered at 1400°C in microwave furnace, Inset: Variation of FWHM of A_{1g} mode for BZT - x ZrO_2 (x = 0 to 3 mol. %) samples

Dielectric properties of microwave sintered samples were not superior to samples processed by conventional sintering. Fig 7 shows Raman spectra of BZT - x ZrO_2 (x = 0 to 3 mol. %) samples sintered at 1400°C in microwave sintering furnace. Inset of Fig 7 shows the variation of FWHM of A_{1g} mode for BZT- x ZrO_2 (x = 0 to 3 mol. %) samples. The BZT- x ZrO_2 (x = 0 to 2 mol. %) samples showed signatures of 1:2 ordering in Raman spectra. Lattice vibrational modes and ordering in the

system is studied using Raman spectroscopy and correlated with the order parameter calculated from XRD analysis.

Chapter 7

Substitution of donor ion (La^{3+}) in the A site of BZT lattice is expected to compensate the local charges and hence influence the degree of ordering. Ga ions in the B site of BZT lattice is known to improve the sinterability and quality factor of BZT. Substitution of smaller ions (La in A site, Ga in B site) may lead to non-linear changes in the dielectric constant and τ_f due to alio-valent substitution. In this study BLZTG [$Ba_{1-x}La_x(Zn_{(1+x-2y)/3}Ta_{(2-x-y)/3}Ga_y)O_3$] (x,y-0, 0.01, 0.025, 0.05, 0.075, 0.1) were synthesized by solid state reaction. The microstructure and microwave dielectric properties have been studied and their structure property relationships have been correlated here.

Rate of densification of BZT is improved by the presence of La and Ga ions even at a lower temperature of 1500°C. Grain growth is enhanced and grain morphology changes with increase in concentration of La and Ga ions (Fig 8(a)). Since the changes in grain morphology in pure BZT and in BLZTG systems were found to be closely related to the presence of secondary phase and the crystal structure, the samples were characterized by XRD. Crystal structure and changes in ordering as examined by X-ray diffraction pattern reveal that the intensities and peak positions of fundamental reflections in BZT and BLZTG systems remain identical whereas there is a change in superlattice reflections.

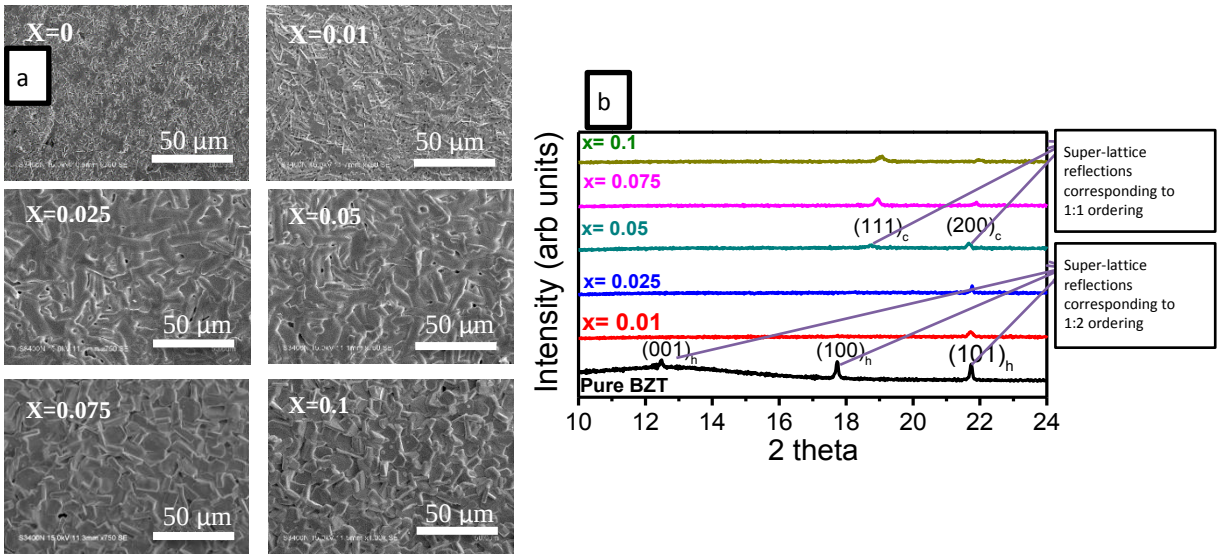

Fig 8 (a) Microstructure of BLZTG (x = 0 to 0.1 mol.%) samples sintered at 1550°C (b) X-ray diffraction pattern indicating super lattice reflection of BLZTG (x = 0 to 0.1 mol.%) samples sintered at 1550°C

Fig 8 (b) shows the x-ray diffraction pattern indicating super lattice reflection of BLZTG (x=0 to 0.1 mol.%) samples sintered at 1550°*C.* Pure BZT and BLZTG (x, y = 0.01, 0.025) were

indexed based on hexagonal unit cell. Super lattice reflections corresponding to B site ordering in pure BZT ($(100)_h$ and $(101)_h$)begins to disappear with the addition of La, Ga ions. When x=0.05, new set of super lattice reflections corresponding to 1:1 ordering begins to evolve and the unit cell is indexed based on cubic system.

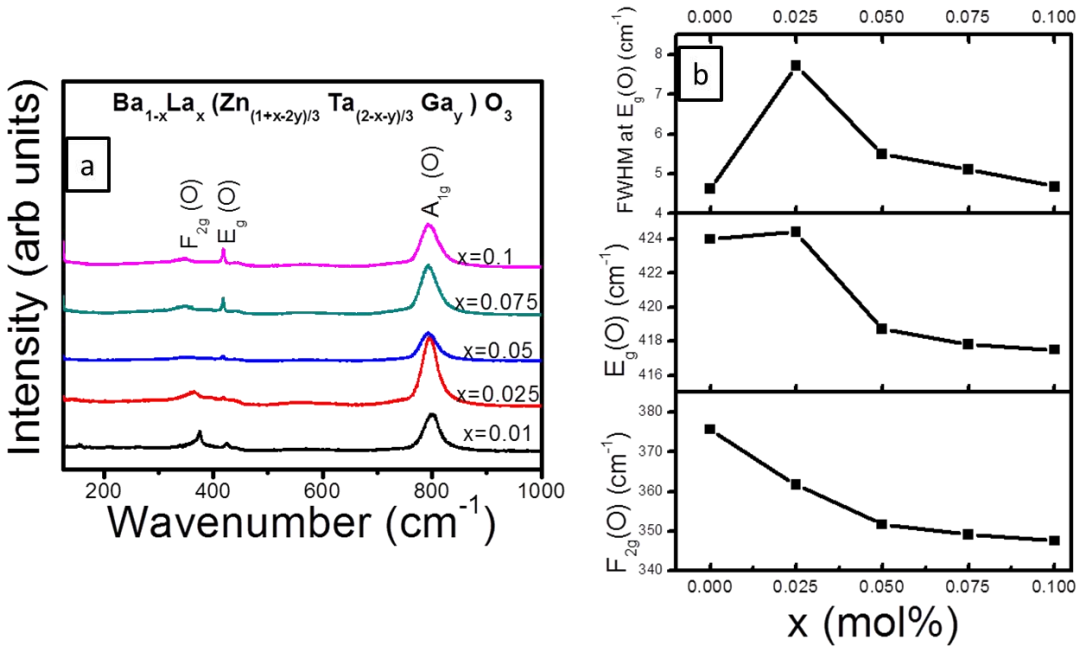

Fig 9 (a) Raman spectrum of BLZTG (x = 0.01 to 0.1 mol.%) sample sintered at 1550°C (b)Variation of Raman modes of BLZTG (x = 0.01 to 0.1 mol.%) as a function of composition

The influence of La and Ga ions in the local structure of BZT is studied using Raman spectroscopy. Fig 9(a) shows the Raman spectrum of BLZTG (x=0 to 0.1 mol.%) sample sintered at 1550°C. The peaks corresponding to the torsional modes of vibration of B site atoms (375 cm^{-1} and 424 cm^{-1}) broaden and shift with increasing concentration of La and Ga. FWHM of peak at 424cm^{-1} remains minimum for pure BZT due to the presence of 1:2 ordering. Variation of Raman modes of BLZTG (x = 0 to 0.1 mol.%) as a function of composition is shown in Fig 9(b). The broadening of peak (as reflected by increase in FWHM) for x = 0.025 could be attributed to the loss in B site ordering which is accordance with the x-ray diffraction pattern. FWHM tends to decrease for x = 0.05 which could be due to the onset of 1:1 ordering. The results are in agreement with order parameter calculated from x-ray diffraction pattern.

The dielectric properties of BLZTG system was evaluated to study its influence on changes in ordering of the system. There is a sharp decrease in Q×f with increase in x for samples sintered at 1600°C. There was a marginal increase in Q×f when x=0.025 which may be attributed to the presence of Ga ion in B site. Further decrease in Q×f is due to increase in 1:1 ordering. The dielectric constant

value of BLZTG system tends to increase with increasing concentration of dopants. Non-linear change of ε_r vs. composition was observed for the BLZTG complex perovskites. τ_f of dielectric mainly depends on τ_ε which is influenced by ordering, octahedral tilting and ionic polarizability. Since there is a change in ordering as well as the dielectric permittivity, τ_f of BLZTG increases with increasing concentration of dopants.

Chapter 8

This chapter gives the summary and conclusions of the results of the present work and also the scopes for future research in this area

Processing of pure BZT

- Volatilization of Zn is minimized and densification is improved (98% of TD) by suitably optimizing the process parameters followed by reaction bed sintering.
- Superior dielectric properties have been achieved without annealing.

Colloidal Processing

- Issues during scaling up to large rectangular bars were addressed by processing BZT by colloidal method (slip casting, gelation using egg albumin and conventional gel casting).
- Maximum densification has been achieved for samples processed by conventional gel casting. Variation in densification with respect to different processing methods is also reflected in microstructures.
- Correct combination of process parameters followed by sintering led to high density and good microwave dielectric properties without annealing thus improving the chance for commercial exploitation of the material.

Microwave sintering

- Addition of oxide dopants has enhanced the densification and led to higher sintering density of ~97% of TD at a lower sintering temperature of 1400°C using microwave sintering.
- Processing time to develop a highly dense ceramic has been drastically reduced by microwave sintering

BLZTG system

- BLZTG system shows better densification at a lower temperature of 1500°C. The atomic arrangement of BLZTG system is more accurately represented by a cubic unit cell for compositions with x>0.05. Microstructural analysis of BLZTG system reveal the presence of equi-axed grains with increase in concentration in accordance with the change in the crystal structure

Scope of future work

The feasibility of active alloy brazing BZT with Ti6Al4V alloy using different filler materials has been investigated and primary leak test results of brazed joints have been reported as a part of scope of future work.

- Fabrication of RF window
- RF window qualification tests
    - Visual inspection - cracks, deformation or for any gross leaks
    - Helium leak detector (HLD) test is carried out to establish its UHV compatibility
    - RF performance – Insertion loss and return loss

REFERENCES

[1] W. Wersing, 'High frequency ceramic dielectrics and their application for microwave components' in: Electronic Ceramics, pp. 67–119, Edited by B. C. H. Steels. Elsevier Applied Science, London, UK (1991).

[2] A. J. Moulson, and J. M. Herbert, 'Dielectrics and Insulators' in: Electroceramics, pp. 300-310, Chapman and Hall, London, UK (1990).

[3] P.K. Sharma, K.K. Ambulkar, P.R. Parmar, C.G. Virani, A.L. Thakur, L.M. Joshi and S.C. Nangru, J. Phys: Conference Series., 208, 012024 (2010).

[4] Mailadil T. Sebastin, '$A(B'_{1/3}B''_{2/3})O_3$ complex perovskites' in Dielectric materials for wireless communication, pp 261-320 Elsevier, London, UK (2008).

[5] K. Leong, J. Mazierska and J. Krupka, 1997 IEEE MTT-S Int. Microw. Symp., Dig. 3, 1639 (1997).

[6] B.W. Hakki and P.D. Colemann, IEEE Trans. Microw. Theory Tech.,18, 402 (1960).

[7] W.E. Courtney, IEEE Trans. Microw. Theory Tech., 18, 476 (1970).

[8] Karen A. Cummings and Subhash H. Risbud, J. Phys. Chem. Solids., 61, 551 (2000).

[9] H. Matsumoto, H. Tamura and K. Wakino, Jpn. J. Appl. Phys., 30, 2347 (1991).

[10] Z. Yue, F. Zhao, Y. Zhang and L. Li. Yue, Mater. Let., 58, 1830 (2004).

[11] S. Nomura and K. Kaneta, Jpn. J. Appl. Phys., 33, 507-508 (1984).

[12] Y-W. Kim, J-H. Park and J-G. Park, J. Eur. Ceram. Soc., 24, 1775 (2004).

[13] I.M. Reaney, I. Qazi and W.E. Lee. J. Appl. Phys., 88, 6708 (2000).

[14] J.-I. Yang, S. Nahm, C.-H. Choi, H.-J. Lee, J.-C. Kim and H.-M. Park. Jpn. J. Appl. Phys., 41, 702 (2002).

[15] J.-I. Yang, S. Nahm, S.-J. Yoon, H.-M. Park and H.-J. Lee. Jpn. J. Appl. Phys., 43, 211 (2004).

[16] M.-H. Kim, S. Nahm, W.-S. Lee, M.-J. Yoo, J.-C. Park and H.-J. Lee. Jpn. J. Appl. Phys. 43, 1438 (2004).

[17] Y.-H. Jeong, M.-H. Kim, S. Nahm, W.-S. Lee, M.-J. Yoo, N.-K. Kang, et al, Jpn. J. Appl. Phys., 44, 956 (2005).

[18] M.R. Varma and N.D. Kataria, J. Mater. Sci. Mater. Electron.. 18, 441 (2007).

[19] M.R. Varma, S. Biju and M.T. Sebastian, J. Eur. Ceram. Soc., 26, 1903 (2006).

[20] M.N. Rahaman, Ceramic Processing and Sintering. Taylor & Francis, 2003. Second edition, USA

[21] S. Dhara and P. Bhargava, J. Am. Ceram. Soc., 84, 12 (2001).

[22] M. Kokabi, A.A. Babaluo, and A. Barati, J. Eur. Ceram. Soc., 26, 15 (2006).

LIST OF PUBLICATIONS

A. List of peer-reviewed publications from the thesis work

- "Effect of colloidal processing on densification and dielectric properties of $Ba(Zn_{1/3}Ta_{2/3})O_3$ Ceramics", Swathi Manivannan, Andrews Joseph, P.K Sharma, K.C. James Raju, Dibakar Das, ***Ceramics International (2017), 10.1016/j.ceramint.2017.06.147***

- "Effect of microwave and conventional sintering on densification, microstructure and dielectric properties of $BZT–xCr_2O_3$ ceramics", Swathi Manivannan, Andrews Joseph, P.K. Sharma, K.C. James Raju, Dibakar Das, ***Ceramics International (2015), 10.1016/j.ceramint.2015.05.035***

- "Investigation of brazing of $Ba(Zn_{0.33}Ta_{0.67})O_3$ ceramic with Ti6Al4V alloy", Suresh Beera, Swathi Manivannan, Amit kumar Singh, Pramod Kumar Sharma, G Madhusudan Reddy, Dibakar Das, ***Ceramics International (2015), 10.1016/j.ceramint.2016.02.006***

- "Effect of Flux Addition on Mechanical and Microwave Dielectric Properties of Barium Zinc Tantalate Ceramics", Swathi Manivannan, V. S. Surya Chandra, P. K. Sharma, K. C. James Raju, and Dibakar Das, ***Trans. Ind. Ceram. Soc (2014), 10.1080/0371750X.2014.922419***

Patent

"A Process of Manufacturing Barium Zinc Tantalate Ceramics for Microwave Application"Swathi Manivannan, D. Das, V. S. Surya Chandra, K. C. James Raju, Pramod Kumar Sharma, ***Patent filed with IPO, Application No.:1591/CHE/2013***

B. Manuscripts to be communicated soon

- "Effect of Additives on densification and microwave dielectric properties in Microwave and Conventionally Sintered Barium Zinc Tantalate Ceramics",

Swathi Manivannan, Santhosh Kumar Gunapu, Pramod Kumar Sharma, K.C James Raju, Dibakar Das (*Manuscript under preparation*)

- "Ordering in $Ba_{1-x}La_x(Zn_{(1+x-2y)/3}Ta_{(2-x-y)/3}\ Ga_y)O_3$ Ceramics", Swathi Manivannan, Santhosh Kumar Gunapu, Pramod Kumar Sharma, K.C James Raju, Dibakar Das (*Manuscript under preparation*)

C. List of Conference Oral and poster presentations

- "Effect of Additives on Densification and Thermal Conductivity of Barium Zinc Tantalate Ceramics", Swathi Manivannan, P.Kumar Sharma, Tanjore V. Jayaraman, Dibakar Das, ***oral presentation in Characterization of Minerals, Metals, and Materials Symposium, 2016 TMS Annual Meeting & Exhibition, Nashville, Tennessee, USA***

- "Densification behavior and dielectric properties of gel cast Barium Zinc Tantalate ceramics", Swathi Manivannan, P.Kumar Sharma, Dibakar Das, ***oral presentation in Characterization of Minerals, Metals, and Materials Symposium, 2016 TMS Annual Meeting & Exhibition, Nashville, Tennessee, USA***

- "Structure and Microwave Dielectric Properties correlation in $Ba_{1-x}La_x(Zn_{(1+x-2y)/3}Ta_{(2-x-y)/3}Ga_y)O_3$ Ceramics", Swathi Manivannan, Santhosh Kumar Gunapu, Pramod Kumar Sharma, K.C James Raju, Dibakar Das, ***Characterization of Minerals, Metals, and Materials Symposium, 2015 TMS Annual Meeting & Exhibition, Orlando, Florida, USA***

- "Effect of Processing parameters on structural and microwave dielectric properties of Barium Zinc Tantalate Ceramics", Swathi Manivannan, D V Santhosh Kumar Gunapu , K. C. James Raju, P.K Sharma, Dibakar Das, ***Poster ID – EC28, presented in ICAFM – 2014, Trivandrum***

Chapter – 1

Introduction

CHAPTER 1

INTRODUCTION

Microwave dielectric ceramics have influenced the wireless technology with a wide range of applications including satellite broad casting, global positioning systems, personal communication devices, etc.,. Dielectric ceramics have modernized wireless communication technology by enabling miniaturization of devices. The importance of these ceramics is growing as they are able to transfer more information due to higher frequency of microwaves (300 MHz to 300 GHz) in comparison with the radio waves (300 KHz to 300 MHz) [1]. Investigation on processing, structure and dielectric properties of the ceramics were studied in detail to meet the increasing demand of the oxide ceramics with desired properties to various applications. Thermal shock resistance, chemical stability and higher resistivity of ceramics allow application in advanced functional devices [2]. Application of microwave dielectric ceramics as dielectric resonators and RF window component are discussed in subsequent sections.

1.1.1 Dielectric resonator (DR):

The term 'Dielectric Resonator' was first coined by Richtmeyer in 1939, where he has explained the possibility of using dielectric materials with an appropriate shape and high ε_r as a microwave resonator. DRs are generally constituted by a cylindrical piece of ceramic with low loss and high relative permittivity that will allow the standing EM radiation to sustain within the volume due to reflection at the dielectric – air interface [3]. Rutile single crystals were found to exhibit properties of dielectric resonator in early 1960s and further studies on low loss dielectric ceramics pioneered in search of new materials to meet the increasing demand in base station and hand set application [4]. DRs form a crucial module in microwave circuits due to its ability to sustain a standing electromagnetic radiation within it. DRs are capable of confining the EM radiation and hence find application as antennas, filters and

oscillators [5]. The dielectric loss of the ceramic materials are greatly influenced by various extrinsic factors (density, microstructure, porosity, defects, etc.,). Hence, studies on processing of ceramics and effect of various additives on structure/property have gained more importance to facilitate commercial production of DRs.

1.1.2 RF window:

Many aspiring energy projects have been going on in present days and one of such projects is Tokamak based fusion reactor. RF power is used as one of the non-inductive methods to maintain the plasma current under steady state condition [6,7]. Lower Hybrid Current Drive (LHCD) system based on a grill type antenna has In vessel system comprising of antenna, RF window and transmission line. RF window, used in the transmission line, acts as a vacuum barrier and transmits the microwave power. Hence it is one of the critical components that limit the power that is coupled to plasma. RF window consists of a single titanium frame with 2×32 slots in which ceramic components are inserted. The ceramic samples should be brazed to the Ti frame to provide leak proof joints. The in vessel system is supposed to give good RF performance and UHV compatibility [8].

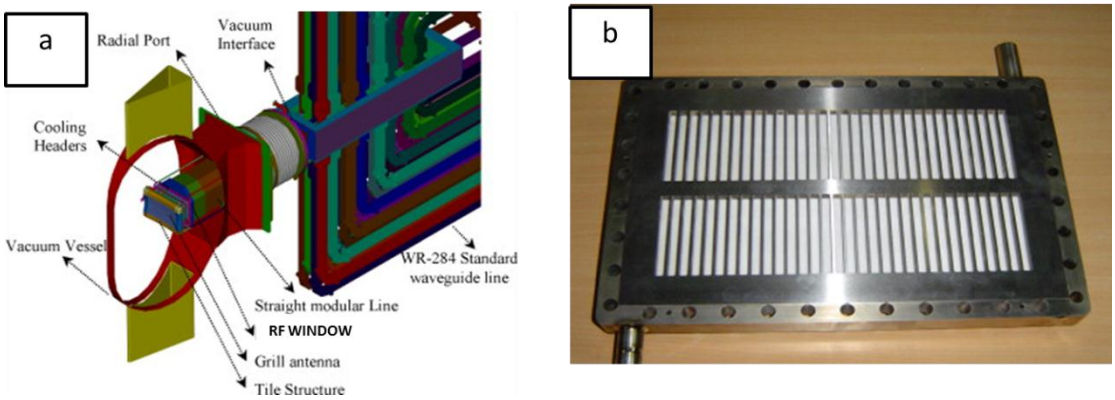

Fig 1.1 (a) Schematic view of In-vessel LHCD system on SST 1 Tokamak (b) RF window with single titanium frame and 64 slots with ceramics components

1.2 Material Requirements:

The desirable material properties for application as dielectric resonator are

1. High quality factor

The quantitative measure of power loss in microwave system is denoted by quality factor. For perfect crystals, quality factor is inverse of dielectric loss (tan δ).

$$Q = 2\pi \frac{maximum\ energy\ stored\ per\ cycle}{average\ energy\ dissipated\ per\ cycle} \quad (1)$$

The dielectric loss in mainly attributed to the interaction of phonons with the applied filed. The total quality factor (or loaded quality factor, Q_L) is the sum of loss due to dielectric ($1/Q_d$), conduction of metallic plates ($1/Q_c$) and radiation ($1/Q_r$). External losses ($1/Q_{ext}$) due to coupling also contribute to decrease in unloaded quality factor.

$$\frac{1}{Q_l} = \frac{1}{Q_d} + \frac{1}{Q_c} + \frac{1}{Q_r} + \frac{1}{Q_{ext}} \quad (2)$$

Since Q value determines the selectivity of a resonator to a given frequency, higher Q values are required for enhanced performance of the resonator.

2. High dielectric constant

The wavelength inside the dielectric (λ_d) is inversely proportional to the square root of its permittivity. Hence high ε_r materials are preferred as dielectric resonators as they can enable circuit miniaturization.

$$\lambda_d = \frac{\lambda_0}{\sqrt{\varepsilon_r}} \quad (3)$$

where, λ_0 is the wavelength in vacuum

3. Small temperature coefficient of resonant frequency

The stability of resonant frequency with variation in temperature is indicated by temperature coefficient of resonant frequency (τ_f). For resonator applications, τ_f

values should be close to zero. τ_f is related to temperature coefficient of permittivity(τ_ε) and linear expansion coefficient (α_l) by the following relation

$$\tau_f = -\alpha_l - \frac{\tau_\varepsilon}{2} \quad (4)$$

The desirable properties of dielectric ceramic used in RF window application are

1. *Low dielectric loss / High quality factor*

   Dielectric loss represents energy dissipation due to intrinsic and extrinsic parameters. Intrinsic losses depends on the crystal structure while extrinsic loss depends on density, microstructural defects, grain boundaries, vacancies, dopants, etc., Hence, for application as RF window, dielectric ceramics should have lower dielectric loss to enable least power dissipation.

2. *High dielectric constant*

   The interaction of ac field with the crystal lattice modifies the equilibrium of phonon system. This leads to dielectric relaxation which is accompanied by energy dissipation. In microwave frequency, energy gets dissipated in the form of heat and so the window section is prone to have higher temperature during operation. Thick sections of RF ceramic window are prone to cracks due to slow dissipation of heat leading to ultimate failure of the window [7,9]. For a fixed resonant frequency, dimension of high ε_r ceramic dielectric required will be less in comparison with low ε_r dielectric. Hence high dielectric constant dielectric material is required.

3. *Good temperature stability and high dielectric strength*

   Since energy dissipation in the form of heat occurs during operation, drift in resonant frequency with increase in temperature is not favorable. Hence temperature coefficient of resonant frequency should be close to zero. High dielectric strength is also a pre-requisite to prevent breakdown of ceramic.

4. *High thermal conductivity*

   Heat generated during operation needs to be dissipated at a faster rate and high thermal conductivity is required to prevent crack generation due to localized heat spots [10].

5. *High mechanical strength*

   Structural loads lead to fracture in ceramics and hence high mechanical strength is required for dielectric material used as RF window

6. *Ability to braze to the frame material*

   Ceramic window sections were to be inserted in the slot of frame material. In order to ensure UHV compatible leak proof assembly, the sections are to brazed to frame material. Hence feasibility to braze multiple ceramic sections to the frame is also an important property [11].

1.3 A ($B'_{1/3}$ $B''_{2/3}$) O_3 complex perovskites:

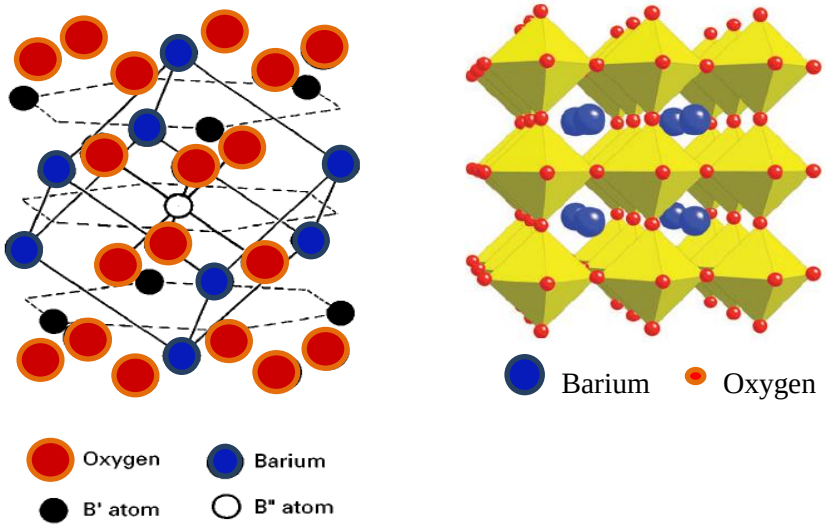

Fig 1.2 Schematic representation of a A ($B'_{1/3}$ $B''_{2/3}$) O_3 complex perovskites

Ceramics with ABO_3 perovskite structure and related compounds have dominated the electro ceramics industry. The perovskite structure is one of the most widely studied classes of structures due to its ability to accommodate extensive range of atomic substitutions and hence offer a robust series of properties. In ABO_3

perovskite structure, B site ions occur in the oxygen octahedra formed due to close packing of AO_3 layers. When the cation-oxygen bond lengths are in equilibrium distance, the unit cell remains undistorted and hence the symmetry remains cubic.

The stability of the perovskite for particular set of cation and anion is dependent on the Goldschmidt tolerance factor (τ).

$$\tau = \frac{r_A + r_O}{\sqrt{2}(r_B + r_O)} \quad (5)$$

For ideal perovskite, the value of τ is equal to one but structures with lower symmetry can also exist as perovskites. The perovskite structure can accommodate alio-valent substitution in A site and B site and the general formula is given as $A(B'_xB''_y)O_3$ or $(A'_xA''_y)BO_3$. One of such complex perovskite structure $A^{2+}(B^{2+}_{1/3}\ B^{5+}_{2/3})\ O_3$ in which higher valence B^{5+} ions occur twice than that of lower valence B^{2+} ions. [12]

$A\ (B'_{1/3}\ B''_{2/3})\ O_3$ complex perovskites are the most extensively investigated family in microwave dielectric ceramics. A site is generally constituted by Ba, Ca and Sr. A broad series of B site substitutions (Zn, Mg, Ni, Sr, Ca, Mn, Cd, etc., at B' site and Ta, Nb in B'' site) allow tailoring of properties to meet various demands in application. The cubic perovskite cell is constituted by three AO_3 layers, one layer of B^{2+} and two layers of B^{5+}.

The first material to be studied in this class of structure was $Ba\ (Sr_{1/3}\ Ta_{2/3})\ O_3$ in which some extra weak reflections were observed in x-ray diffraction pattern. Galasso et al accounted these weak reflections to hexagonal superstructure formed due to 1:2 ordering of Sr and Ta ions in the B site. The ordering of B site ions along the <111> direction of cubic unit cell led to the formation hexagonal unit cell with lattice parameters, $a_{ord} = a_c\sqrt{2}$ and $c_{ord} = a_c\sqrt{3}$ and $P\bar{3}m1$ symmetry. 1:2 ordered tantalates and niobates have gained considerable importance due to their low dielectric loss and high dielectric constant [13].

1.4 Microwave dielectric properties measurement:

1.4.1 Quality factor:

Quality factor of the samples were measured by $TE_{01\delta}$ mode dielectric resonator method, using a variable cavity based test fixture manufactured by QWED [14]. The dielectric ceramic puck is kept inside the copper cavity. The inner surface of the cavity is coated with silver and the sample is placed at the center on the quartz spacer. The aspect ratio of the samples is maintained between 2 – 2.5 range to ensure mode separation. Approximate value of resonant frequency for isolated dielectric resonator is calculated from dimension of the sample. After identifying $TE_{01\delta}$ mode resonance frequency, quality factor of various samples were measured using a Vector Network Analyzer under weak coupling condition, where loaded quality factor ≈ unloaded quality factor.

Fig 1.3 Cavity test fixture for $TE_{01\delta}$ mode dielectric resonator method

1.4.2 Dielectric constant:

The dielectric constant of the material is measured by Hakki and Coleman method modified by Courtney. The sample is placed symmetrical with two probes and the various resonant modes are identified using a vector network analyser [15]. The $TE_{01\delta}$ mode resonance frequency is identified and the span is reduced further to have enhanced resolution. The centre frequency is accurately identified and the dimensions of the sample, diameter D and Length L, are measured.

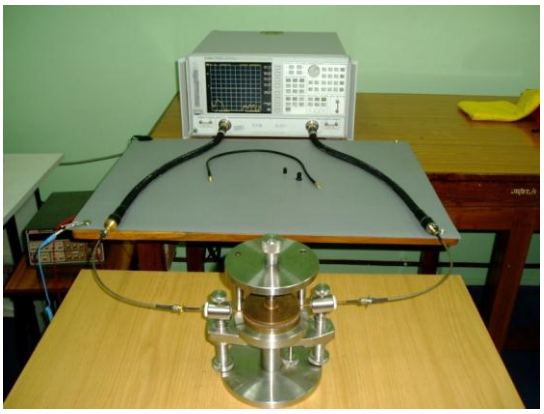

Fig 1.4. Hakki and Coleman setup to measure dielectric constant

From the mode chart parameter values (α_1 and β_1), dimensions of ceramic puck and center frequency (f_r), the dielectric constant is calculated using the formula given below

$$\varepsilon_r = 1 + \left(\frac{c}{\pi D f}\right)^2 . \left(\alpha_1^2 + \beta_1^2\right) \qquad (6)$$

1.4.3 Temperature coefficient of resonant frequency:

The temperature coefficient of resonant frequency is measured by placing the sample in invar cavity. The sample is slowly heated at a rate of 3°C/min in the range of 25°C – 80°C.

Fig 1.5 Cavity setup for measurement of temperature coefficient of resonant frequency

The shift in the resonant frequency due to increase in temperature in the reflection mode is noted over the temperature range of 25°C – 80°C using vector network analyser. The temperature coefficient of resonant frequency is calculated using the formula given below

$$\tau_f = \frac{1}{f_0} \cdot \frac{\Delta f}{\Delta T} \; ppm/^o C \qquad (7)$$

1.5 References

[1] I.M.Reaney, D. Iddles, J. Am. Ceram. Soc., 89, 7 (2006)

[2] W. Wersing, 'High frequency ceramic dielectrics and their application for microwave components' in: Electronic Ceramics, pp. 67–119, Edited by B. C. H. Steels. Elsevier Applied Science, London, UK (1991).

[3] R. D. Richtmyer, J. App. Phys. 10, 391 (1939)

[4] A. Okaya, Proc. IRE., 48, 1921-24 (1960).

[5] A. J. Moulson, and J. M. Herbert, 'Dielectrics and Insulators' in: Electroceramics, pp. 300-310, Chapman and Hall, London, UK (1990).

[6] C. Hamlyn-Harris, A. Borthwick, J. Fanthome, C. Waldon, M. Nightingale, N. Richardson, Fusion Eng. Des. 84, 887–894(2009)

[7] K.A. Cummings, S.H. Risbud, J. Phys. Chem. Solids., 61, 551 (2000).

[8] P.K. Sharma, K.K. Ambulkar, P.R. Parmar, C.G. Virani, A.L. Thakur, L.M. Joshi and S.C. Nangru, J. Phys: Conference Series., 208, 012024 (2010).

[9] Y. Saito, IEEE Transactions on Electrical Insulation 2 (2), 243–250(1995).

[10] S. Michizono, Y. Saito, S. Yamaguchi, S. Anami, N. Matuda, A. Kinbara, IEEE Transactions on Electrical Insulation 28 (4) 692–699 (1993).

[11] J. S. Pimenta et al J. Braz. Soc. Mech. Sci. & Eng; 32, 4:468-474 (2010).

[12] Mailadil T.Sebastin, '$A(B'_{1/3}B''_{2/3})O_3$ complex perovskites' in Dielectric materials for wireless communication, pp 261-320 Elsevier, London, UK (2008).

[13] P.K. Davies, H.Wu, A.Y. Borisevich, I.E. Molodetsky, and L. Farber Annu. Rev. Mater. Res., 38:369–401(2008).

[14] K. Leong, J. Mazierska, J. Krupka, 1997 IEEE MTT-S Int. Microw. Symp. Dig. 3 1639-42 (1997).

[15] B.W. Hakki and P.D. Colemann, IEEE Trans. Microw. Theory Tech.,18, 402 (1960).

Chapter – 2

Literature review

CHAPTER 2
LITERATURE REVIEW

2.1 Overview of ceramics for RF window application:

High purity dense alumina ceramics is the most common material for RF window application. The effect of various sintering additives and densification and RF performance of aluminium oxide window sections has been reported already [1]. Feasibility of using Beryllium oxide as window section has been tested but this material is not preferred due to its toxicity [2]. Sapphire window sections showed luminescence and were able to transfer only one fourth of the power transmitted by alumina. Aluminium Nitride window sections suffered from serious drawbacks (poor RF performance, low resistivity and multipacting) which will lead to failure of RF window [3]. Even though alumina is considered as ideal material for window sections, it is worthwhile to investigate an alternate material for RF window application.

2.2 Candidate complex perovskite materials for DR applications:

Structure and property correlation of A $(B'_{1/3}\ B''_{2/3})\ O_3$ complex perovskites have gained enough attention and numerous studies were done to tailor different properties by various atomic substitutions. $Ba(Mg_{1/3}Ta_{2/3})O_3$(BMT) , $Ba(Zn_{1/3}Ta_{2/3})O_3$ (BZT) and $Ba(Zn_{1/3}Nb_{2/3})O_3$ (BZN) systems have been extensively studied due to their attractive dielectric properties that are ideal for microwave DR applications. The stability of B site ordering differs for niobate and tantalate systems inspite of having similar ordered structures. This behavior is attributed to the difference in covalency of the two systems.

Matsumoto et al [4] reported Ba $(Mg_{1/3}Ta_{2/3})O_3$ (BMT) with good dielectric properties ($Q\times f$ – 430000 GHz, ε_r - 24, τ_f - 8ppm/°C). But the disadvantage involved in preparing BMT is that it requires high sintering temperature (1650°C) due to poor

sinterability followed by long hours of annealing to establish B site ordering. Solid state synthesis of Ba $(Zn_{1/3}Nb_{2/3})O_3$ was reported by Yue et al (Q×f - 96000GHz, ε_r - 42, τ_f - 30ppm/°C)[5]. Several authors tailored the dielectric properties of BZN by doping with Co, Ga, Ce, etc. Also the effect of glassy additives on sinterability and dielectric properties has been studied. In order to have good temperature stability (τ_f ~ 0 ppm/°C), several authors tried to prepare solid solution with SZN, but the quality factor of the samples drastically reduced [6-8]. $Ba(Mn_{1/3}Ta_{2/3})O_3$ ceramics also had low loss (Q×f - 104000 GHz) and high dielectric constant (ε_r - 27). But the system requires special atmosphere during sintering which hampered the commercial exploitation of the material [9]. A number of studies on preparation of Ba $(Mg_{1/3}Nb_{2/3})O_3$ (BZN) by chemical and solid state routes were reported. BMN samples with small Mg deficiency showed better properties (Q×f - 96000GHz, ε_r - 32, τ_f - 30ppm/°C). The relatively high τ_f of this system prevents it from practical applications [10].

2.2.1 Ba $(Zn_{1/3}Ta_{2/3})O_3$ (BZT) ceramics:

Barium zinc tantalate Ba $(Zn_{1/3}Ta_{2/3})O_3$ (BZT) is a well-known dielectric ceramics with excellent microwave dielectric properties and having high dielectric constant (ε_r), low loss (tanδ) and very low temperature coefficient of resonance frequency (τ_f) in the microwave frequency range and a high quality factor is an important material for wireless communication devices [11]. This material which belong to $A(B'_{1/3}B''_{2/3})O_3$ complex perovskites has potential for applications in satellite broadcasting at frequencies higher than 10 GHz and as a very high Q dielectric resonator (DR) in mobile phone base stations or combiner filter for PCS applications. The value of the quality factor is dependent on the degree of 1:2 ordering of B site ions and hence Q is sensitive to sample processing conditions [12].

BZT ceramics, with such excellent microwave dielectric properties are suitable for different microwave and millimeter wave device applications including filters in base station of mobile and satellite application, dielectric resonators,

microwave windows in fusion reactors, multilayer ceramic capacitors (MLCC) etc [13].

But, the main disadvantage in processing BZT ceramics for such applications is the high processing (sintering) temperature requirement to develop a highly dense material, followed by a high temperature annealing process for prolonged time duration (to obtain the desired crystallographic structure. The problem becomes even severe in processing co-fired (simultaneous heat treatment of the BZT ceramics with a low melting temperature metals, such as Ni, Cu) MLCC substrate in particular [14]. The major drawback in processing BZT ceramics at high temperatures is the volatilization of low melting Zn from the BZT composition rendering the final product containing lot of defects including the presence of other phases. The problem has been addressed in the prior art in many ways [15].

One such way known is by adding a small amount of other oxides (dopants), such as Al_2O_3, Ga_2O_3, ZrO_2, or TiO_2 to BZT to compensate for the Zn loss from the system [16-19].

Zn loss from the system has also been prevented by sintering it at relatively lower temperatures in presence of some sintering additives such as boron trioxide (B_2O_3) and in few literatures it is shown with copper oxide (CuO) as well. Lithium salts also help in low temperature sintering of BZT ceramics, without loss of Zn. BZT sintering without Zn loss has also been realized with combined addition of B_2O_3 and lithium fluoride (LiF_2) in various reducing sintering atmospheres particularly for the processing of copper based MLCC [20,21].

Suppression of Zn loss followed by enhancement in densification of BZT ceramics has been observed in presence of other oxides, such as ZrO_2 and TiO_2, as a result of grain growth observed in liquid phase sintering [22]. B_2O_3 and Li salts reduce the sintering temperature of BZT ceramics but the presence of glassy matrix (as a result of liquid phase sintering) in the sintered product make the system inherently weak and the final product does not have adequate mechanical strength [23].

Even though the addition of other oxides and salts helps in reducing the sintering temperature and Zn loss from the system (thereby increasing the density and hence reducing the porosity) the presence of other cations (such as Ni, Zr, Ti, Ga etc) alter the ionic environment of the native ions (such as Ba, Zn, Ta, O_2 etc) and hence affect the dielectric properties.

Several efforts have also been made to use dopant consisting of similar ions as that of BZT in order to suppress the extended defects arising from other oxides and salts doping in BZT matrix. Doping with barium tungstenate ($BaWO_4$) under zinc oxide (ZnO) muffling (covering the BZT pellet with ZnO powder) conditions results in improved structural and dielectric properties [24].

Nanosized BZT powder, synthesized by wet chemical route, were doped with Ga_2O_3 and sintered by muffling with calcined BZT powder. But, only 90% of the theoretical density has been achieved [25].

Several efforts have been made to suppress the Zn loss from BZT ceramics thereby improving the structural and dielectric properties. The density and microstructure of the sintered BZT composition (in global scale, with very less magnification) has not been reported in prior arts. Apart from having acceptable microwave dielectric properties the BZT product has to be mechanically robust as well with as minimum porosity as possible (as high density close to the theoretical density as possible).

2.3 References

[1] K.A. Cummings, S.H. Risbud, J. Phys. Chem. Solids., 61, 551 (2000).

[2] M. Pisharody, P. Barnes, E. Chojnacki, R. Durand, T. Hayes, et al, IEEE Particle Accelerator Conference, Dallas, TX, 3, 1720–1722 (1995).

[3] M. Neubauer, R. P. Johnson, R. Rimmer, T. Elliot, M. Stirbet, Proceedings of PAC09, Vancouver, BC, Canada WE5PFP042, 2089 (2009).

[4] M. Hiroyuki, T. Hiroshi, W. Kiku, Jpn. J. Appl. Phys, 30, 9S, 2347 (1991).

[5] Z. Yue, F. Zhao, Zhang, Gui and L. Li, Mater. Letters., 58, 1830-1834 (2004).

[6] K. Endo, K. Fujimoto, K. Murakawa, J. Am. Ceram. Soc., 70, 9, C-215–C-218, (1987).

[7] S. Kamba, H. Hughes, D. Noujni, S. Surendran, R. C Pullar, et al., J. Phys. D: Appl. Phys., 37, 14 (2004).

[8] M. R. Varma, M.T. Sebastian, J. Eur. Ceram. Soc., 27, 2827–2833 (2007).

[9] S. Nomura and K. Kaneta, Jpn. J. Appl. Phys., 23, 1, 4 (1984).

[10] M. Y. Chen, C. T. Chia, I. N. Lin, L. J. Lin, C. W. Ahn, Shan Nahm, J. Eur. Ceram. Soc., 26, 10, 1965-1968 (2006).

[11] S. B. Desu, and H. M. O'Bryan, J. Am. Ceram. Soc., 68, 546–551 (1985).

[12] H. Tamura, D.A. Sagala and K. Wakino, Jpn. J. Appl. Phys., 25, 787-791 (1986).

[13] A. J. Moulson, and J. M. Herbert, 'Dielectrics and Insulators' in: Electroceramics, pp. 300-310, Chapman and Hall, London, UK (1990).

[14] I. Kim, T. Oh, Y. Kim, J. Mater. Sci. Lett., 12, 182–184 (1993).

[15] H. Tamura, T. Konoike, Y. Sakabe, K. Wakino, Comm. J. Am. Ceram. Soc., 67, 4, C59–61(1984).

[16] F. Roulland, G. Allainmat, M. Pollet, S. Marinel, J. Eur. Ceram. Soc., 25, 2763–2768 (2005).

[17] J.-I. Yang, S. Nahm, C.-H. Choi, H.-J. Lee, J.-C. Kim, H.-M. Park, Jpn. J. Appl. Phys., 41, 702 (2002).

[18] Y.-H. Jeong, M.-H. Kim, S. Nahm, W.-S. Lee, M.-J. Yoo, N.-K. Kang, et al., Jpn. J. Appl. Phys., 44, 956–960 (2005).

[19] M. R. Varma, N. D. Kataria, J. Mater. Sci. Mater. Electron., 18, 441–446 (2007).

[20] C.J. Lee, G. Pezzotti, S. H. Kang, Deug J. Kim, K. S. Hong, J. Eur. Ceram Soc., 26, 1385-1391(2006).

[21] J.-In Yang, S. Nahm, C.-H. Choi, H.-J Lee, H. M. Park., J. Am. Ceram. Soc., 85, 1, 165–168 (2002).

[22] J.-I. Yang, S. Nahm, S.-J. Yoon, H.-M. Park, H.-J. Lee, Jpn. J. Appl. Phys., 43 211–214 (2004).

[23] F. Roulland, R. Terras, S. Marinel, Mater. Sci. Eng., B.,104, 156-162 (2003).

[24] J. S. Kim, J.-W. Kim, C.I. Cheon, Y.-S. Kim, S. Nahm, J.D. Byun, J. Eur. Ceram. Soc., 21, 2599–2604 (2001).

[25] M. R. Varma, S. Biju, M.T. Sebastian, J. Eur. Ceram. Soc., 26, 1903–1907 (2006).

Chapter – 3

Objective of the work

CHAPTER 3

OBJECTIVE OF THE WORK

The present aim of this thesis work is to synthesize and investigate the structural and microwave dielectric properties of $Ba(Zn_{1/3}Ta_{2/3})O_3$ (BZT) ceramics for the following applications as

- Ceramic window sections to be used in high power microwave windows in fusion systems
- Microwave dielectric resonator to be used in communication devices

The ceramic material to be used as dielectric resonator is expected to have very high density, uniform microstructure, high thermal conductivity, good thermal stability and excellent microwave dielectric properties. BZT ceramics are extremely useful for application as microwave window section in fusion reactors, in particular. The window has to offer an ultrahigh vacuum tight sealing (BZT composition with density close to TD) as well as to deliver (transmit) the high power microwave into the reactor to sustain the plasma.

The significant factors to be investigated to develop such a ceramic material for the given applications are

- Development of a suitable and an efficient processing route to synthesis the bulk ceramic material, which includes its synthesis methods, compaction behaviours, densification/sintering kinetics, etc.
- The influence of the processing conditions and chemical composition of the material on its structural and microwave dielectric properties.

This investigation will provide the flexibility to design the composition of the ceramic material and also to tune its dielectric properties by varying the processing parameters. This study will also lead us to new insights in this material and to achieve a comprehensive understanding of the contributing factors and physical phenomena by in-depth experimental investigation.

Although there has been tremendous progress in the development of microwave dielectric materials in the past, there is still a need for developing efficient, economical and stable MW dielectric materials for the ever increasing growth in this field. Hence based on a thorough literature analysis, with the drawbacks discussed in the previous chapter, the following objectives were set to develop mechanically robust BZT ceramics with highest density (close to the theoretical density), high dielectric constant, low loss (high quality factor, Q), very low and stable temperature coefficient of resonance frequency and high thermal conductivity suitable for high power microwave and millimeter wave device applications.

- Study the effect of different process parameters during consolidation and sintering to achieve robust BZT ceramics with high microwave dielectric properties
- Investigate the effect of colloidal processing on the densification and dielectric properties of BZT
- Study the influence of microwave sintering in minimizing zinc volatilization
- Investigate the change in ordering and sinterability of BZT with specific site doping of A site and B site with suitable dopants.

Chapter – 4

Synthesis, Characterization and Microwave dielectric properties of pure BZT

CHAPTER 4

SYNTHESIS, CHARACTERIZATION AND MICROWAVE DIELECTRIC PROPERTIES OF PURE BZT

$Ba(Zn_{1/3}Ta_{2/3})O_3$ (BZT) is a complex perovskite which has shown superior dielectric properties matching close to an ideal microwave dielectric resonator material and mainly used for DR applications. Density and dielectric properties of this BZT ceramics depends upon the way it is processed and hence the steps for processing and the sintering conditions must be carefully monitored and controlled for the best results. Therefore various processing conditions, techniques have been employed and careful attention has been paid for the preparation of the BZT samples.

The main disadvantages in processing BZT ceramics are discussed in detail in Chapter 2. Also, studies on effect of dopant addition on BZT and its consequences on density and microwave dielectric properties of BZT were elaborated in Chapter 2.

For applications such as microwave window sections for fusion reactor, mechanically robust BZT ceramics with high density and uniform microstructure is required. The obviousness of correct combination of different processing parameters will lead to the desired properties and this has been elaborated in this chapter:

4.1 Synthesis by solid state reaction:

Synthesis by solid state reaction method is one of the most widely used techniques for synthesis of dielectric ceramics. The rate of reaction is high in this method and involves a solvent less reaction. Precursors were taken in the form of oxides and bicarbonates in stoichiometric proportions and homogenously mixed by ball-milling for several hours. The mixed oxides/ carbonates were then heat treated to achieve the target composition [1]. In this study, solid state synthesis method was

employed as to cost effectively produce large quantity of powders for preparation of BZT samples with large dimensions.

$Ba(Zn_{1/3}Ta_{2/3})O_3$ samples were prepared by conventional solid-state reaction. The starting materials used were analytical reagent (AR) grade of

- Barium carbonate ($BaCO_3$),
- Zinc oxide (ZnO) and
- Tantalum oxide (Ta_2O_5)

$BaCO_3$, ZnO (Sigma Aldrich, USA) and Ta_2O_5 (NFC, Hyderabad) powders with > 99% purity were taken. Stoichiometric quantities were weighed, ground, homogenized and milled for 12 hours in a planetary ball mill (Fritsch Pulverisette 7) with yttria stabilized zirconia (ZrO_2) balls and isopropyl alcohol as medium. The dried powders were calcined and were subjected to particle size reduction with ZrO_2 balls and isopropyl alcohol as medium. The powder batches so obtained were compacted in high chromium high carbon hardened steel die using a uniaxial hydraulic press in presence of polyvinyl alcohol (PVA) as binder. After 24 hours of drying at 100 °C, the green pellets so obtained were characterized for its green densities by dimensional method. The density of the sintered pellets was estimated using the Archimedes' method following the ASTM standard (C 373 – 88).

The sintered pellets of both BZT were characterized for phase analysis using

1) XRD (X- ray diffraction) –
   For crystal structure determination X-ray diffraction technique (Bruker D8 Advance) using Cu-Kα (1.54058 Å) radiation has been used in the 2θ range 10°-90°.
2) Micro structural analysis of the sintered pellets was carried out using HITACHI S-3400N Scanning Electron Microscopy (SEM). The samples were polished to ensure a smooth surface finish prior to SEM characterization.
3) The microwave characteristics were measured using Agilent E8361C Network Analyzer. Dielectric properties (dielectric constant (ε_r) and unloaded quality

factor) were measured by cavity resonator technique by using Vector Network Analyzer (Agilent E8361C) in $TE_{01\delta}$ mode [2,3].

4) The temperature coefficient of resonant frequency τ_f is measured by placing the sample in invar cavity and monitoring the shift in the resonant frequency over the temperature range of 25 °C – 80 °C [4].

The flowchart (in Figure 4.1) shows the preparation, processing and characterization of BZT.

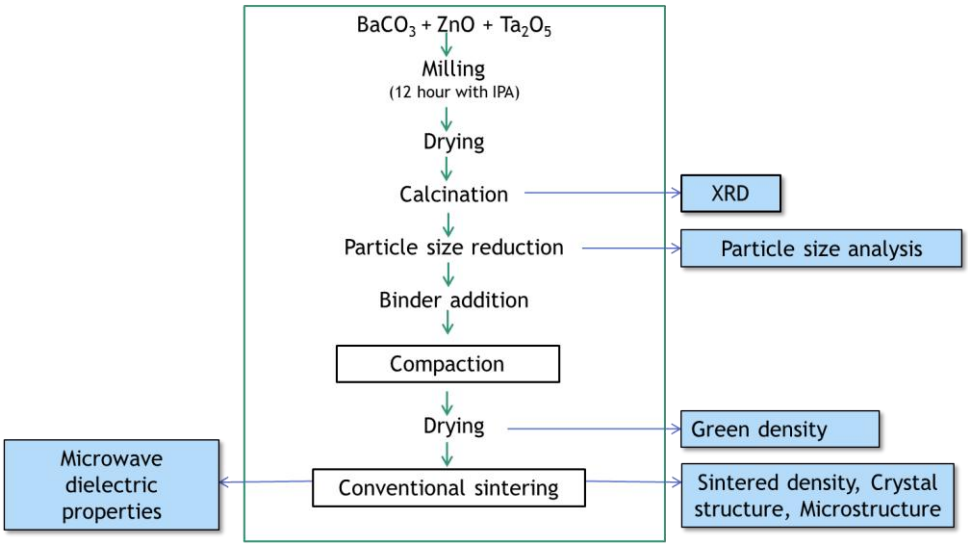

Fig 4.1 Process flowchart illustrating preparation and characterization of pure BZT

4.2 Processing study

4.2.1. Effect of starting particle size:

Microstructure of the green body after the shaping process plays a vital role in determining the rate of sintering. Particle packing, which is greatly influenced by the starting particle size and distribution, has a significant effect on the sintering kinetics [5].

The dried powder containing stoichiometric quantities of $BaCO_3$, ZnO and Ta_2O_5 were calcined at a temperature of 1250 °C for 6 hours to ensure complete phase formation. Presence of trace amount of unreacted phases will lead to zinc volatilization leading to the formation of zinc deficient phases during sintering. BZT

ceramics gets crystallized in cubic structure with apparently disordered B site ions (Zn and Ta). The x-ray diffraction pattern of the calcined BZT powder is shown in figure 4.2. A broad super structure reflection at 2θ = 17.7° is shown in the inset of Fig 4.2. This peak corresponds to (100) reflection and it indicates the presence of smaller 1:2 ordered domains. The result is in accordance with the reference [6] wherein the presence of smaller domains of trigonal perovskite phase had been reported.

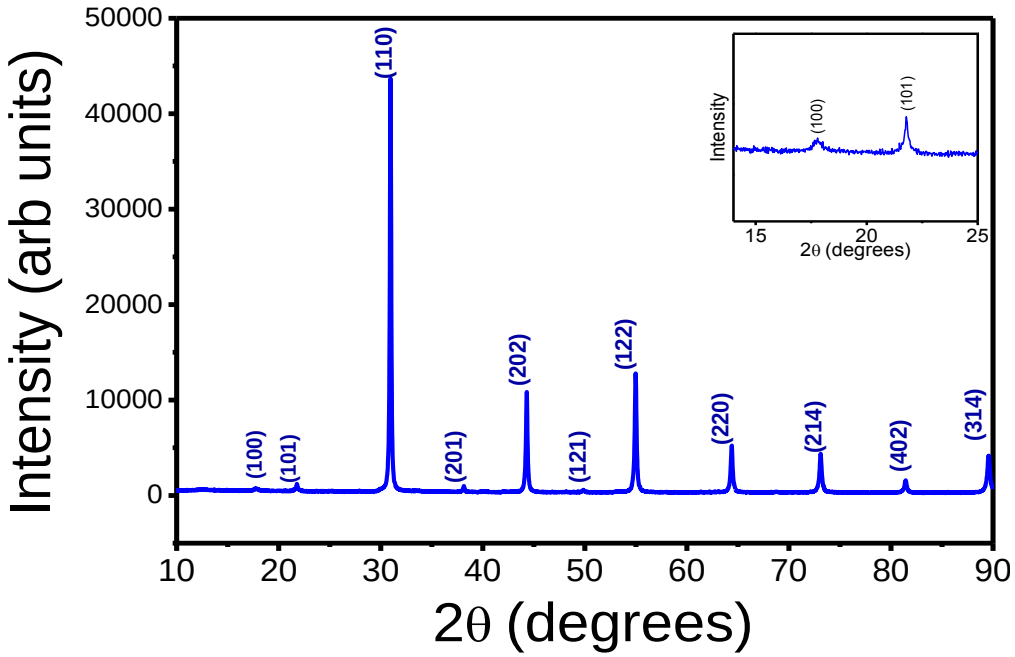

Fig 4.2 X-ray diffraction pattern of BZT after calcination at 1250 °C/6 hours

Inset: Superstructure reflection corresponding to 1:2 ordering

The calcined powder was subjected to different hours of milling to enable particle size reduction prior to compaction process. The milled powders were then sintered at 1600 °C for 2 hours. The effect of milling time on density and quality factor of BZT was shown in figure 4.3. The as calcined powder gets densified to ~ 94% TD. Calcined powders milled for 8 hours after sintering had maximum sintered density of ~ 96% TD. Further increase in milling time led to decrease in densification. The quality factor of the samples also followed the same trend as that of the sintered density.

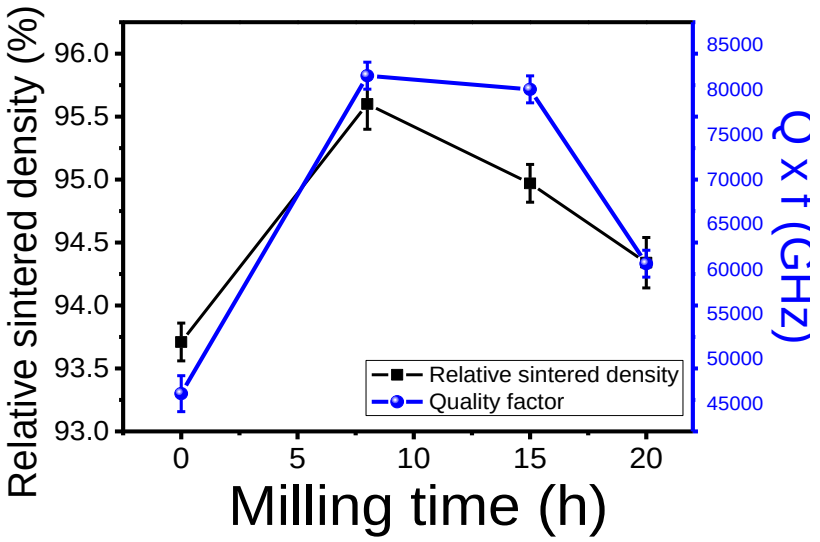

Figure 4.3 Effect of milling time on sintered density and quality factor of BZT

The as calcined powder possessed the minimum Q×f value (~ 46200 GHz) which could be attributed to low sintered density. Sample milled for 8 hours had shown the maximum quality factor of 81500 GHz. There was a marginal decrease in the Q×f values with further increase in milling time. The effect of starting particle size on the density and dielectric properties of BZT was shown in Table 4.1.

Table 4.1 Summary of effect of starting particle size on density and dielectric properties of BZT

Milling time	**Particle size (µm)**	**Relative density (%)**	**Dielectric constant**	**Q × f (GHz)**
As calcined	3.02	93.71	27.71	46200
8 h	1.01	95.6	29.37	81550
15 h	0.84	94.97	28.5	80030
20 h	0.69	94.34	28.1	60650

It can be clearly seen from the table that the mean particle size decreases with increase in milling time. The as calcined powder had the highest mean particle size of

3.02µm. Maximum density and good microwave dielectric properties were obtained for sample having a mean particle size of 1.01 µm. Dielectric constant is greatly influenced by the presence of porosity in the sample. Sample with maximum sintered density possessed high dielectric constant. Further decrease in particle size did not improve the sintering kinetics and hence led to poor densification and dielectric properties. Hence, from the density and dielectric property ($Q \times f$, ε_r) measurement values, milling time of 8 hours is considered optimum.

4.2.2 Effect of Compaction pressure:

BZT powder after calcination at a temperature of 1250 °C for 6 hours and 8 hours of milling is subjected to granulation. 10% solution is made with Poly vinyl alcohol (binder) and it is added to the calcined powder to enhance the green strength of the compact. Granulation is done prior to compaction to enable good flow ability of the powder and hence ensures better die filling. Pure BZT samples were subjected to different compaction pressures (100 to 200 MPa) to derive the optimum pressure for compaction.

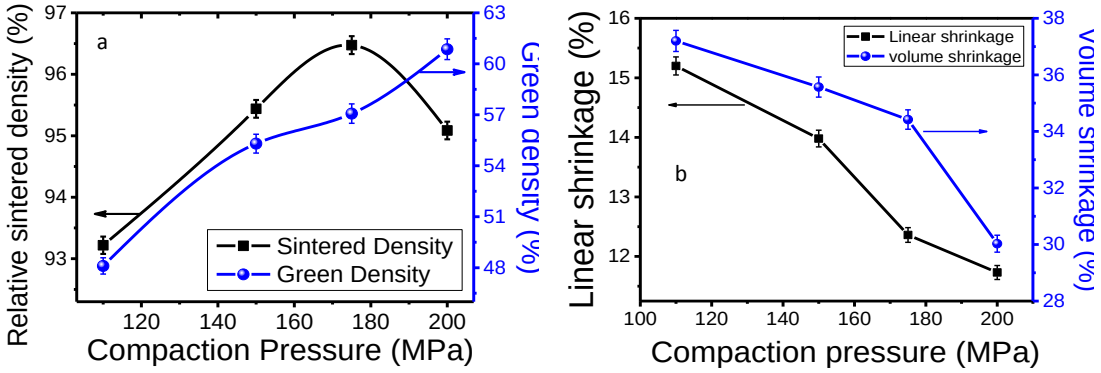

Figure 4.4 (a) Effect of compaction pressure on green density of the samples and its subsequent effect on sintered (at 1600 °C for 2 hours) density, (b)Variation of linear shrinkage and volume shrinkage as a function of compaction pressure

Fig 4.4 a shows the effect of compaction pressure on green density of the samples and its subsequent effect on sintered density when sintered at 1600 °C for 2

hours. Green density of the samples increased with increase in compaction pressure. The values are seen to vary from ~48% to ~60% of TD. A maximum sintered density of ~96.5% of TD has been observed for sample compacted at 175 MPa pressure. Further increase in compaction pressure (upto 200 MPa) has resulted in lowering the sintered density. Decrease in sintering density at higher pressure could be attributed to the presence of layering crack in the sample due to larger spring back/ strain relaxation at higher compaction pressure. Variation of linear shrinkage and volume shrinkage as a function of compaction pressure is shown in Fig 4.4 b. Linear and volumetric shrinkages tend to decrease with increasing compaction pressure due to better particle packing. Linear shrinkage of samples with minimum compaction pressure is relatively high (~15.2%) in comparison with the sample with maximum compaction pressure (~12%). Volume shrinkage of the samples tends to decrease with increase in compaction pressure and a minimum of ~30% was achieved.

4.2.3 Effect of Sintering Temperature and dwell time:

The sintering phenomena in polycrystalline materials are accompanied by several matter transport paths which occur simultaneously with increase in temperature [5]. Hence the final microstructure is greatly influenced by both the peak temperature and the dwell time at peak temperature.

BZT powder calcined at 1250 °C for 6 hours and subjected to particle size reduction for 8 hours is compacted (with optimum pressure of 175 MPa) after granulation with the addition of polyvinyl alcohol as binder. The green density of the samples was measured and it is ensured that it is more than 50% of the theoretical density to ensure good sinterability. The samples were subjected to different sintering temperatures- 1400 °C, 1500 °C, 1550 °C and 1600 °C. The dwell time was about 2 - 4 hours.

Effect of sintering temperature and dwell time on densification of pure BZT is shown in Fig 4.5a. It can be seen that the sintered density increases with increase in sintering temperature and dwell time at peak temperature. At lower sintering temperature of 1400 °C, the samples were densified only to 88%TD.

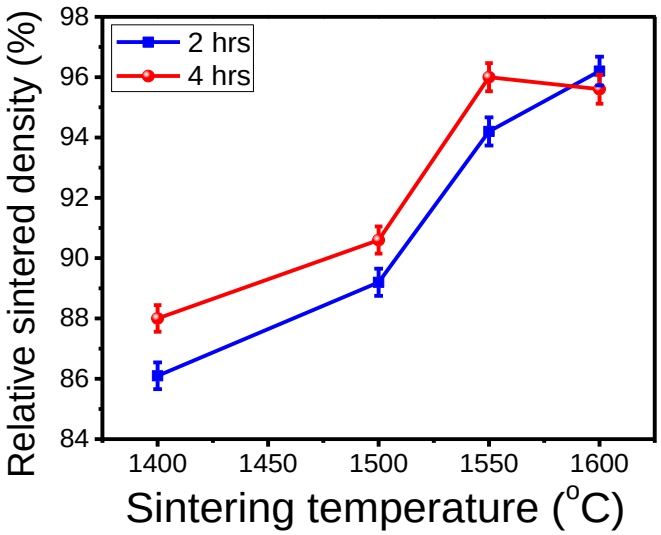

Fig 4.5a Effect of sintering temperature and dwell time on densification of pure BZT

Increasing the dwell time from 2 hours to 4 hours did not improve the densification predominantly. At 1500 °C, 89%TD was obtained and increase in dwell time at 1500 °C led to marginal increase in sintered density. 95%TD was obtained when the samples were sintered at 1550 °C and increase in dwell time at this temperature improved the density to 96%TD. Maximum sintered density (96.3%TD) was obtained for sample sintered at1600 °C for 2 hours. Increase in dwell time at this temperature led to decrease in density. This could be attributed to the exaggerated grain growth or due to formation of zinc deficient secondary phases. In order to analyze the crystal structure and the formation of zinc deficient secondary phase with increase in sintering temperature, x-ray diffraction pattern of the samples were recorded.

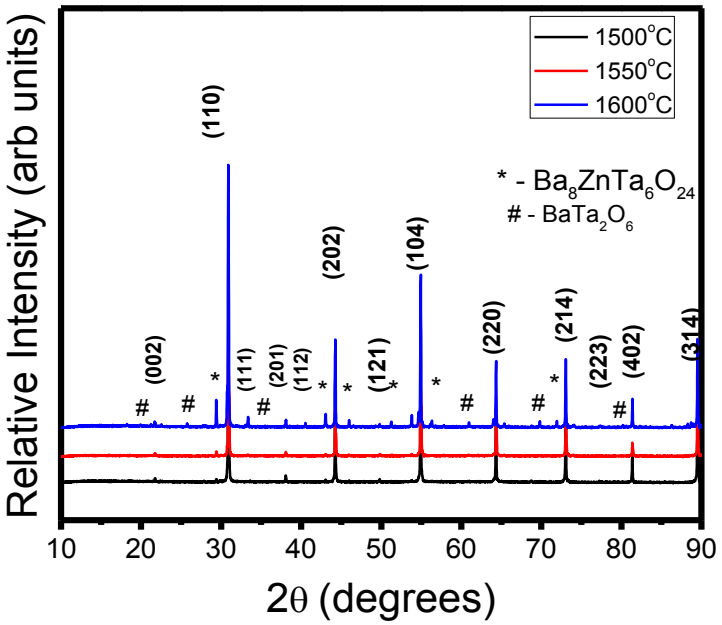

Fig 4.5b X-ray diffraction pattern of pure BZT sintered at 1500 - 1600 °C for 4 hours

Fig 4.5b shows the x-ray diffraction pattern of pure BZT sintered at different temperatures. The pattern is indexed as a hexagonal unit cell. The super-lattice reflections corresponding to ordering of B site ions were not seen in the as sintered sample. It can be seen from the diffraction pattern that the sample sintered at higher temperatures ($T \geq 1550$ °C) had $BaTa_2O_6$ and $Ba_8ZnTa_6O_{24}$ as secondary phases. The occurrence of these phases become more predominant in sample sintered at 1600 °C.

Fig 4.5c shows the elemental mapping result of sample sintered at 1600 °C. Elemental distribution of the sample sintered at 1600 °C indicates that the sample sintered at higher temperatures shows non-uniformity in the distribution of zinc.

Sample sintered at higher temperatures had a skin layer (white colour) which corresponds to the formation of zinc deficient secondary phase as seen in XRD and SEM results. Though increase in temperature led to increase in sintered density of the sample, higher sintering temperatures led to zinc volatilization which is known to be detrimental for dielectric and mechanical properties of the sample.

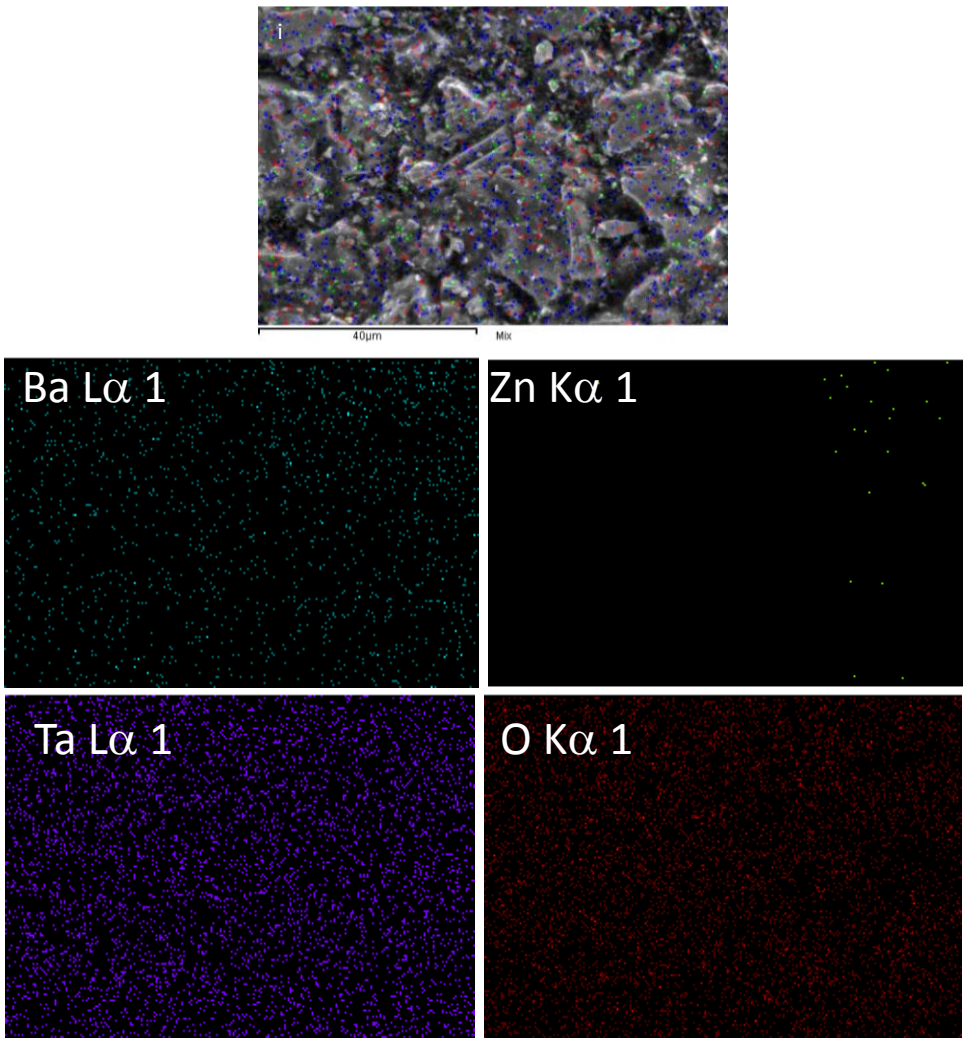

Fig 4.5c Elemental mapping of pure BZT sintered at 1600 °C for 4 hours

Heating rates have a significant role to play in densification of ceramics. Samples were sintered at 1600 °C for 2 hours with a faster heating ramp to suppress zinc volatilization. This led to decrease in densification due to improper binder burn-out. Binder is added to impart handling strength to the green sample and improper binder removal leads to residual carbon in the final sintered sample which leads to decrease in the final sintered density. The heating schedule was then modified to ensure complete and homogenous removal of binder by incorporating a soak at 500 °C and 800 °C for 1 hour and a heating rate of 3 °C /min to the peak temperature. High rate of heating leads to the formation of elastic strains which can adversely

affect the dielectric properties. The heating schedule adopted for sintering of BZT ceramics is illustrated in Fig 4.5d.

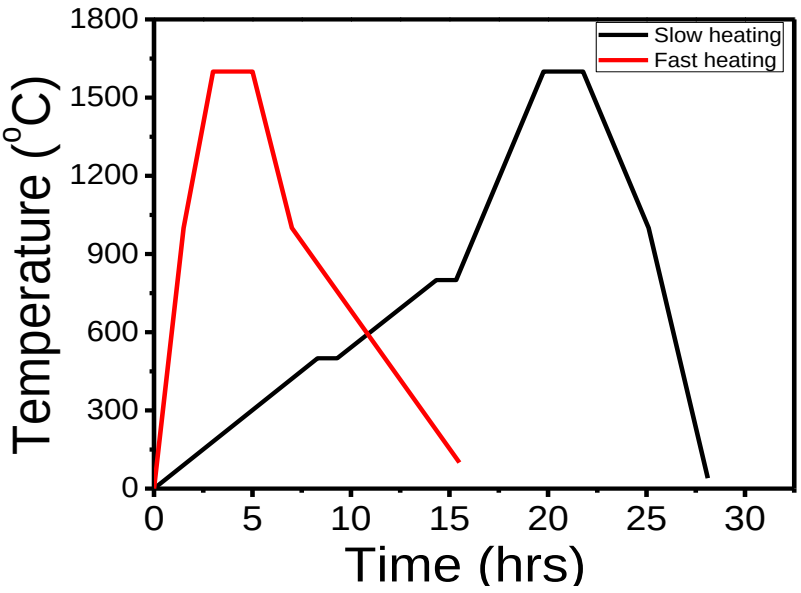

Fig 4.5d Heating schedule adopted for sintering BZT ceramics

The sintered density of the sample with fast heating rate and no soak at 500 °C led to 94% of TD. When a slow heating rate was followed - 1 °C /min upto 500 °C followed by a soak of 1 hour at 500 °C / 800 °C and 3 °C upto to the peak temperature led to a maximum density of 97% of TD.

4.2.4 Effect of flux addition:

One of the approaches to suppress zinc volatilization during sintering is to add a low melting phase to pure BZT prior to sintering to reduce the peak sintering temperature. Since highly dense BZT samples are required for RF windows, B_2O_3 is added to improve the sinterability of BZT samples. The effect of B_2O_3 addition, prior to compaction processing, on the microstructure, microwave dielectric properties and mechanical properties of BZT ceramics is investigated. It has already been reported that B_2O_3 improves the 1:2 ordering despite increasing the density of BZT ceramics at lower temperatures [7]. Also it is reported that presence of glassy phase in the ceramic aids in filling the pores present in the metalized layer by migration through capillary

action [8]. Since metallization and brazing processes were required in the fabrication of RF window sections, B_2O_3 addition was considered to aid in densification as well as for metallization/brazing. Three different weight percentages (0.1%, 0.25%, 0.5%) of B_2O_3 was chosen and added to the calcined powder and milled for 3 hours to ensure homogenous mixing. The powder so obtained was compacted and sintered at lower temperature of 1450 °C and 1500 °C.

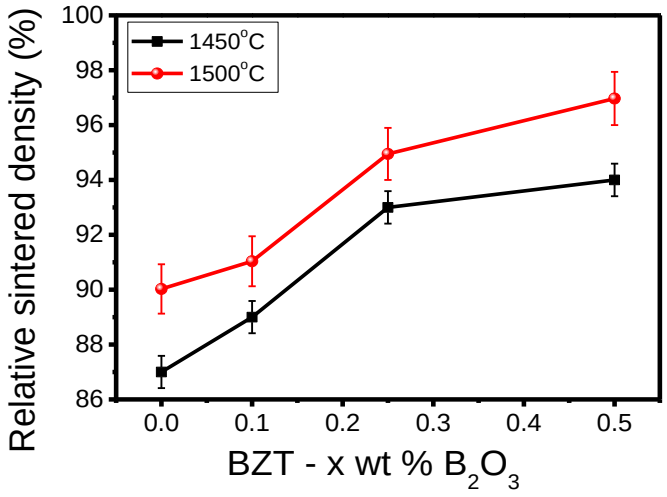

Fig 4.6a Variation of density for the samples containing B_2O_3 at two different sintering temperatures

Fig 4.6a shows the variation of density for the samples containing B_2O_3 at two different sintering temperatures. It can be clearly seen that sintered density increased with increase in concentration of B_2O_3 addition as well as sintering temperature. Sintering of BZT with 0.5% B_2O_3 at a temperature of 1450 °C led to 95% TD. Sintering with lower percentages of B_2O_3 led to poor densification at a temperature of 1450 °C. 97% of the theoretical density was achieved for the sample with 0.5% B_2O_3 sintered at 1500 °C. Pure BZT requires higher sintering temperature (>1550 °C) to achieve sintered density >95%TD. In order to analyse the changes in crystal structure and variation in ordering of the system containing B_2O_3, x-ray diffraction pattern was recorded.

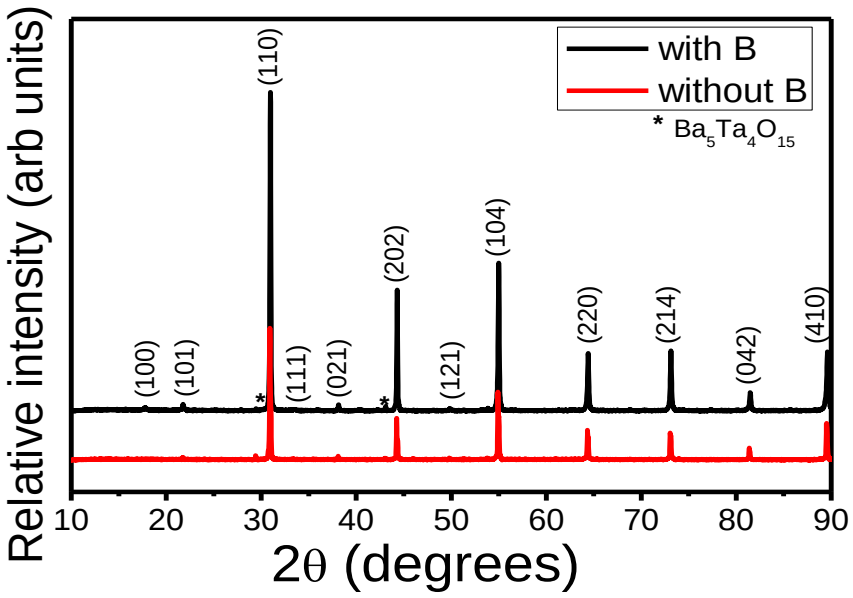

Fig 4.6b X-ray diffraction pattern of the pure BZT and sample containing 0.5% B_2O_3 sintered at 1500 °C

Sintering at higher temperatures (1500 °C) led to volatalization of zinc and hence a zinc deficient secondary phase existed in the sample surface, which is reflected in the X-ray diffraction of the samples shown in Fig 4.6b. The extent of this zinc deficient secondary phase is too high for pure BZT samples, which appeared as a different color in the periphery of the samples. The X-ray diffraction pattern of the BZT sample containing B_2O_3 shows the presenec of the (100) peak, which is a characteristic of the existence of 1:2 ordering of the B site cations in the BZT crystal lattice [9]. Percentage of B_2O_3 was not increased beyond 0.5% because higher percentages generally decrease the quality factor inspite of 1:2 ordering, which is attributed to the presence of liquid phase [7]. Also mechanical strength of the sample is greatly influenced by the glassy phase formed due to the addition of flux.

The RF window sections require a smooth surface finish for subsequent metallization. Hence surface roughness of the sintered samples is a very crucial parameter that decides the adherence of the metal layer to the ceramic. Polishing of samples containing 0.5 wt% of B_2O_3 led to irregular surface finish which is indicated in Fig 4.6(c). This may be attributed to grain pull out caused due to the presence of weaker glassy phase. Fig 4.6e illustrates the surface of pure BZT after polishing. The

surface finish of pure BZT samples were smooth showing the porosity caused due to lesser densification. Fig 4.6(d) and 4.6(f) indicates the fracture surface of sample with and without B_2O_3 respectively. The grain boundaries remain fused for samples containing B_2O_3 even after thermal etching at temperatures 150 °C less than the sintering temperature while pure BZT samples show clear and sharp grain boundaries.

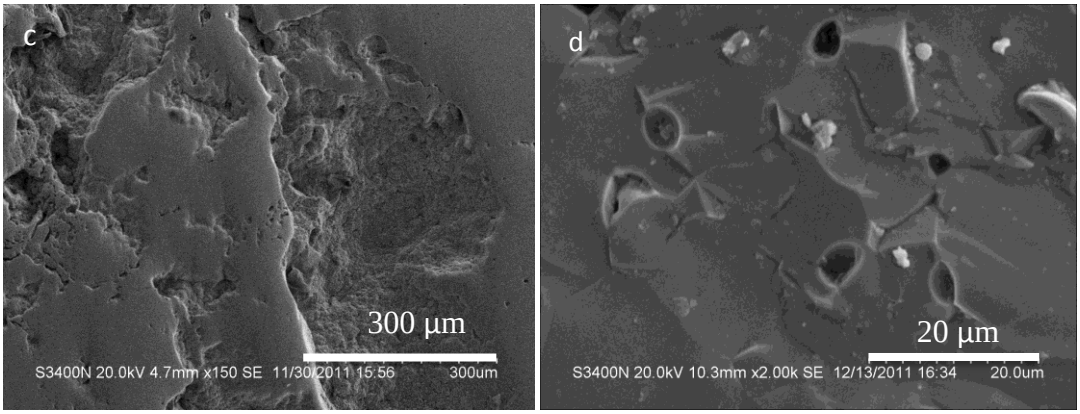

Fig 4.6c Polished sample surface of sample containing 0.5% B_2O_3 sintered at 1500 °C, 4.6d Fracture surface of 0.5% B_2O_3 sample sintered at 1500 °C

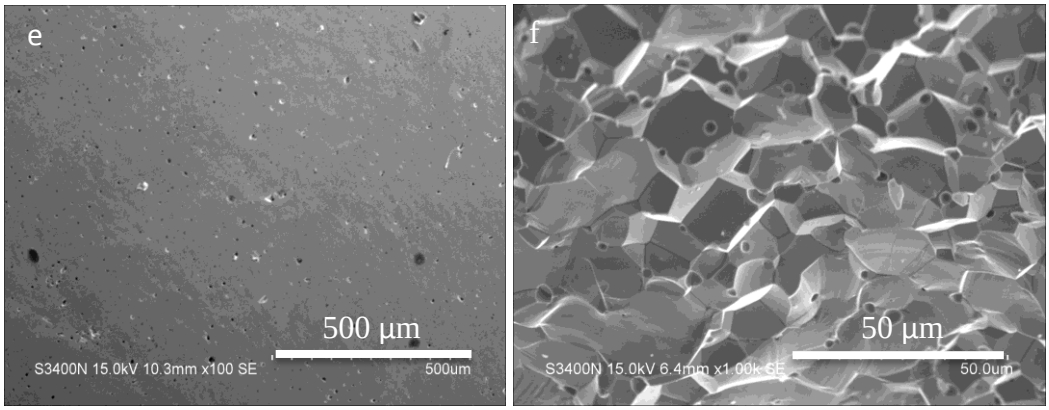

Fig 4.6e Polished sample surface of pure BZT sample sintered at 1600 °C, 4.6f Fracture surface of pure BZT sample sintered at 1600 °C ,

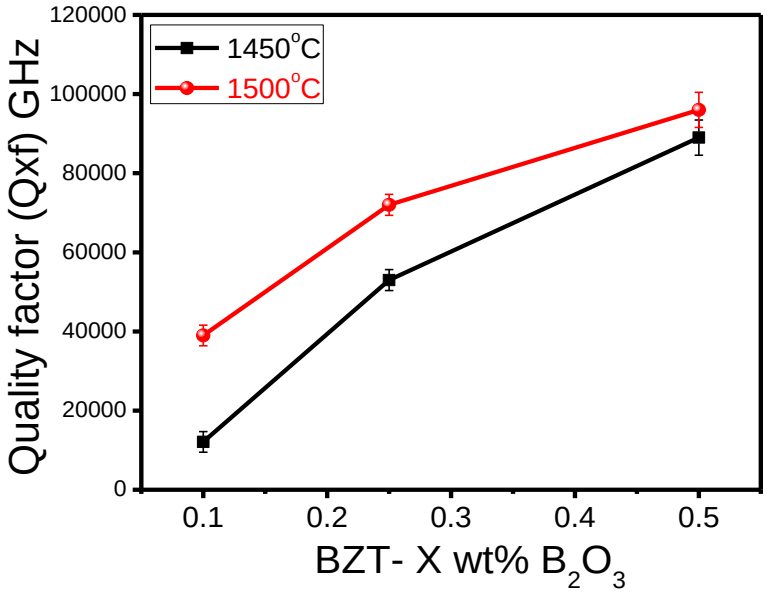

Fig 4.6g Variation of quality factor for the samples containing B_2O_3 at two different sintering temperatures

Fig 4.6g shows the variation of quality factor for the samples containing B_2O_3 at two different sintering temperatures (1450 °C and 1500 °C). Sample, containing 0.1% of B_2O_3, sintered at 1450 °C showed least quality factor, Q×f = 12100 GHz. Samples containing 0.5% B_2O_3 sintered at 1450 °C and 1500 °C showed maximum quality factor of 89000 GHz and 96000 GHz respectively. The quality factor of the pure BZT samples sintered at 1550 °C and 1600 °C were 73000 and 80000 GHz respectively. The increased quality factor of the B_2O_3 containing BZT samples could be attributed to ordering of the Zn and Ta atom in the B site of the perovskite lattice. The signature of ordering of the B site ions in the perovskite lattice is also seen in the XRD data. The temperature co-efficient of resonance frequency (τ_f) of the samples, containing B_2O_3, varied from 2 to 7 ppm/ °C. But, pure BZT samples showed a τ_f of -2 ppm/ °C.

Vickers hardness of the sample was measured using semi- automatic microhardness tester (MVH – Auto, Omnitech). Vickers hardness test revealed that the hardness of the sample containing flux (0.5 wt% B_2O_3) was lesser (0.79 GPa) than the hardness of pure BZT which is around 2 GPa.

Density as well the quality factor of the samples increases with increase in the percentage of B_2O_3 addition and the sintering temperature. Pure BZT samples exhibit a quality factor lesser than the B_2O_3 containing samples. This may be attributed to the density as well as to the presence of zinc deficient phase. In spite of higher density and good microwave dielectric properties exhibited by the B_2O_3 containing samples, these samples were unable to withstand the polishing action required to generate a smooth surface finish for subsequent metallization. Since metallization followed by brazing of the components is an essential process in the fabrication of window sections, B_2O_3 containing samples are not suitable for RF window application.

4.2.5 Effect of sintering atmosphere:

BZT ceramics are quite sensitive to the structure and property for small changes in the bulk chemistry and stoichiometry. Sintering environment has a great effect on the properties of BZT because of the presence of low volatilizing zinc in the formulation. Different sintering environments were created by muffling the green BZT pellets with different powder compositions. Heating rates and other processing parameters were kept constant to evaluate the effect of different sintering atmospheres on the final properties of BZT pellet.

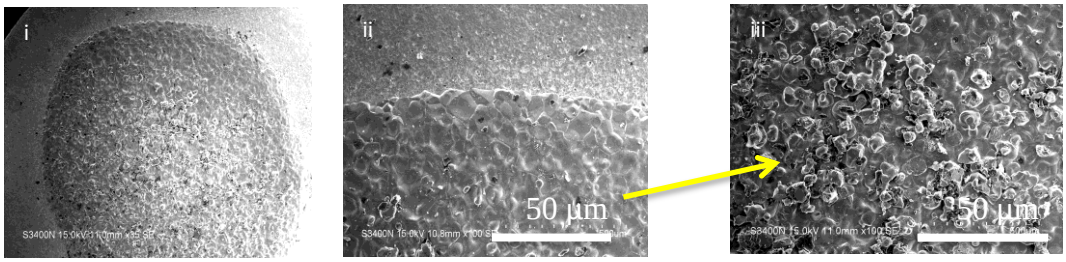

Fig 4.7a Microstructures (at different magnification) indicating the nucleation of ZnO on sample surface

In order to reduce the zinc volatilization, the pellet was sintered with ZnO powder. Such reaction bed sintering with ZnO has led to nucleation of ZnO on the surface of the sample which is indicated in the microstructures shown in Fig 4.7a. The microstructure of the ZnO is different from that of the BZT sample surface. Sintering in the presence of Zn pellets did not suppress zinc volatilization and the intensity of

the zinc deficient phase is quite high in X-ray diffraction analysis (Fig 4.7b). Density of the samples was close to 95% of the theoretical density but the dielectric properties were adversely affected due to volatilization of zinc. Q × f for samples sintered in the presence of Zn pellets exhibited a value of 70,000 GHz.

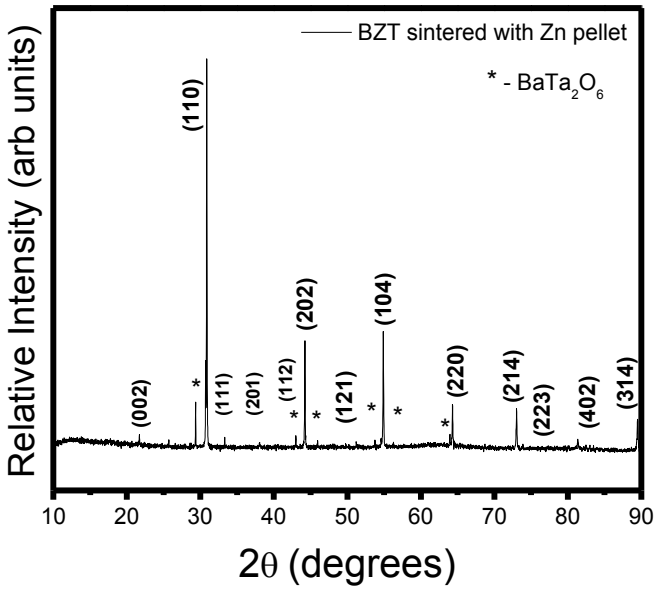

Fig 4.7b XRD pattern of sample sintered with Zn pellet

Sintering in the presence of positive oxygen partial pressure at a temperature of 1300 °C led to a porous microstructure with very poor density (~72% of theoretical density). Microstructure of sample sintered in positive oxygen partial pressure is given in Fig 4.7c.

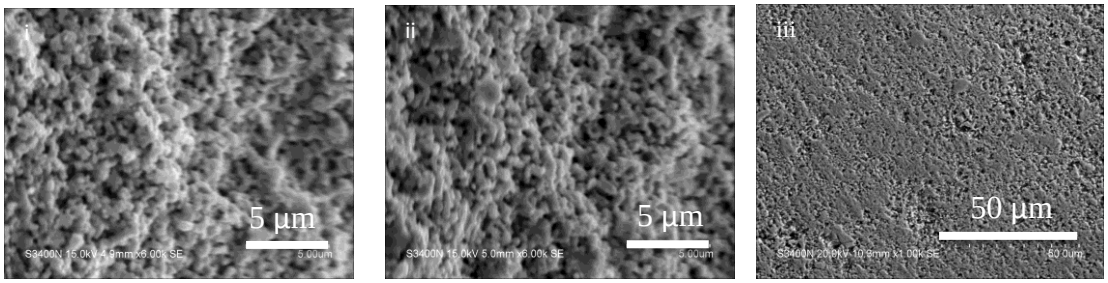

Fig 4.7c Microstructures of samples sintered in positive oxygen partial pressure

Reaction bed sintering with calcined BZT powder at 1600 °C for 2 hours resulted in uniform microstructure with good microwave dielectric properties. Volatilization of zinc is minimized and suppression in formation of zinc deficient secondary phase led to marginal improvement in densification.

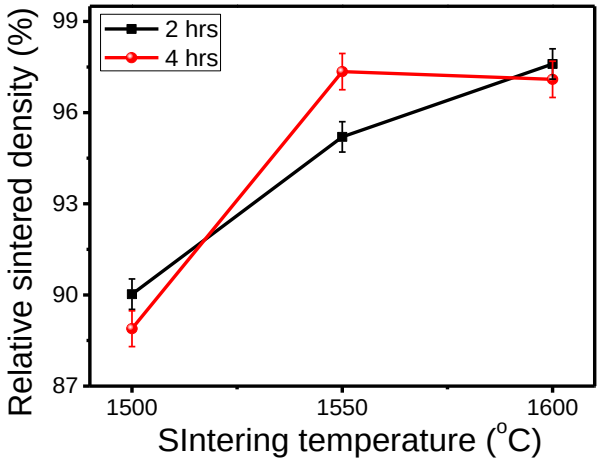

Fig 4.7d Effect of reaction bed sintering on densification of pure BZT

Fig 4.7d shows the effect of peak sintering temperature on densification of BZT by reaction bed sintering. For shorter dwell time of 2 hours, higher temperature of 1600 °C is required to achieve density close to 98%TD. Sintered density is almost close for samples sintered at 1550 °C for 4 hours and 1600 °C for 2 hours. The density and dielectric properties of sample sintered at various sintering temperatures by reaction bed sintering is shown in Table 4.2.

Table 4.2 Density and dielectric properties of sample sintered at various sintering temperatures and dwell time by reaction bed sintering

Dwell time : 2hrs				
Sintering temperature	**Density**	**%TD**	**Q x f**	**τ_f**
1500 °C	7.13	90.02	28900	-2.35
1550 °C	7.54	95.20	72300	-1.28
1600 °C	7.73	97.60	114000	-0.2

Dwell time : 4 hrs				
Sintering temperature	**Density**	**%TD**	**Q x f**	**τ_f**
1500 °C	7.04	88.88	33800	-2.54
1550 °C	7.71	97.34	99400	0
1600 °C	7.69	97.10	103090	-0.17

It can be clearly seen that increase in peak temperature and decrease in dwell time ensures better density with good microwave dielectric properties. Fracture surface and elemental mapping results of sample sintered by reaction bed sintering at 1600 °C for 2 hours is shown in Fig 4.7e.

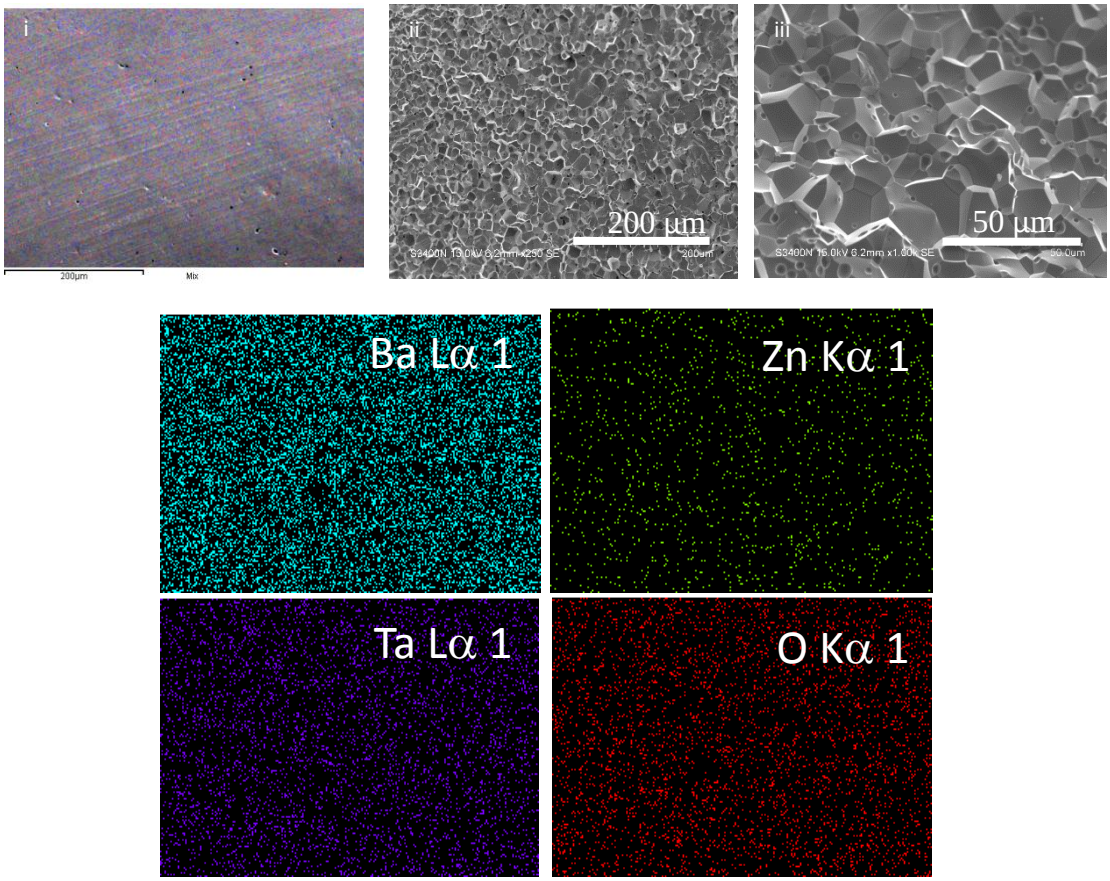

Fig 4.7e Microstructure and elemental mapping of sample sintered by reaction bed sintering

Dense and uniform microstructure with clear grain boundary is revealed in the fracture surface of sample sintered at 1600 °C for 2 hours. Elemental mapping of the

sample reveal that the distribution of zinc is more uniform leading to better densification and good microwave dielectric properties. Since samples sintered at 1550 °C for 4 hours and 1600 °C for 2 hours has the maximum density, the starting particle size of the calcined powder was varied for these two temperatures. The results for the effect of starting particle size at different sintering temperatures and dwell time are tabulated in Table 4.3. The sintering kinetics remains better for sample with starting particle size of 1 µm thus leading to higher density.

Table 4.3 Effect of starting particle size at different sintering temperatures and dwell time during reaction bed sintering

Sintering temp (°C) (Dwell time) (hours)	**Milling time (hours)**	**Density (g/cm^3)**
1550 °C (4 hrs)	8	7.71
	15	7.66
	20	7.56
1600 °C (2 hrs)	8	7.73
	15	7.68
	20	7.63

It can be seen that maximum density and superior microwave dielectric properties were achieved for the samples when processed with right combination of different processing parameters (starting particle size, compaction pressure, sintering environment, sintering temperature and dwell time at peak temperature).

4.3 References

[1] R.E.Carter, J. Chem. Phys., 34, 2010 (1961).

[2] B.W. Hakki, P.D. Colemann, IEEE Trans. Microw. Theory Tech. 18, 402–410 (1960).

[3] W.E. Courtney, IEEE Trans. Microw. Theory Tech., 18, 476 (1970).

[4] Mailadil T. Sebastin, 'Measurement of microwave dielectric properties and factors affecting them' in Dielectric materials for wireless communication, 40-42 Elsevier, London, UK (2008).

[5] M.N. Rahaman, Ceramic Processing and Sintering. Taylor & Francis, 2003. Second edition, USA.

[6] M. Bieringer, S. Moussa, L.D. Noailles, A. Burrows, C.J.Kiely et al., Chem. Mater.,15, 586–597 (2003).

[7] C.J. Lee, G.Pezzotti, Shin H. Kang, Deug J. Kim, Kug Sun Hong, J. Eur. Ceram Soc., 26, 1385-1391 (2006).

[8] S. Ghosh, A. Sengupta, K.S. Pal, N. Dandapat, R. Chakraborty, S. Datta, And D. Basu, Metall. Mater. Trans. A., 43, 3, 912-920 (2011).

[9] A. Ioachim, M.I. Toacsan, L. Nedelcu, L. Mihut, High-Q BZT Ceramics for microwave application, 6th WSEAS International Conference on Applied Electromagnetics, Wireless And Optical Communications (Electroscience '08), Trondheim, Norway, (2008).

Chapter – 5

Colloidal processing of BZT

5.1 Introduction

- Issues during scale up to large rectangular window sections

5.2 Experimental procedure for colloidal processing of BZT

5.2.1 Slurry preparation

5.2.1.1 Slip casting

5.2.1.2 Gelation using EW

5.2.1.3 Conventional gel casting

5.3 Results and discussion

5.3.1 Slip casting

5.3.2 Gelation using EW

5.3.3 Conventional gel casting

5.4 References

CHAPTER 5

COLLOIDAL PROCESSING OF BZT

5.1 Introduction

Issues during scale up to large rectangular bars:

The BZT samples prepared to optimize the process parameters are cylindrical and rectangular samples of the following dimensions

i. 8mm diameter and 4mm height
ii. 10mm diameter and 5mm height
iii. 28mm length, 14mm breadth and 4mm height

For microwave window application, large rectangular bars (76mm × 7mm × 3.3mm) with high density, uniform microstructure and good microwave dielectric properties are prerequisites. Processing of large rectangular slabs of dimensions 55mm × 10mm × 5mm by compaction with the parameters optimized for smaller samples after sintering exhibited both warpage and density gradient. Even though the use of binder to increase the compact strength, reduction of applied pressure to reduce the extent of spring back and the use of lubricant to reduce the die wall friction were enabled to reduce the defect formation, conventional compaction processing of large rectangular slabs lead to density gradients which in turn causes crack like voids in the sintered body.

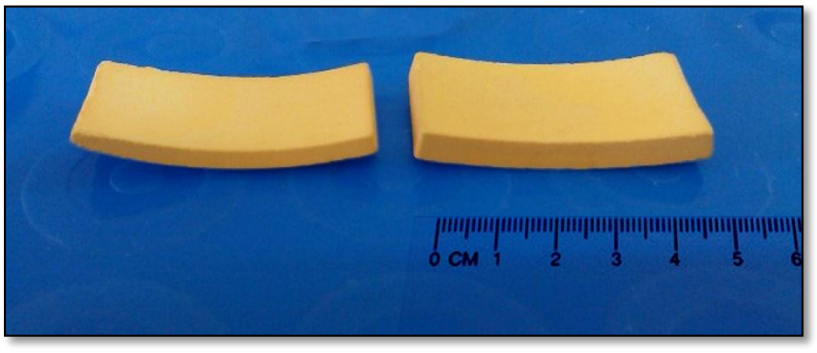

Fig 5.1a BZT sample processed by compaction route showing warpage

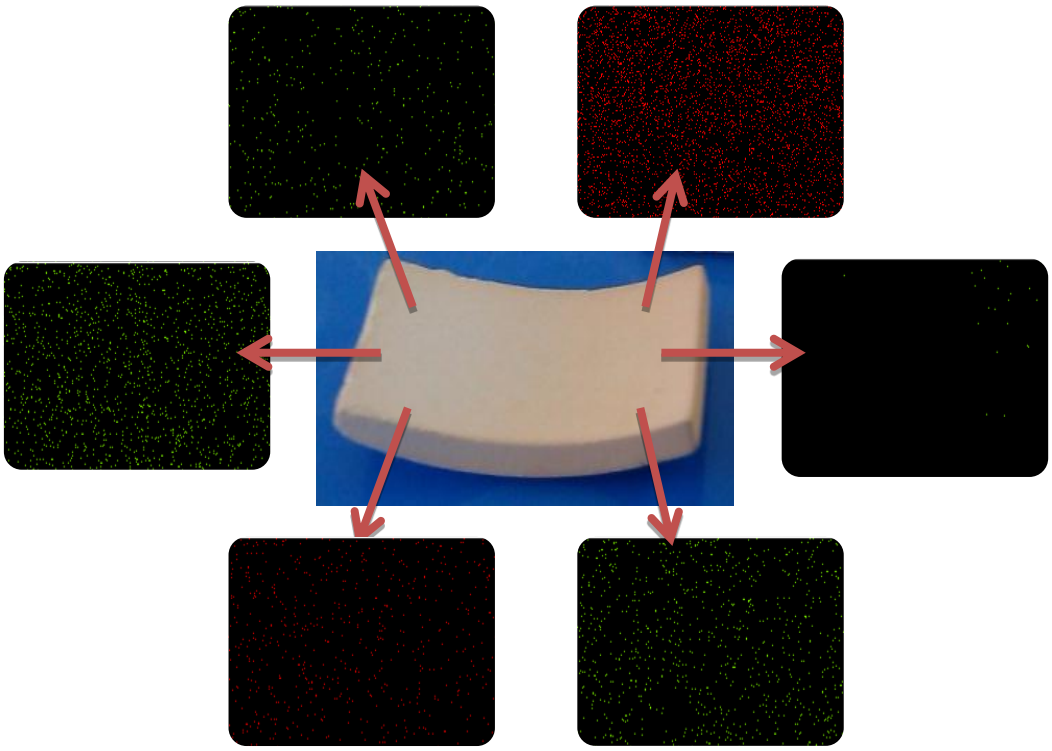

Fig 5.1b Elemental distribution of Zinc at various regions on sintered BZT sample

Stress gradients due to die-wall friction are enhanced with increasing ratio of length to diameter (L/D) of the compact. Presence of such gradients has led to cracking and warping of the samples (Fig 5.1a). The density variation in the sample is in between 96% to 98% of the theoretical density. Microstructural analysis (as shown in Fig 5.1b) of the rectangular slabs has revealed that the distribution of zinc is not uniform in the sample. Elemental distribution of Zinc at various regions on the sample is not uniform and there are regions deficient of Zinc. The change in colour after sintering is also not uniform throughout the sample. X-Ray diffraction analysis of the sintered samples at different depth of the sample from the surface has shown extra peaks corresponding to the zinc deficient phases and intensity of those peaks change with respect to the sintering environment. The intensity of these peaks varies with the zinc content in the sample and it is influenced greatly by the sintering environment. Though shaping by compaction followed by reaction bed sintering with correct combination of process parameters resulted in dense ceramics, reaction bed sintering of large rectangular bars required large quantity of BZT powder to suppress zinc volatilization. Colloidal processing of ceramics are known to produce better particle

packing than die compaction method and hence better uniformity in the green body thus leading to enhanced densification and control of microstructure during sintering [1]. BZT powders were produced by different synthesis routes [2] and the effect of different additives on sinterability and dielectric properties were studied in detail in the previous reports [3-8]. Open literatures pertaining to the effect of consolidation process on the density and dielectric properties of BZT were scarce. S. Liu et al [9] have elaborated injection moulding of BZT and its effect on densification and dielectric properties of BZT. In this chapter, densification and dielectric behavior of BZT ceramics processed by different consolidation techniques has been compared.

5.2 Experimental procedure for colloidal processing of BZT:

In this study, processing of BZT powders was carried out using colloidal routes such as, slip-casting and gel-casting and also by conventional die-pressing route. The effects of consolidation technique on densification and microstructure evolution and their subsequent influences on the microwave dielectric properties have been investigated in this work. Slip casting is a well-established shaping technique in which consolidation is effected by capillary suction of micro porous Plaster of Paris (POP) moulds [1]. Gel casting is recognized as one of the prospective near net shaping process in developing green ceramics with high mechanical strength [10]. Use of egg white as an eco-friendly binder for gel casting of ceramics has been adopted in developing low toxic green bodies [11]. In the present study, colloidal processing and its effect on densification, microstructure evolution and microwave dielectric properties of BZT have been studied for the first time.

5.2.1 Slurry preparation:

Stoichiometric quantities of raw materials were weighed and homogeneously mixed by milling with IPA as medium. The powders were then calcined and milled based on the optimized process parameters described in Chapter 4. The particle size of calcined and milled BZT powder was assessed by using DLS technique (Nanosizer, Malvern, UK) and the surface area of the milled powders were also measured (using Tristar II, Micromeritics). Fig 5.2a shows the SEM microstructure of the calcined and

milled BZT particles. The particle size distribution of BZT powders is shown as an inset in the figure. An average particles size of ~1µm was measured for BZT from the SEM microstructure. Fig 5.2 b also shows the particle size distribution of milled BZT powder measured using the DLS method. BZT calcined and milled powder also had a mean particle size of ~1 µm (as assessed by DLS technique using Nanosizer, Malvern, UK) and a surface area of 1 m^2/g (Tristar II, Micromeritics).

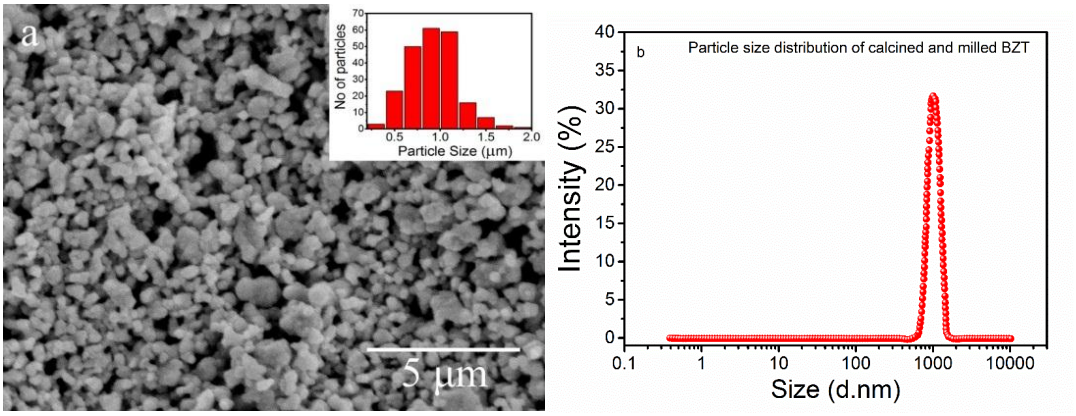

Fig 5.2 (a) SEM microstructure of calcined and milled BZT particles
Inset: Histogram showing the distribution of particles sizes of calcined and milled BZT powders, (b) Particle size distribution of calcined and milled BZT particles measured using DLS method

5.2.1.1. Slip casting:

Calcined BZT powder after particle size reduction was dispersed in an aqueous medium to form slurries having solid loading in the range of 50 to 80 wt.% using Darvan 821A (R. T. Vanderbilt Co., Inc., Norwalk, CT, USA) as a dispersant and polyvinyl alcohol (PVA) as a binder. In order to determine the optimum amount of dispersant, amount of darvan was varied from 0.1 wt.% to 3.5 wt.% of BZT powder in premix containing BZT and water with a solid loading of 60 wt%. The suspension was then milled for 12 hrs in polypropylene bottles in a roller mill using YSZ grinding balls of 3mm diameter at 1:1 powder to balls ratio. The rheological properties of suspensions were determined using Anton Paar Rheometer (MCR 102) with parallel plate geometry. The sample temperature was controlled within ±0.1°C using water as a heat transfer fluid. Iso-electric point (IEP) and stability of 0.1 wt% of

BZT suspension with and without darvan were characterized by zeta potential measurements. Zeta potential of dilute BZT slurries was measured using electrophoretic mobility. pH values were adjusted by adding HCl and NaOH solution.

Rheological behavior of the slurries with different solid loading was measured at constant and varying shear rates to determine the flow properties. Grinding media was removed from the suspension by filtering through sieve and octanol was added as an anti-foaming agent prior to casting. The suspensions were cast in Plaster of Paris (POP) moulds to obtain solid discs (25 mm in diameter and 10 mm in height, 10 mm in diameter and 5 mm in height). The green densities of the green cast samples were measured after 24 hours of drying at 100°C and the values have been reported as percentage of theoretical density of BZT.

5.2.1.2 Gelation using egg white (EW):

Egg white was added to water in different ratios and was stirred using magnetic stirrer for 2 hours. Octanol was added as an anti-foaming agent. The froth was removed after stirring and this premix was used to prepare BZT slurry. The gelation behavior of the slurry was studied by measuring complex viscosity of suspensions with increase in temperature. BZT powder was added in batches to the premix and optimized amount of darvan was added as dispersant to attain maximum solid loading. The suspension was then milled for 12 hrs in polypropylene bottles on a roller mill using YSZ grinding balls of 3 mm diameter at 1:1 charge to balls ratio. The slip so obtained was subsequently casted in a preheated mold (80°C) coated with petroleum jelly. The samples were then slowly demoulded and dried at room temperature for about 24 hours. Then the samples were dried in a humidity chamber at 60°C with relative humidity (RH) of 95%. RH was decreased slowly to 45% in a period of 12 hours. The samples so obtained were subjected to sintering with a very slow heating rate upto a temperature of 800°C to completely remove the binder and other additives added during casting.

5.2.1.3 Conventional gel casting:

2.5 wt.%, 5 wt.% and 10wt.% aqueous solutions of monomer (MAM) and cross-linker (MBAM) in 6:1 ratio were used as premix for slurry preparation. During slurry preparation, BZT powder was added in steps to attain the desirable solid loading of 88 wt%. Polyacrylic acid ammonium salt (Darvan 821 A) was added as dispersant in quantity of 1.5 wt.% of powder to the premix. The slurries were prepared in polypropylene bottles using zirconia milling media of ~ 3 mm diameter with 1:1 weight ratio of powder to milling media. All slurries were milled/ mixed for a period of 24 hours. The amount of initiator taken for a particular volume of slurry determines the time taken for gelation. Hence, for 5% and 10% monomer and cross-linker (M&C) solutions, three different initiator concentrations were chosen and their rheological behaviors were subsequently studied. The gelation behavior of the slurry was studied by measuring storage modulus (G′) in the oscillatory mode at a frequency of 1 Hz and at a constant strain of 0.5%. After the addition of initiator and catalyst, the slip is subsequently casted in a preheated mold coated with petroleum jelly. The samples were then slowly demoulded and dried under controlled humidity conditions (50°C with RH of 95% for 12 hours). RH was decreased slowly to 45% in a period of 12 hours and temperature was increased to 60°C step wise.

5.3 Results on colloidal processing of BZT

Figure 5.3 shows the X-ray diffraction of BZT powders calcined at 1250°C. The diffraction peaks of the phase pure BZT powders have been indexed to hexagonal crystal system with $P\bar{3}m1$ space group using JCPDS card no 18-0201. XRD of sintered samples processed by different colloidal processing technique did not show any extra peak after sintering except for the presence of zinc deficient secondary phase ($Ba_8ZnTa_6O_{24}$) indicating that no extra phases or additional impurities were formed during slurry preparation and further processing. BZT samples processed by colloidal processing were sintered at temperatures more than 1450°C. Literatures have reported zinc volatilization at temperatures more than 1400°C [12,13] and hence

the presence of secondary phase could be attributed to zinc deficient $Ba_8ZnTa_6O_{24}$ phase formed during sintering.

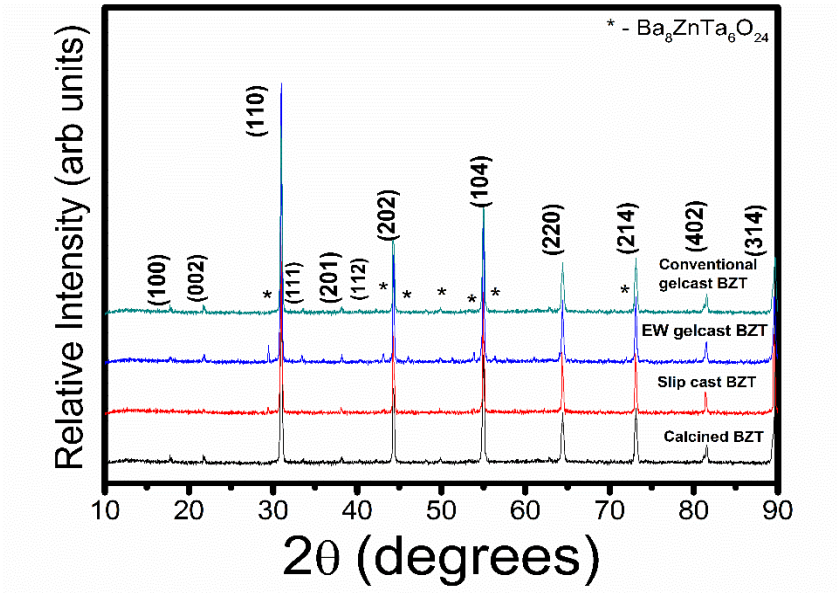

Fig 5.3 X-ray diffraction spectra of (a) BZT after calcination (b) slip cast BZT (c) BZT gel cast using EW and (d) Conventional gel cast BZT

5.3.1 Slip casting:

Stable colloidal suspension can be achieved by dispersing the powder in aqueous medium having a pH away from the Isoelectric point (IEP) [14]. The variation of zeta potential of BZT suspensions with and without darvan as a function of pH is shown in Fig 5.4. It is clear that the zeta potential of suspension in the absence of darvan did not exceed 48 mV in the pH range of 9 – 10, whereas, the zeta potential of BZT in the presence of darvan retained a high negative value of nearly 62 mV over a pH range of 9-10. It was also observed that the IEP of BZT suspension was close to a pH of 2.5. Formation of strong double layer repulsion can be achieved through the generation of highly charged surface by suitably adjusting the pH away from the IEP [15]. In the case of BZT suspensions with darvan as a dispersing agent, highly negative potential was achieved in the alkaline medium range. The extent of dissociation of monomer units in the dispersant increases in alkaline regime and thus

enhances the adsorption of polymer chains on to ceramic particles surfaces [14,15]. It is therefore preferred to prepare the dispersions at higher pH levels to obtain a stable aqueous colloidal suspension.

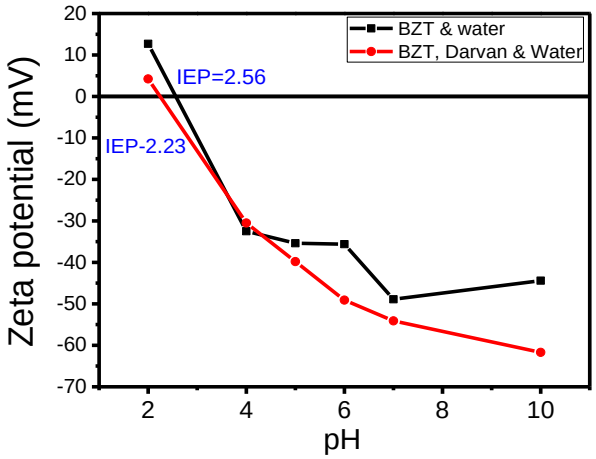

Fig 5.4 Variation of zeta potential of BZT suspensions as a function of pH

The effect of dispersant concentration on the viscosity of suspensions with 60 wt.% solid loading is shown in Fig 5.5, which presents plot of viscosity at different concentrations of the dispersant at a constant shear rate. Rheological behavior was characterized under constant shear rate (250/s) in controlled shear mode using rheometer with a parallel plate arrangement (25 mm). Viscosity of the suspension initially decreases with increase in darvan concentration and remains almost unchanged for a particular concentration regime. The decrease in viscosity with increase in darvan concentration upto 1.5 wt.% could be attributed to the increase in the electrostatic repulsive forces caused due to the surface coverage of BZT particles by the darvan molecules. The electrostatic repulsive forces attain a level that is strong enough to overcome the Vander Waal attraction force, when the concentration of darvan ranges from 1.5 wt.% to 2.5 wt.%. At this concentration regime of darvan, suspension remains stabilized due to increased repulsive forces. Further addition of darvan leads to increase in viscosity values, which could be attributed to the weaker repulsive forces caused due to the compression of the electrical double layer leading to coagulation of the BZT particles [15].

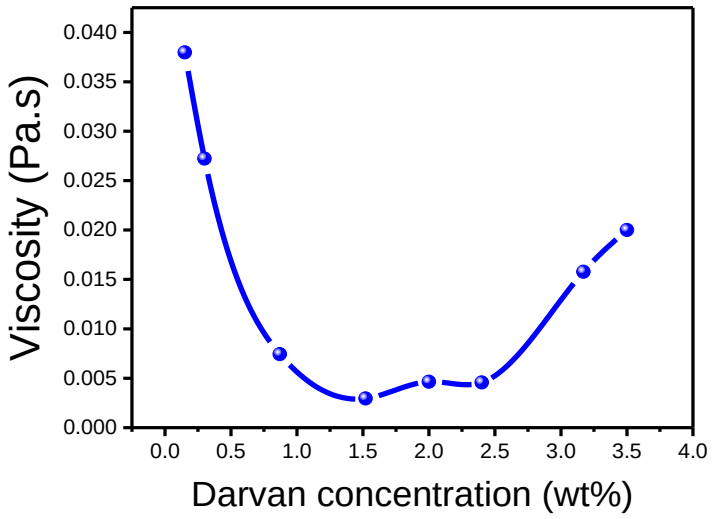

Fig 5.5 Effect of dispersant concentration on the viscosity of BZT suspensions

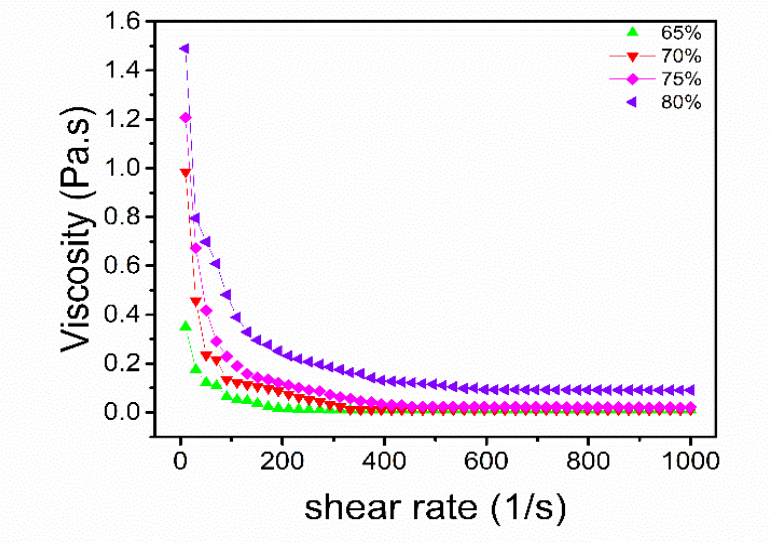

Fig 5.6 Variation of viscosity of BZT suspensions as a function of shear rate for different solid loading

Fig 5.6 represents the viscosity of suspensions as a function of shear rate for various solid loading. A steady increase in viscosity can be observed with increase in solid loading. Decrease in viscosity has been observed with increasing shear rate. The suspensions exhibit shear-thinning behavior upto a shear rate of 250/s beyond which

they exhibit Newtonian behavior. Higher values of viscosity at lower shear rates could be attributed to the dominance of inter-particle forces at lower shear rate.

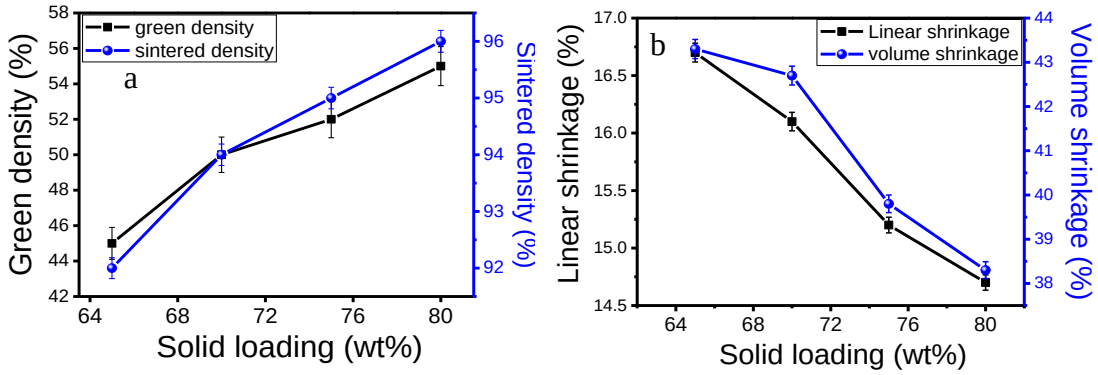

Fig 5.7 (a) Variation in green and sintered densities as a function of solid loading of the suspensions, (b) Variation of linear and volume shrinkages as a function of solid loading of the suspensions

Green densities of samples tend to increase with increasing solid loading and a minimum solid loading of 70wt% is required to achieve a relative green density of 50%. The samples were sintered at 1550°C/4h and the sintered samples were characterized for its shrinkage (linear and volume) and density. Fig 5.7a shows the variation in green and sintered densities with increase in solid loading of the suspensions. Sintered density also increases with increasing solid loading and a maximum relative sintered density of 96% has been achieved by slip casting. Shrinkage behavior of the sintered samples with increasing solid loading of the suspensions has been shown in Fig 5.7b. Linear and volumetric shrinkages tend to decrease with increasing solid loading due to better particle packing at higher solid loading. Linear shrinkage of samples with lower solid loading is relatively high (~16.7%) in comparison with the sample with higher solid loading (~14.5%). Volume shrinkage of the samples tends to decrease with increase in solid loading and a minimum of ~38.3% was achieved for the sample with 80% solid loading. The sample with maximum sintered density showed a quality factor (Q×f) of 63900 GHz and ε_r of 28.5.

5.3.2 Gelation using egg white

The suspensions containing different percentages of egg white in the premix solution were characterized for viscosity values with varying shear rates. Variation in viscosity with increasing shear rates of suspensions with different egg white content is shown in Fig 5.8.

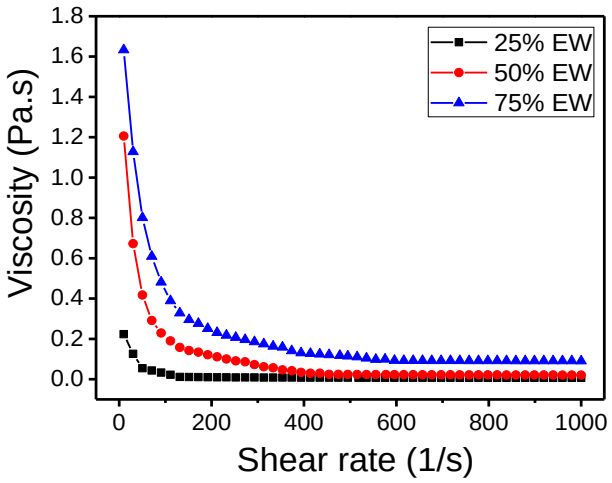

Fig 5.8 Variation of viscosity as a function of shear rate for suspensions with different egg white contents

The viscosity values tend to increase with increasing quantity of egg white in the premix solution. The suspensions show shear thinning behavior upto a shear rate of 400/s beyond which they exhibit Newtonian behavior. Gelation behavior was studied by measuring complex viscosity of suspensions with increase in temperature. Fig 5.9 shows the variation in complex viscosity with increase in temperature for the suspensions with different egg white content in the premix solution. Complex viscosity values tend to increase with increase in temperature and the gelation temperature tends to decrease with increase in the egg white content in the premix solution (Inset Fig 5.9).

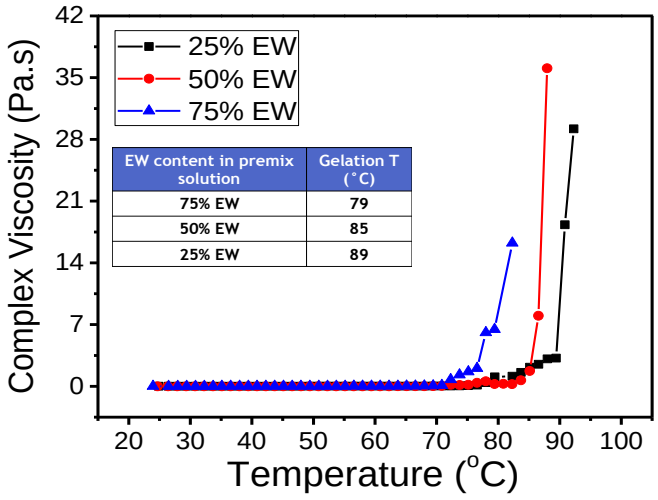

Fig 5.9 Variation of complex viscosity as a function of temperature for suspensions containing different egg white contents
Inset: Variation in gelation temperature for different egg white content in the premix

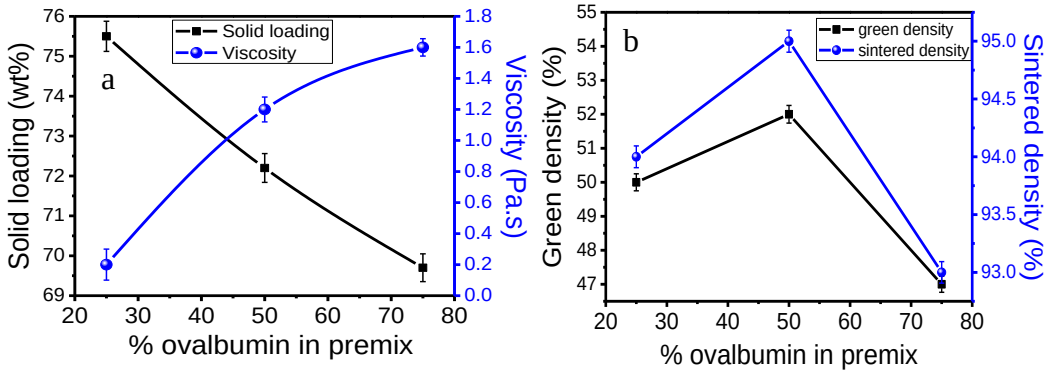

Fig 5.10 (a) Variation of solid loading and viscosity as a function of egg white content in the premix solution, (b) Variation of relative green and sintered densities as a function of egg white content in the premix

The effect of egg white content on the maximum solid loading and their corresponding viscosity is shown in Fig 5.10a. Maximum solid loading that was achieved in the suspensions decrease with increase in egg white content of premix solution. Viscosity of suspensions with maximum solid loading tends to increase with increase in the egg white content in the premix solution. The variation in relative green and sintered densities of the samples cast from suspensions with different egg white content is shown in Fig 5.10b. Relative green and sintered density values tend

to increase with increase in egg white content in premix upto 50 wt% beyond which it decreases.

Maximum solid loading achieved in premix containing 75% egg white is only 69 wt% leading to lower green and sintered densities. The decrease in green and sintered densities in samples containing 25% egg white could be attributed to poor consolidation due to small quantity of egg white in the premix. Premix containing 50% egg white with a maximum solid loading of 73 wt% tends to give maximum green and sintered densities due to good dispersion properties of the slurry. Green microstructure of samples prepared from premix containing different solid loading is shown in Fig 5.11a and it can be observed that premix with 25% and 50% egg white contents reveal uniform dispersion and relatively higher particle packing. Premix containing 75% egg white with a maximum solid loading of 69 wt% tends to get agglomerated due to non-uniform dispersion in the highly viscous premix.

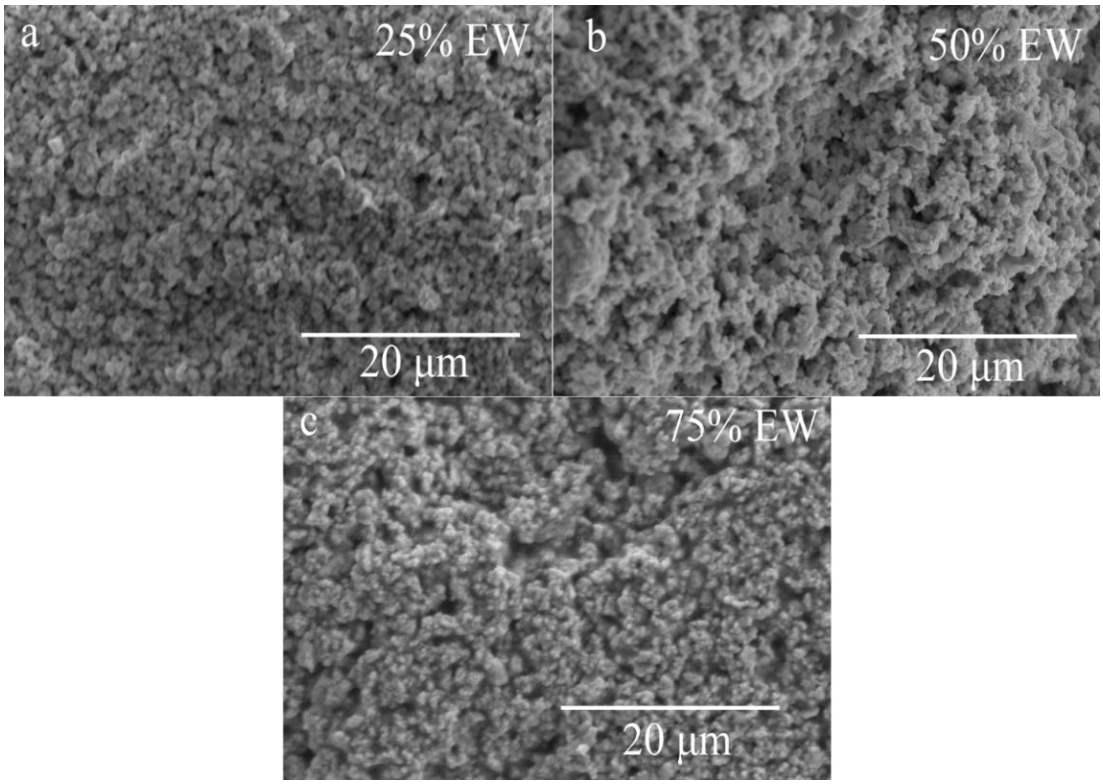

Fig 5.11a Green microstructures of samples prepared from premix containing different percentages of egg white a) 25% EW, b) 50% EW c) 75% EW

Microstructures of sintered specimens are shown in Fig 5.11b. It can be clearly seen from the microstructures that the samples contained large pores even after sintering at higher temperature (1600°C), which is in accordance with the sintered density data. The dielectric properties of sintered samples with different egg white (EW) concentrations are given in Table 5.1. The sample containing 50% EW showed maximum quality factor (59100 GHz), which could be attributed to higher sintered density. The quality factors of samples consolidated using egg white are less compared to those of slip cast samples. The possible reason could be attributed to the formation of bubbles due to foaming nature of egg white. In spite of the presence of anti-foaming agent, agglomeration of the BZT particles due to high viscosity might lead to porosity in the green samples. The trapped pores during sintering might lead to poor densification and inferior dielectric properties consequently.

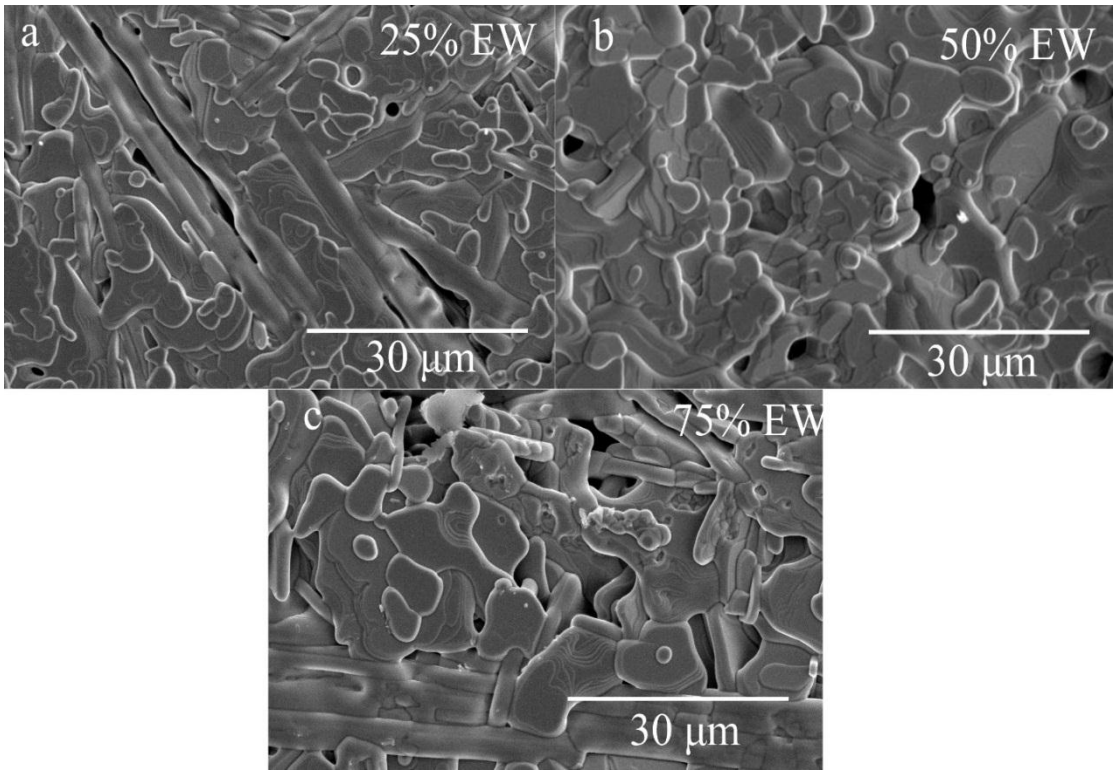

Fig 5.11b Microstructures of sintered samples prepared from premix containing different percentages of egg white a) 25% EW, b) 50% EW c) 75% EW

Table 5.1 Summary of the green density and sintered density and the dielectric properties of sintered samples with different egg white (EW) concentrations

DESCRIPTION	RELATIVE GREEN DENSITY (%)	RELATIVE SINTERED DENSITY (%)	Q × f (GHz)	ε_r
25% ovalbumin	50	94	58300	28.1
50% ovalbumin	52	95	59100	28.3
75% ovalbumin	47	93	47200	27.9

5.3.3 Conventional gel casting:

The chemical interaction of ceramic particles in suspension was studied by monitoring the viscosity and storage modulus with increase in temperature. An aqueous solution containing different percentages of MAM (monomer) and MBAM (cross-linker) (2.5 wt.%, 5 wt.% and 10 wt.%) with respect to the powder in the ratio of 6:1 was taken as the premix solution for slurry preparation. In order to ensure gel formation, storage modulus of the premix solution was measured.

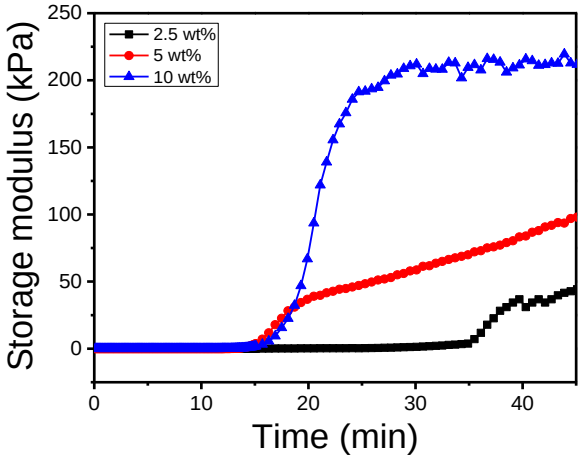

Fig 5.12 Variation of storage modulus as a function of time for different concentrations of monomer and cross-linker

Fig 5.12 shows the storage modulus of premix solution containing different percentages of monomer and cross linker (M & C). Premix containing 2.5 wt.% of monomer and cross-linker showed an increase in the storage modulus value beyond 35 min after the addition of 10 wt.% APS solution (initiator) and TEMED (catalyst) and a maximum value of 50 kPa was obtained. When the M & C percentage is increased to 5%, gelation started around 15 min and a maximum value of 100 kPa was obtained. Further increase in the concentration of monomer and cross-linker (upto 10wt.%) led to a high storage modulus value of 225 kPa. The amount of initiator taken determines the time taken for gelation and hence the initiator concentration in the premix solution (5 and 10 wt.%) is varied and rheological behavior was studied.

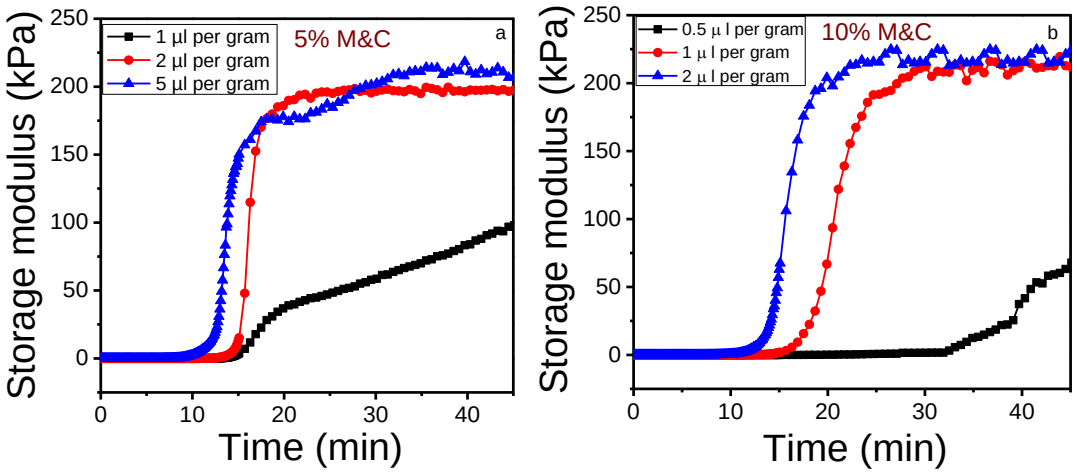

Fig 5.13 Variation of storage modulus as a function of time for different initiator concentrations (a)5% M and C , (b) 10% M and C

Fig 5.13 shows the variation of storage modulus as a function of time for different initiator concentrations. For premix solution containing 5% MAM and MBAM, higher storage modulus values were obtained for an initiator concentration of 2µl and 5 µl per gram of slurry. In case of sample with 2µl of initiator per gram of slurry, the gelation started within 15 mins of initiator addition. Further increase in the initiator concentration (5µl per gram of slurry) led to rapid gelation within 10 minutes of initiator addition. For lower concentrations of initiator, polymerization started within 20 mins and a storage modulus value of 100 kPa was obtained. Hence, from

the storage modulus values and time taken for initiation of gelation, 2 µl of initiator per gram of slurry is considered optimum for premix solution containing 5% MAM and MBAM. In case of premix with 10% MAM and MBAM, 1µl per gram of slurry was considered optimum and the polymerization reaction started within 15 mins from the time initiator was added. For concentration as low as 0.5 µl per gram of slurry, storage modulus was so low that the gel formed may not have sufficient rigidity to hold the shape of the cast. Higher concentration (2 µl per gram of slurry) of initiator led to gelation at temperatures lower than the peak temperature. In such cases, thermal stresses are prone to occur in the cast sample due to inhomogeneous temperature distribution. Hence, for samples containing 5% and 10% MAM and MBAM, 2µl per gram of slurry and 1µl per gram of slurry were considered as optimum concentration of initiator.

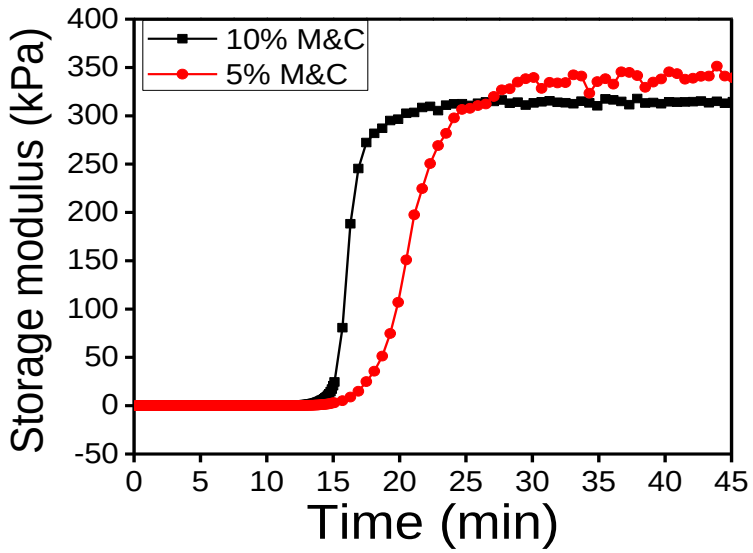

Fig 5.14 Storage modulus of BZT suspensions prepared from premix containing 5 and 10wt.% of MAM and MBAM with optimized initiator concentration

Fig 5.14 shows the storage modulus of BZT suspensions prepared from premix containing 5 and 10 wt.% of MAM and MBAM with optimized initiator concentration. Storage modulus values of BZT suspensions were higher than those of the premix solution and the onset temperature for gelation remained same for both premix and BZT suspensions. Higher storage modulus values of suspensions could be

attributed to the presence of BZT powder in the polymer matrix contributing to increased stiffness of gel. Samples with different solid loading containing optimized concentrations of monomer, cross-linker and initiator were cast and sintered at 1550°C/ 4 hours. Variation in green and sintered densities as a function of solid loading is shown in Fig 5.15a. Solid loading > 70 wt% is required to achieve green density > 50% of TD. Sintered density also increases with increase in solid loading and a maximum relative sintered density ~ 98% has been achieved for sample with 88% solid loading. Linear and volume shrinkages (as shown in Fig 5.15b) tend to decrease with increase in solid loading, which is due to better particle packing density. Shrinkage values remain least for conventional gel cast sample in comparison with slip cast and samples cast with egg white thus enabling near net shaping of BZT.

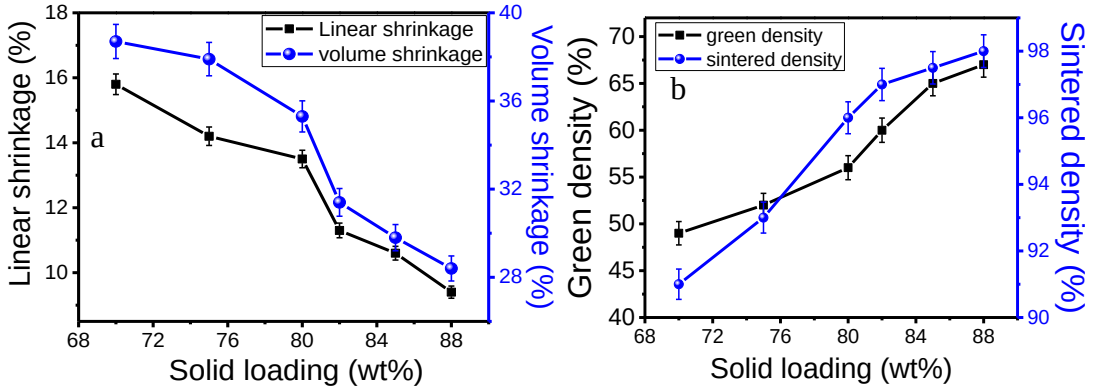

Fig 5.15 (a) Variation of green and sintered densities as a function of solid loading of the BZT suspensions, (b) Variation of linear and volume shrinkages as a function of solid loading of the BZT suspensions

Green microstructures of samples with different solid loadings are shown in Fig 5.16a. The microstructures reveal the increase in particle packing with increase in solid loading, which is in accordance with the green density values. The sample with 88% solid loading tends to show maximum particle packing and thus has a higher green density value.

Microstructures of sintered samples (as shown in Fig 5.16b) indicate the improvement in densification with increase in solid loading. Sample with 88% solid loading reveals a dense microstructure in comparison with samples cast by slip

casting and gelation using egg white. The variation in dielectric properties of samples with different solid loading is given in Table 5.2. The increase in quality factor and dielectric constant values with increase in solid loading follows the same trend as that of sintered density values. The increase in quality factor is marginal beyond 85% solid loading. Maximum quality factor of 93700GHz and dielectric constant of 29.5 have been achieved for sample with maximum solid loading containing optimum concentrations of monomer, cross linker and initiator.

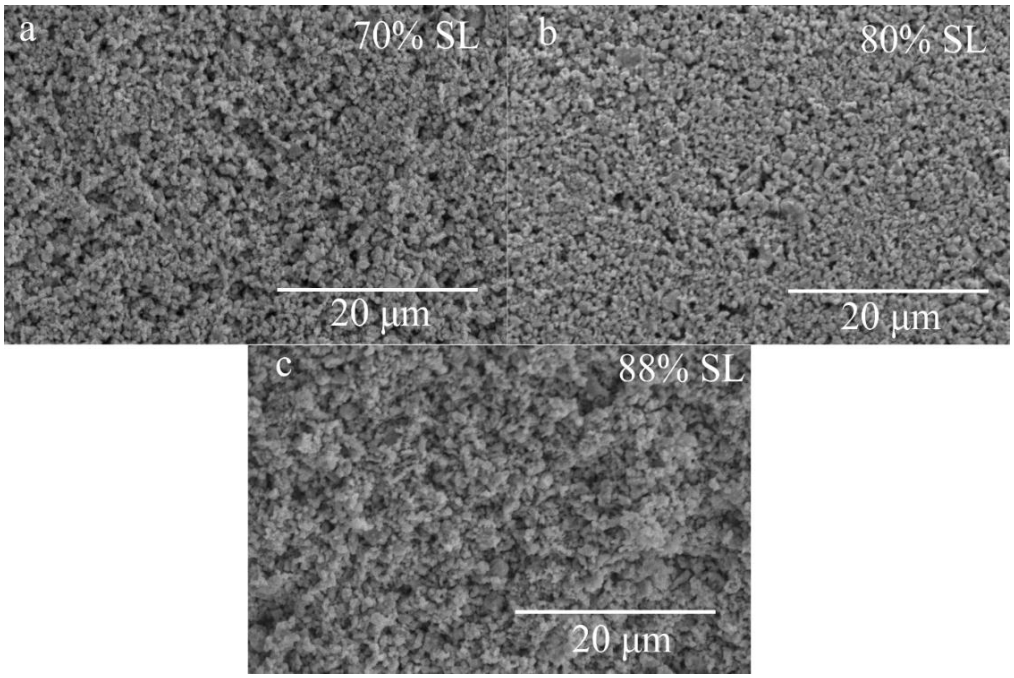

Fig 5.16a Green microstructures of samples with different solid loading containing 5% monomer and crosslinker a) 70% SL, b) 80% SL, c) 88% SL

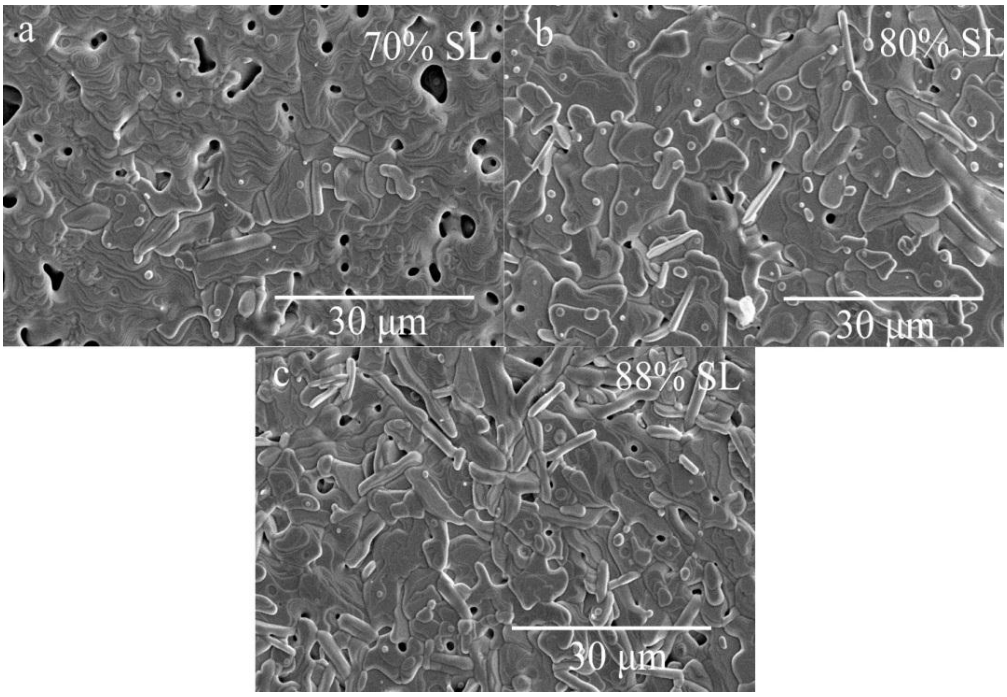

Fig 5.16b Microstructure of sintered samples with different solid loading a) 70% SL b) 80% SL c) 88% SL

Table 5.2 Summary of the dielectric properties of sintered samples with different solid loading

Solid loading	**Q × f**	**ε_r**
wt%	**(GHz)**	
70	27600	28.4
75	36400	28.9
80	67600	29.1
82	72300	29.3
85	89350	29.28
88	93700	29.54

The effect of colloidal processing on the densification behavior and microstructure development of Ba $(Zn_{1/3}Ta_{2/3})O_3$ (BZT) ceramics and their subsequent effect on the dielectric properties has been studied. Linear shrinkage and volume

shrinkage of samples remain least for conventional gel casting and maximum for slip casting. Maximum densification has been achieved for samples processed by conventional gel casting. Variation in densification with respect to different processing methods is also reflected in microstructures. Correct combination of process parameters followed by sintering led to high density and good microwave dielectric properties without annealing thus improving the chance for commercial exploitation of the material. Also, for application such as dielectric antennas, filters and resonators different geometries (spherical, conical, hemispherical, etc.,) are required which can be easily achieved through near net shaped processing techniques.

5.4 References

[1] M.N. Rahaman, Ceramic Processing and Sintering. Taylor & Francis, 2003. Second edition, USA

[2] M. R. Varma, S. Biju, M.T. Sebastian, J. Eur. Ceram. Soc. 26, 1903–1907 (2006)

[3] F. Roulland, G. Allainmat, M. Pollet, and S. Marinel, J. Eur. Ceram. Soc., 25, 12, 2763–2768 (2005).

[4] J.-I. Yang, S. Nahm, C.-H. Choi, H.-J. Lee, J.-C. Kim, and H.-M. Park, Jpn. J. Appl. Phys., 41 702 (2002).

[5] J.-I. Yang, S. Nahm, S.-J. Yoon, H.-M. Park, and H.-J. Lee, Jpn. J. Appl. Phys., 43, 1, 211–214 (2004).

[6] M.-H. Kim, S. Nahm, W.-S. Lee, M.-J. Yoo, J.-C. Park, and H.-J. Lee., Jpn. J. Appl. Phys., 43 [4R] 1438 (2004).

[7] Y.-H. Jeong, M.-H. Kim, S. Nahm, W.-S. Lee, M.-J. Yoo, N.-K. Kang, and H.-J. Lee, Jpn. J. Appl. Phys., 44, 2, 956–960 (2005).

[8] M.R. Varma and N.D. Kataria, J. Mater. Sci. Mater. Electron., 18, 4, 441–446 (2007).

[9] S. Liu, V. A. Merrick, N. Newman, J. Eur. Ceram. Soc., 26, 3273–3278 (2006).

[10] M. Kokabi, A.A. Babaluo, and A. Barati, J. Eur. Ceram. Soc., 26, 15, 3083–

3090 (2006).

[11] S. Dhara and P. Bhargava, J. Am. Ceram. Soc., 84, 12, 3048–3050 (2001).

[12] I.M. Reaney, I. Qazi, and W.E. Lee, J. Appl. Phys., 88, 11, 6708 (2000).

[13] M. Bieringer and S. Moussa, Chem Mater, 5, 586–597 (2003).

[14] F. Boschini, A. Rulmont, R. Cloots, and R. Moreno, J. Eur. Ceram. Soc., 25, 13, 3195–3201 (2005).

[15] E. Ewais, A.A. Zaman, and W. Sigmund, J. Eur. Ceram. Soc., 22, 16, 2805–2812 (2002).

Chapter – 6

Microwave sintering of BZT

CHAPTER 6

MICROWAVE SINTERING OF BZT

6.1 Introduction:

A wide variety of dopants and additives were tried to stabilize the perovskite phase enabling sintering at lower temperatures. The effect of various additives on density, microstructure and microwave dielectric properties by conventional sintering was discussed in detail in the prior arts. But, any subtle changes in the intrinsic crystal structure and the presence of secondary phases in the sample, with same nominal composition, adversely affect the dielectric properties. Use of microwave power for sintering of ceramics leads to faster heating rates, low processing times and enhanced densification rates leading to uniform microstructure compared to those obtained in conventional sintering [1]. Hence, in order to address the issues faced during scale up to large rectangular window sections, microwave sintering of BZT was studied. Literatures relating the effect of microwave sintering on the density and dielectric properties of BZT were scarce.

It is generally seen that electrically insulating ceramics are poor absorbers of microwaves at room temperature. Dielectric losses of such ceramics increase with increasing temperature and starts coupling with microwaves beyond a certain critical temperature T_c. Hence, insulating ceramics are sintered by hybrid heating, where susceptors are used to increase the temperature of the material upto the critical temperature T_c. [2]. If the critical temperature of the ceramic is too high, then the other approach to conduct microwave sintering is to use a second phase that couples effectively with microwaves [3].

In this chapter, different additives which is known to couple effectively with microwaves, is added to BZT. The variation of density and microstructure with increase in sintering temperature is studied and compared with those obtained by conventional sintering. The effect of these additives on B-site ordering and quality factor of BZT samples are also studied and discussed in this chapter.

6.2 Experimental Procedure:

$Ba(Zn_{1/3}Ta_{2/3})O_3$ powder was calcined and milled by conventional solid-state reaction using the optimized processing parameters described in chapter 4. The powder after particle size reduction was mixed with different mol. % (0.5, 1 and 2) of Cr_2O_3 / Fe_2O_3 / ZrO_2. The additive oxides (Cr_2O_3 / Fe_2O_3 / ZrO_2) were intimately mixed with calcined BZT powder. The powder batches so obtained were compacted uniaxially under optimized compaction pressure in presence of polyvinyl alcohol (10% PVA solution) as binder. Pellets so obtained were characterized for green densities by dimensional method after 24 hours of drying at 100 °C. The samples were subsequently subjected to binder burnout at 500 °C for 2 hours at a slow heating rate of 1 °C/min. The samples were then subjected to conventional sintering in a high temperature programmable furnace. Microwave sintering was carried out in Microwave lab furnace MKH-4,8 Linn High therm, where heating is effected by six air - cooled microwave generators (continuous wave magnetron). The maximum microwave capacity is 6 x 800 W in frequency range between 2400 to 2500 MHz.

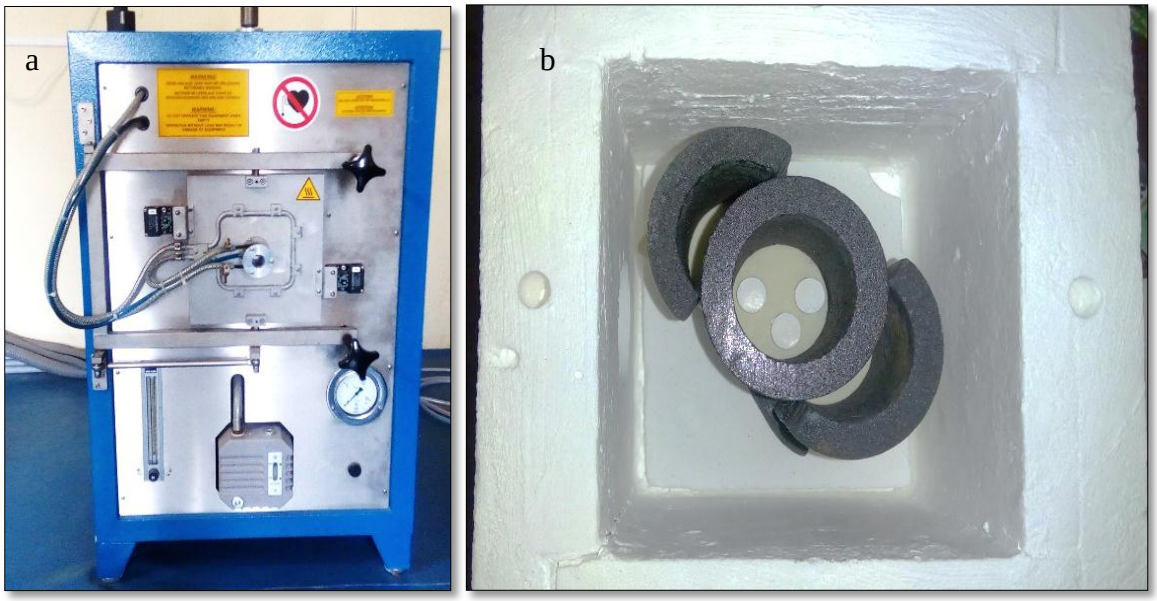

Fig. 6.1 (a) Microwave furnace MKH-4,8 Linn High Therm (b) The retort with the BZT sample (cylindrical) surrounded sintered by SiC susceptors (dark colour)

Figure 6.1 a shows the Microwave sintering furnace used in this sintering study of BZT ceramics. Figure 6.1 b shows the arrangement used for microwave sintering with hollow SiC rods were used as susceptors. Temperature measurement was carried out by a pyrometer which can read temperatures above 650 °C. The sintered samples were characterized for sintered density, crystal structure, B site ordering and microstructure. Raman spectrum of the samples were recorded at room temperature using Laser Micro Raman spectrometer (Bruker, Senterra) with an excitation source of 532nm, using a laser power of 10mW with a resolution approximately 0.5 cm^{-1}.

6.3 Results and discussion:

6.3.1 Densification:

Uniaxially compacted pure BZT samples (with green density ~ 55% of TD) after calcination did not respond to microwaves effectively at lower sintering temperatures and hence the densification was poor. At 1300 °C, there was no evident densification and a relative density close 58% was obtained. On further increase in temperature to 1400 °C, density increased to 67%. When temperature was further increased to 1450 °C, densification gradually increased to 74%. A maximum density ~84% of TD was obtained for pure BZT even at a temperature of 1500 °C.

In order to accelerate the sintering kinetics, the constituent oxides of BZT ($BaCO_3$, ZnO and Ta_2O_5) were mixed in stoichiometric proportions and compacted using uniaxial hydraulic press. The samples were pre-sintered in conventional furnace at 1300 °C for a shorter duration of 30 minutes. The pellets were crushed, grounded and mixed with calcined BZT powder in different proportions. Microwave sintering of pellets heat treated in conventional furnace led to a maximum density of 65% of TD even at a high temperature of 1500 °C. The rate of densification did not improve when 25% of pre-sintered powder was added to calcined BZT. On further increase in the proportion of pre-sintered powder to 50%, rate of densification of BZT decreased and only a relative density close to 77% were obtained.

In the present study few oxides (Cr_2O_3 / Fe_2O_3 / ZrO_2 / MgO) and non-oxide (Si_3N_4 and SiC), which are known to couple effectively with microwaves, were added as secondary phases to BZT. The effect of these additives on densification and crystal structure were primarily studied to select the optimum additive for BZT.

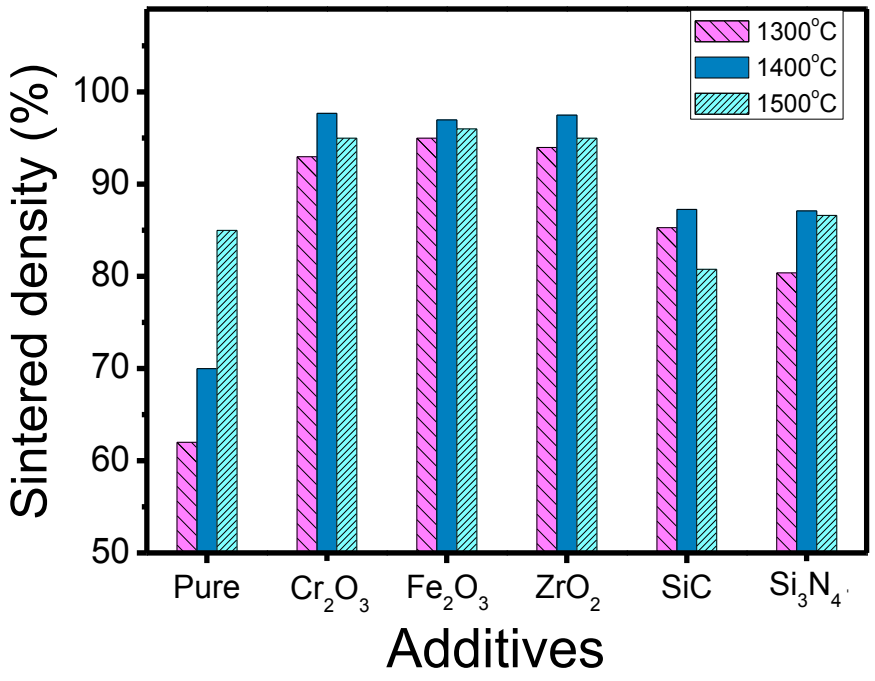

Fig 6.2 Densification behavior of BZT containing different additives for various microwave sintering temperatures.

Figure 6.2 shows the densification behavior of BZT containing different additives for various sintering temperature. It can be clearly seen from the graph that the oxide additives couple with microwaves effectively, thereby improving the density of pure BZT. BZT with Cr_2O_3, Fe_2O_3 and ZrO_2 showed better densification even at lower temperature of 1400 °C. In case of BZT containing MgO as additive, densification starts to improve only at higher temperature of 1500 °C. When non-oxide ceramics were added to BZT, densification was relatively improved in comparison with pure BZT but not as effective BZT containing oxides as additives.

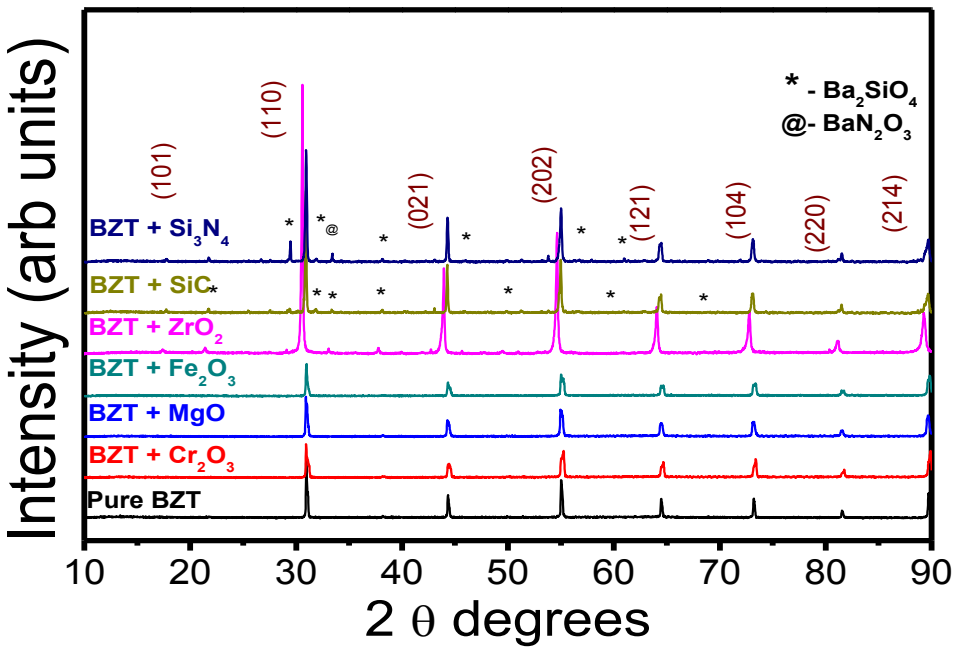

Fig 6.3 X-ray diffraction pattern of BZT samples with different additives sintered using microwaves at 1400°C

The x-ray diffraction pattern of sintered samples with different additives is shown in Figure 6.3. The primary peaks and intensities of the samples with oxide additives match with the fundamental reflections of pure BZT and there were no extra peaks corresponding to unreacted phases present in the sample. Few samples had zinc deficient secondary phase ($Ba_8ZnTa_6O_{24}$) which is formed due to volatilization of Zinc from the system. In case of samples containing Si_3N_4 and SiC as additives, numerous extra peaks corresponding to secondary phases formed due to reaction of Ba with additives were formed. Based on the results of density and x-ray diffraction pattern, oxides (Cr_2O_3, Fe_2O_3 and ZrO_2) were chosen as optimum additives for microwave sintering of BZT.

Figure 6.4 shows the effect of soaking time during microwave sintering on the final sintered density of BZT – xCr_2O_3 (x = 0.5 mol. %) samples. Sintered density close to 91% of TD was obtained in microwave sintering at 1400 °C for a shorter soaking duration (15 min).

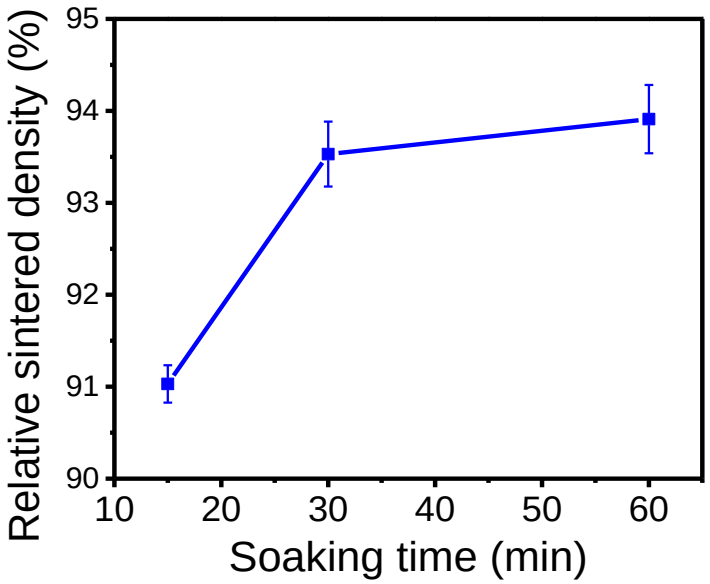

Fig 6.4 Effect of soaking time during microwave sintering on the final sintered density of BZT – xCr_2O_3 (x = 0.5 mol. %) samples sintered at 1400 °C

Increase in soaking time to 30 min increased the density to ~93.5% of TD. Increase in sintered density was marginal with further increase in soaking time (upto 60 min). Soaking time was not increased beyond 60mins as higher soaking time would impair the lifetime of the magnetrons. Microwave sintering is known to give better sintered densities at shorter soaking times compared to those obtained in conventional sintering due to efficient coupling of the samples with microwaves. Similar results were observed in the present study, where better densities were obtained for shorter soaking duration.

The effect of Cr_2O_3 addition on the density of BZT ceramic by microwave and conventional sintering is subsequently studied. Figure 6.5 shows the influence of Cr_2O_3 content on the sintered densities of BZT – xCr_2O_3 (x = 0 to 2 mol.%) samples sintered at 1300 °C - 1500 °C in microwave sintering furnace. Increase in density with increase in sintering temperature was observed to be relatively low for pure BZT when compared with BZT – xCr_2O_3 samples. A maximum density ~84% of TD was obtained for pure BZT even at a temperature of 1500 °C. This could be attributed to relatively poor coupling capacity of BZT with microwaves than that of BZT – xCr_2O_3.

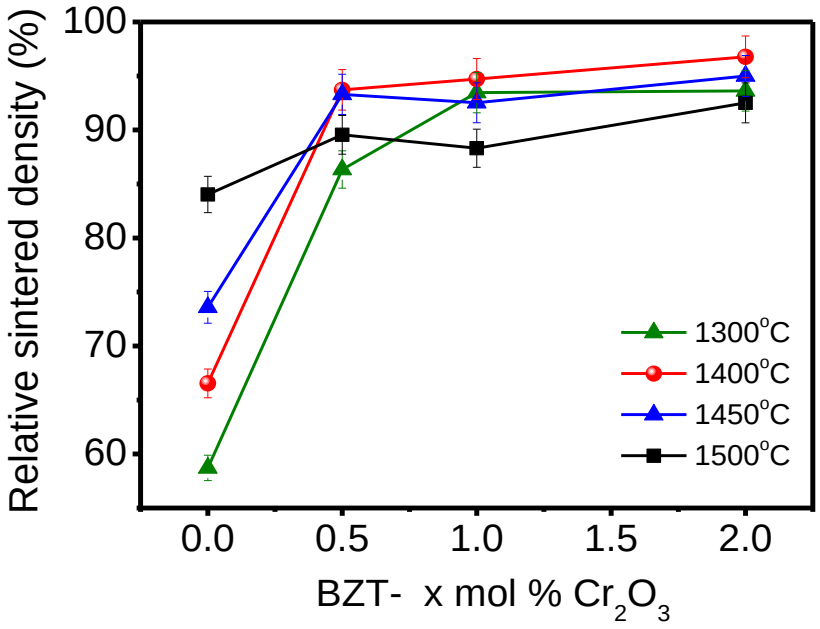

Fig 6.5 Influence of Cr_2O_3 content on the sintered densities of BZT – xCr_2O_3 (x = 0 to 2 mol.%) samples microwave sintered at 1300 °C - 1500 °C

The rate of densification increased rapidly with Cr_2O_3 addition of 0.5 mol. % and with further addition of Cr_2O_3 (upto 2 mol. %) marginal increase in the densification rate was observed. Samples containing 0.5 mol. % Cr_2O_3 when sintered at 1400 °C led to a density of ~94% of TD. Maximum density of 97% of TD was observed for BZT containing 2 mol. % of Cr_2O_3 when microwave sintered at 1400 °C. There is a marginal decrease in density when sintered at 1500 °C.

Conventional sintering of the samples was carried to compare the densification behavior of BZT with increase in temperature over microwave sintering. Figure 6.6 shows the influence of Cr_2O_3 content on the sintered densities of BZT – xCr_2O_3 (x = 0 to 2 mol. %) samples conventionally sintered at 1450 °C - 1550 °C for 2 hours. Density of pure BZT sample was ~88% when sintered at 1500 °C/2 hours. When compared to microwave sintering at 1500 °C, increase in density could be attributed to long soaking time in conventional sintering.

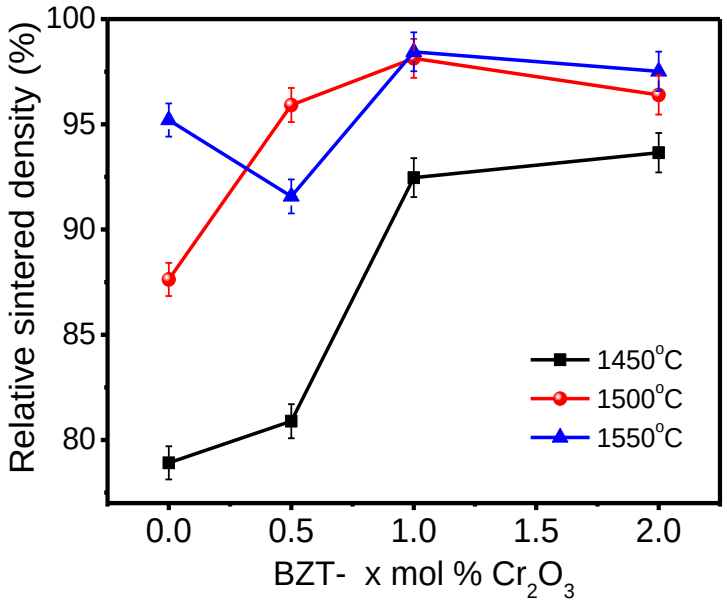

Fig 6.6 Influence of Cr_2O_3 content on the sintered densities of BZT – xCr_2O_3 (x = 0 to 2 mol.%) samples conventionally sintered at 1450 °C - 1550 °C

Conventional sintering temperature was increased further to 1550 °C and density of ~95% was obtained. At lower sintering temperature (1450 °C), sample containing 1 mol. % Cr_2O_3 showed better densification compared to those of pure BZT and 0.5mol. % Cr_2O_3 samples. Very little variation in density was observed with increase in Cr_2O_3 content (upto 2 mol. %). Maximum density (~ 98% of TD) was achieved for the sample containing 1 mol. % Cr_2O_3 when conventionally sintered at a temperature of 1500 °C/ 2 hours. This is the maximum density reported for samples containing Cr_2O_3 as additive. M. R. Varma et al. has reported a maximum density close to 93% of TD for samples containing 0.5 and 1 mol.% Cr_2O_3 when conventionally sintered at 1525 °C/ 6 hours [4]. When 2 mol.% Cr_2O_3 is added to BZT synthesized by decomposition of citrate precursor gel, 87% of TD is achieved after sintering at 1550 °C/ 6 hours [5]. Density of the samples was found to decrease marginally when conventionally sintered at 1550 °C.

Figure 6.7 shows the influence of Fe_2O_3 content on the sintered densities of BZT – xFe_2O_3 (x = 0 to 2 mol.%) samples sintered at 1300 °C - 1500 °C in microwave sintering furnace. The rate of densification of BZT improved with increasing concentration of Fe_2O_3 addition. At lower temperature (1300 °C),

densification of BZT - 0.5 Fe_2O_3 was relatively poor (74%TD) compared to sample containing 0.5mol% Cr_2O_3 (86%TD). Upon increase in temperature (1400 °C), the rate of densification improved and a maximum density of 94%TD was obtained for BZT - 0.5 Fe_2O_3.

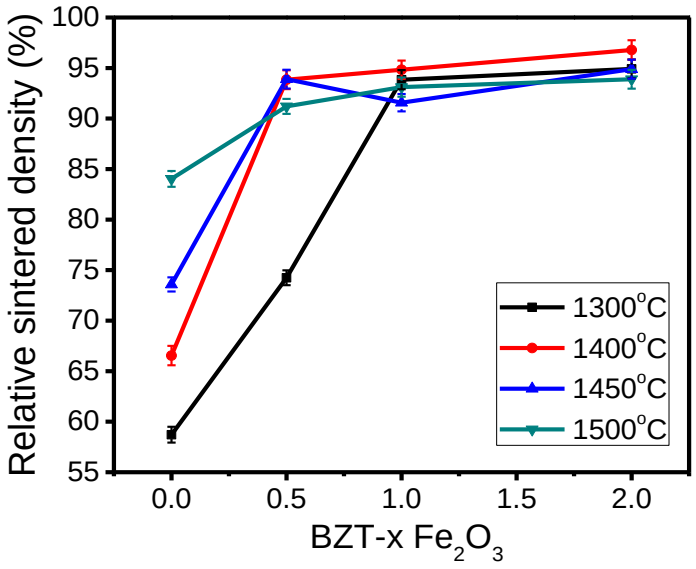

Fig 6.7 Influence of Fe_2O_3 content on the sintered densities of BZT – xFe_2O_3 (x = 0 to 2 mol.%) samples microwave sintered at 1300 °C - 1500 °C

Further increase in temperature did not influence the density much and there is a marginal decrease in density for samples sintered at 1500 °C. Increase in concentration upto 1 mol% addition led to marginal increase in density even with increase in sintering temperature. 97%TD was achieved for BZT - 2 Fe_2O_3 at 1400 °C and there is a decrease in density when samples were sintered at 1500 °C. This could be primarily due to zinc volatilization from the system rendering the samples porous or due to exaggerated grain growth. The densification of BZT with Fe_2O_3 addition for different sintering temperature followed almost similar trend as that of BZT – xCr_2O_3 samples.

Figure 6.8 shows the influence of Fe_2O_3 content on the sintered densities of BZT – xFe_2O_3 (x = 0 to 2 mol.%) samples conventionally sintered at 1400 °C - 1500 °C for 2 hours. Even at a lower temperature of 1400 °C, density of samples increased rapidly with increase in concentration of Fe_2O_3.

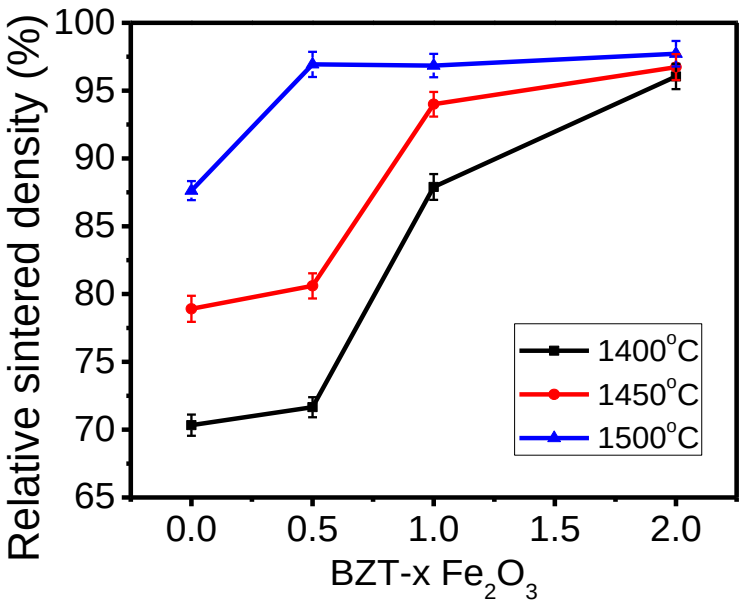

Fig 6.8 Influence of Fe_2O_3 content on the sintered densities of BZT – xFe_2O_3 (x = 0 to 2 mol.%) samples conventionally sintered at 1400 °C - 1500 °C

96%TD has been achieved for samples containing 2mol% of Fe_2O_3 on sintering at 1400 °C. Increase in temperature upto 1450 °C led to increase in density and maximum density of 97% TD was observed in BZT – 2 mol%Fe_2O_3. Higher temperature (1500 °C) is required for achieving density of 97%TD in samples containing 0.5mol% and 1 mol% of Fe_2O_3.

Figure 6.9 shows the variation in density of BZT - $xZrO_2$ (x = 0 to 3 mol%) samples sintered by microwave sintering (1400 °C) and conventional sintering (1550 °C). Microwave sintering of BZT - $xZrO_2$ led to increase in density with increasing concentration of ZrO_2. The rate of densification increases rapidly with ZrO_2 addition upto 2mol. % and with further addition of ZrO_2 (upto 3 mol. %) decrease in the densification rate was observed in microwave sintering. 98% TD was obtained for sample containing 2 mol% of ZrO_2 in microwave sintering. It has been seen in previous reports that BZT samples conventionally sintered with ZrO_2 as additive has improved the densification behavior and dielectric properties of BZT [6].

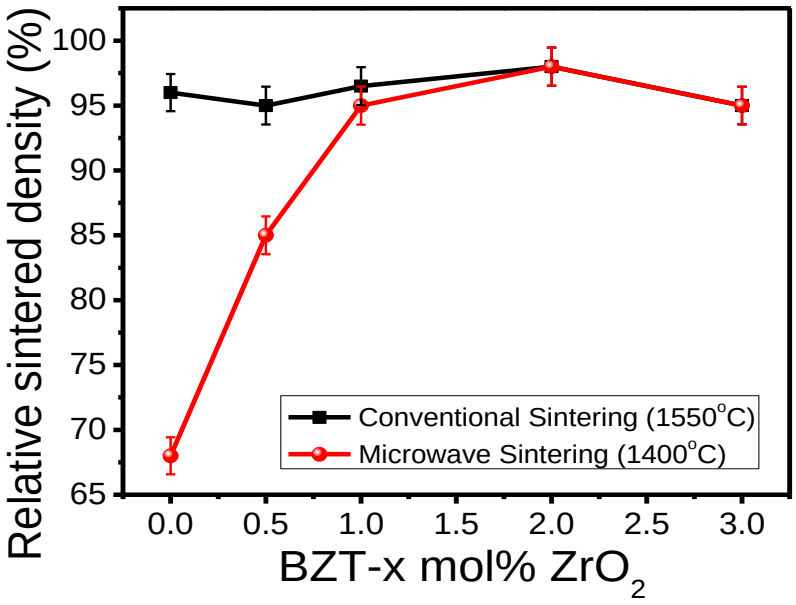

Fig 6.9 Influence of ZrO_2 content on the sintered densities of BZT – $xZrO_2$ (x = 0 to 3 mol.%) samples 1400 °C microwave and 1550 °C conventionally sintered

BZT - $xZrO_2$ (x = 0 to 3 mol%) samples were conventionally sintered at 1550 °C to study and compare the effect of sintering technique on density and final properties. All samples sintered at 1550 °C showed density >95%TD. Maximum density (~98%TD) was achieved for sample containing 2 mol% ZrO_2 and further addition of ZrO_2 beyond 2 mol% lead to decrease in rate of densification by conventional sintering which is in accordance with the results obtained by Yang et al. [6]

6.3.2 Microstructural analysis:

Microstructural analysis of the samples was carried out to study the variation of density with increase in temperature. Figure 6.10 shows the microstructures of pure BZT samples sintered at 1450 °C and 1500 °C in microwave sintering furnace. The samples exist in intermediate stage of sintering and a more continuous pore phase was observed. The area of continuous pore phase decreased with increase in temperature with grains growing closer. Grain growth as well the decrease in pore phase area was observed in the microstructure of sample sintered at 1500 °C.

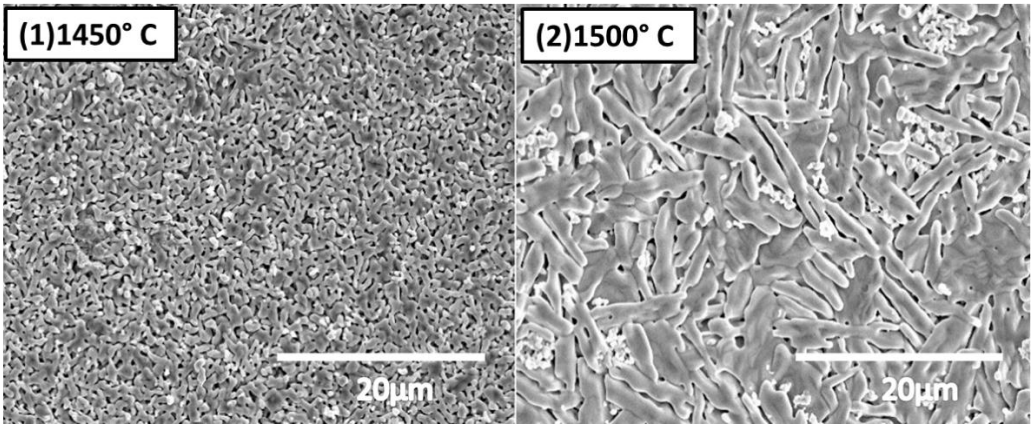

Fig 6.10 Microstructures of pure BZT samples sintered at (1)1450 °C and (2) 1500 °C in microwave furnace

Analysis on the density of BZT – xCr_2O_3 (x = 0 to 2 mol.%) samples reveal that there is marginal drop in density of samples sintered at 1500 °C using microwave furnace. The variation is predominantly seen in samples containing 1 mol. % and 2 mol. % Cr_2O_3 even at a temperature of 1450 °C.

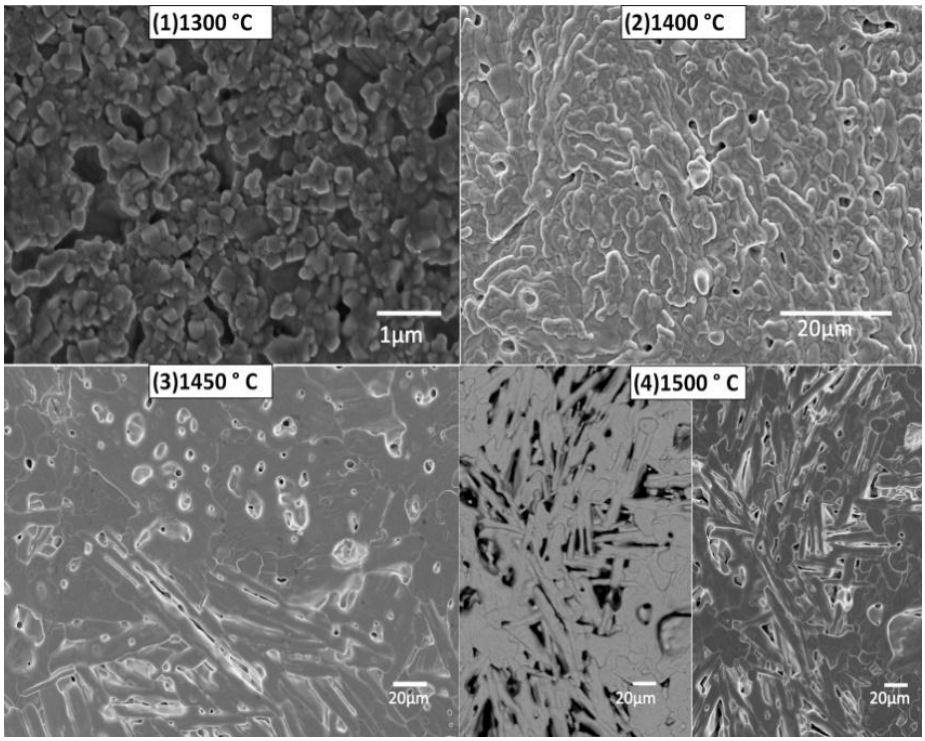

Fig 6.11 Microstructure of BZT – xCr_2O_3 (x = 2 mol.%) samples microwave sintered at 1300 °C -1500 °C

Figure 6.11 shows the microstructure of BZT – xCr_2O_3 (x = 2 mol.%) samples sintered at 1300 °C - 1500 °C in microwave sintering furnace. Presence of small grains was observed for sample sintered at 1300 °C. Grain growth was observed with increase in temperature and irregularly shaped grains with diffused grain boundaries has been observed for the samples sintered at 1400 °C. The co-existence of anisotropic acicular grains and irregularly shaped grains has been seen in sample sintered at 1450 °C. Growth of the acicular grains was observed with increase in temperature. Phase contrast has not been observed in the BSE micrographs taken for the sample sintered at 1500 °C in regions where the acicular grains, irregularly shaped grains and pores co-exist.

Figure 6.12 shows the microstructures of BZT – xCr_2O_3 (x = 0 to 2 mol. %) samples sintered at 1450 °C in microwave sintering furnace. It has been observed that growth of acicular grains increased with increase in addition of Cr_2O_3. Irregularly shaped grains were predominantly observed in samples with 0.5 mol. % Cr_2O_3, whereas, the occurrence of irregular as well as elongated structure were seen in samples containing 1 mol. %. Large acicular grains were mainly seen in the samples containing 2 mol. % Cr_2O_3.

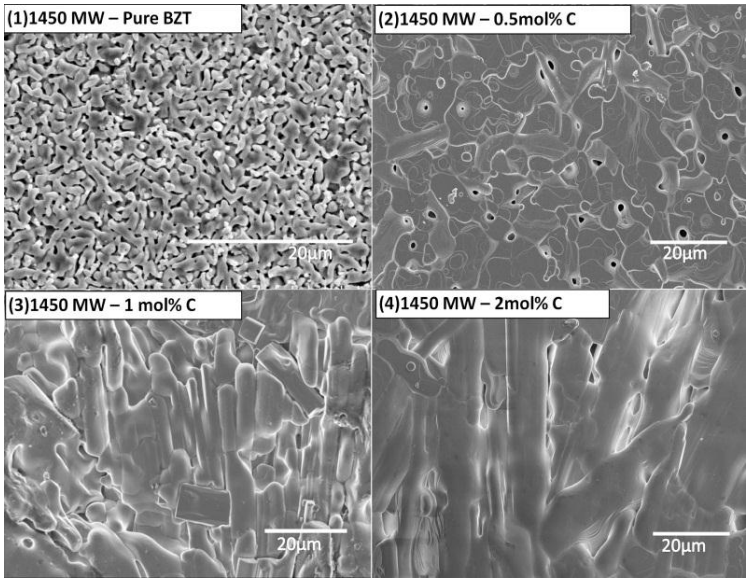

Fig 6.12 Microstructures of BZT – xCr_2O_3 (x = 0 to 2 mol. %) samples microwave sintered at 1450 °C

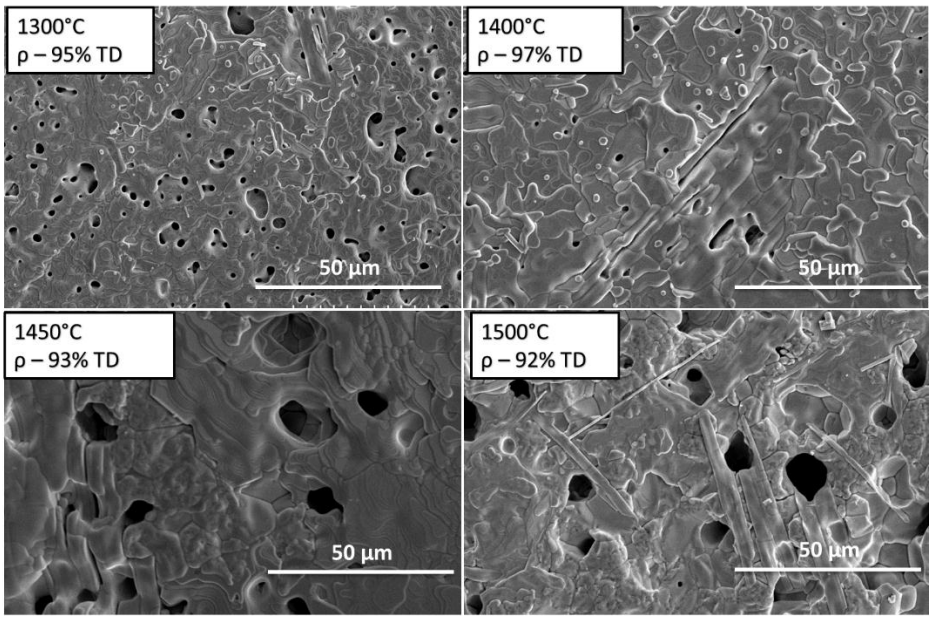

Fig 6.13 Microstructure of BZT – xFe_2O_3 (x = 2 mol.%) samples sintered at 1300 °C - 1500 °C in microwave sintering furnace

Figure 6.13 shows the microstructure of BZT – xFe_2O_3 (x = 2 mol.%) samples sintered at 1300 °C -1500 °C in microwave sintering furnace. Pure BZT, which was in an intermediate stage of sintering even at a temperature of 1450 °C showed drastic increase in density with addition of Fe_2O_3. Even at a lower sintering temperature (1300 °C), there was a drastic decrease in the continuous pore phase area compared to pure BZT and small irregular grains were observed. Increase in temperature led to increase in grain growth of the sample and dense microstructure with small irregular grains were seen in sample sintered at 1400 °C. Anisotropic elongated grains were observed in the dense matrix of irregular grains in samples sintered at 1400 °C. Growth of anisotropic grains predominated with increase in temperature leading to decrease in density.

Figure 6.14 shows the microstructures of BZT – xFe_2O_3 (x = 0 to 2 mol. %) samples sintered at 1450 °C in microwave sintering furnace. It can be seen from the micrographs that presence of Fe_2O_3 during microwave sintering aided in the formation of anisotropic grain growth. Micrographs taken in back scattered electron mode at regions were anisotropic grains and dense matrix consisting of irregular grains did not

reveal any phase contrast. Similar microstructures showing acicular and anisotropic grains were also seen in BZT – xCr_2O_3 samples.

J.S. Kim et al. have observed similar anisotropic grains in $BaWO_4$ doped BZT. It is stated that $BaWO_4$ accelerates the growth of anisotropic grains in an abnormal way and hence influence the final density of the samples [7]. Similar structures have been observed in high-Q Ga_2O_3 doped BZT [8]. Tolmer et al. attributed such structures on pure BZT surface to $BaTa_2O_6$ phase [9]. Acicular grains of single phase $Ba_8ZnTa_6O_{24}$ showing a dense microstructure after two stage sintering was reported by P.K. Davies et al [10]. The growth of acicular grains were observed in BZT – xCr_2O_3 and BZT - xFe_2O_3 (x = 2 mol. %) with increase in temperature. Since volatilization of zinc is prone to occur at higher temperatures (T > 1400 °C), it may lead to the formation of secondary phase ($Ba_8ZnTa_6O_{24}$). The presence of this secondary phase could be attributed to the development of such anisotropic grains. It has been observed that preferential crystallographic orientations existed in $Ba_8ZnTa_6O_{24}$ compacts and has been inferred that the anisotropic grains existed due to the growth of the hexagonal platelets along (001) direction [10].

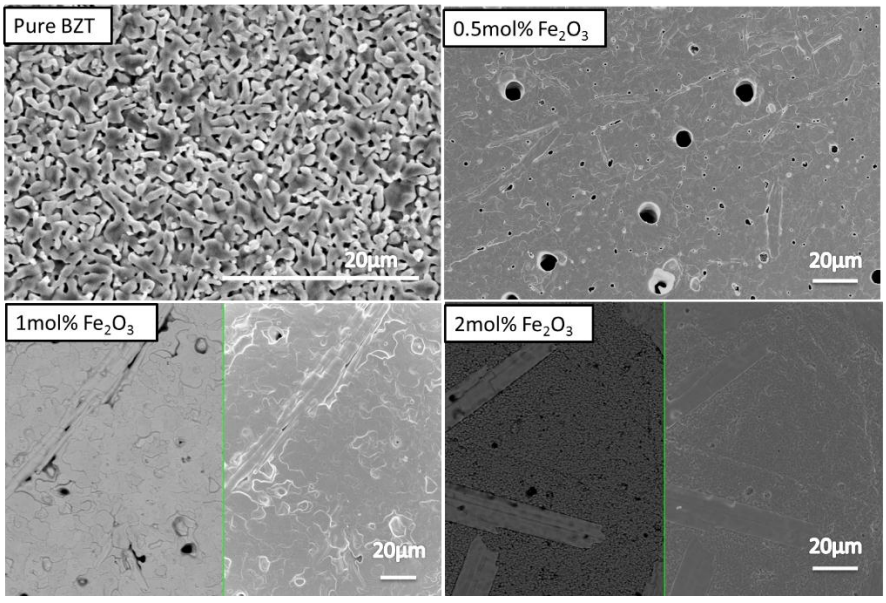

Fig 6.14 Microstructures of BZT – xFe_2O_3 (x = 0 to 2 mol. %) samples microwave sintered at 1450 °C

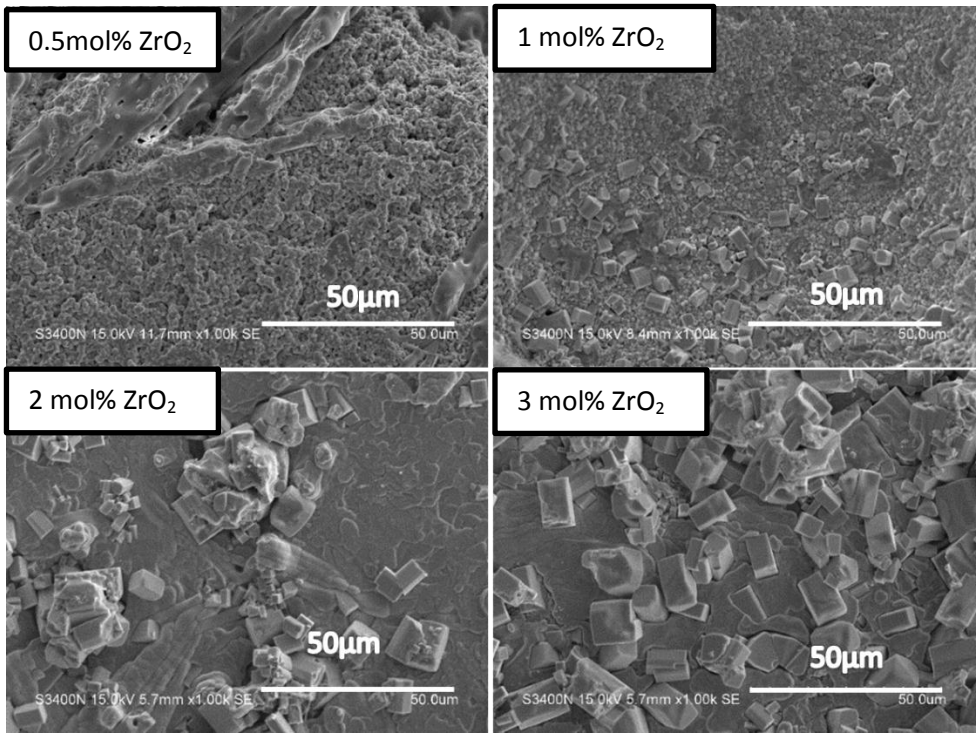

Fig 6.15 Microstructures of BZT – $xZrO_2$ (x = 0 to 3 mol. %) samples microwave sintered at 1400 °C

Figure 6.15 shows the microstructures of BZT – $xZrO_2$(x = 0 to 3 mol. %) samples sintered at 1400 °C in microwave sintering furnace. Even for small addition of ZrO_2 to BZT (0.5 mol%), small grains as well anisotropic grains were observed in the microstructure. As the concentration of ZrO_2 is increased, bar shaped grains tend to evolve in the matrix containing small grains. Grain growth is improved for BZT – 2mol%ZrO_2 samples leading to dense microstructure formed from acicular grains with diffused grain boundary. Clusters of bar shaped grains were seen in the sample with 2 mol% ZrO_2. Growth of bar shaped grains was found to be predominant as concentration of ZrO_2 is increased to 3 mol%.

Similar bar shaped grains were witnessed by Yang et al[6] in conventionally sintered BZT with ZrO_2 as additive and the presence of these grains were attributed to Ta rich phase ($Ba_{0.5}TaO_3$) formed due to presence of Zr^{4+} ions during sintering. Cr^{3+}, Fe^{3+} and Zr^{4+} have ionic radii close to that of B-site ions in the perovskite lattice and hence it is anticipated to enter the B-site of the perovskite unit cell. The increasing amount of acicular grains at larger additive oxide content could result from

larger formation of Zn deficient phase because of Zn vacancies ($V_{Zn}^{//}$) in presence of Cr^{3+} / Fe^{3+} / Zr^{4+} and higher temperatures.

6.3.3 Microwave dielectric properties:

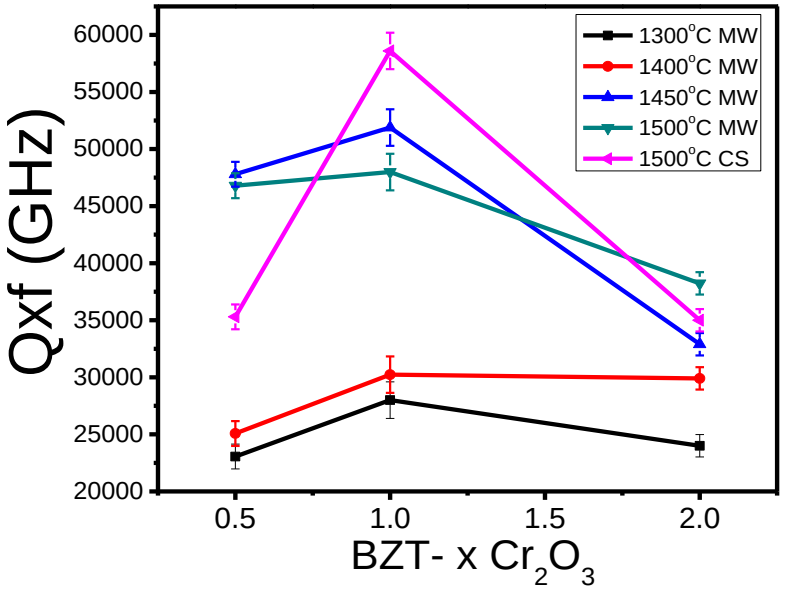

Fig 6.16 Effect of sintering temperature on Quality factor (Q×f) of BZT – xCr_2O_3 (x = 0 to 2 mol. %) samples microwave sintered at 1300 °C -1500 °C and conventionally sintered at 1500 °C

The sintered samples were characterized for microwave dielectric properties to determine the efficiency of BZT – xCr_2O_3 (x = 0 to 2 mol. %) samples for microwave application. Figure 6.16 shows the effect of sintering temperature on Quality factor (Q×f) of BZT – xCr_2O_3 (x = 0 to 2 mol. %) samples sintered in microwave furnace. It has been seen that BZT – xCr_2O_3 (x = 0.5 mol.%) sample, sintered at higher temperatures (1450 °C and 1500 °C) show better Q×f in comparison with the sample sintered at 1400 °C. The reason could be attributed to presence of smaller grains in sample sintered at 1400 °C. With increase in temperature, large anisotropic grains were found to exist which effectively reduces the grain boundary area thus improving the quality factor of the samples. In as sintered samples, BZT – 0.5 Cr_2O_3 maximum quality factor of 47800 GHz has been seen in sample sintered at 1450 °C. Highest quality factor (~51900 GHz) has been achieved in sample containing 1 mol% Cr_2O_3

after sintering at 1450 °C. Further increase in concentration of Cr_2O_3 led decrease in the quality factor. In case of conventionally sintered sample, BZT - $0.5Cr_2O_3$ samples sintered at 1500 °C showed a quality factor of 35300 GHz. Increase in concentration of Cr_2O_3 (upto 1 mol%) led to increase in quality factor value (~58600 GHz) and further increase in concentration led to decrease in the Q×f values.

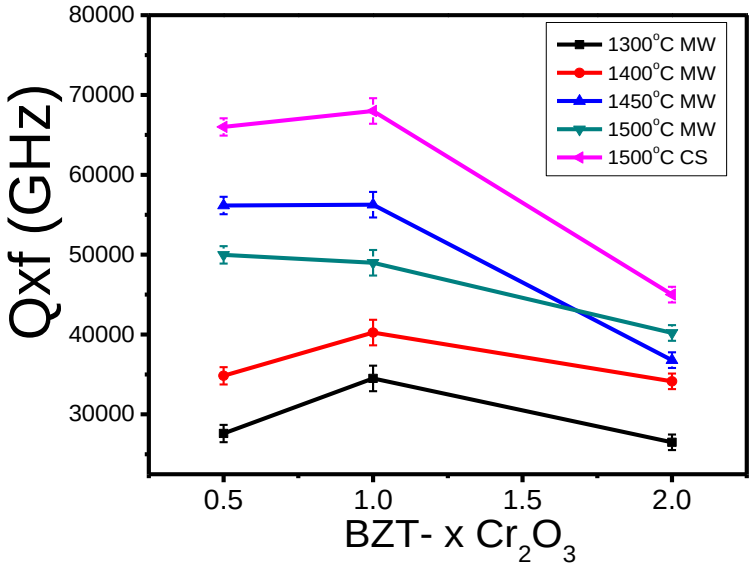

Fig 6.17 Effect of annealing on Quality factor (Q×f) of BZT – xCr_2O_3 (x = 0 to 2 mol. %) samples microwave sintered at 1300 °C -1500 °C and conventionally sintered at 1500 °C

Figure 6.17 shows the effect of annealing on Quality factor (Q×f) of BZT – xCr_2O_3 (x = 0 to 2 mol. %) samples sintered in microwave furnace. The increase in Q×f values with increase in annealing time is better for samples sintered at 1450 °C and 1500 °C compared to those sintered at 1400 °C. Maximum Q×f of 56000 GHz is obtained for sample with 0.5 mol% Cr_2O_3, sintered at 1450 °C and annealed for 12 hours. In case of samples containing 1 mol.% Cr_2O_3, better Q×f values were observed for samples sintered at 1450 °C and 1500 °C than those sintered at 1400 °C. Increase in annealing time beyond 6 hours did not improve the quality factor of the samples. Qxf values reaches a maximum of 57000 GHz after annealing for 6 hours and a marginal decrease is observed on further annealing. In case conventionally sintered sample, maximum quality factor of 68000 GHz has been

achieved for sample with 1 mol% Cr_2O_3 after annealing for 6 hours. The quality factor value of BZT - 0.5Cr_2O_3 did not increase beyond 66000 GHz even after annealing for 12 hours. Higher percentage addition of Cr_2O_3 led to decrease in the quality factor values. In all samples with Cr_2O_3 content more than 0.5mol%, maximum value was obtained after annealing for 6 hours and there was a marginal decrease on further annealing. The reason for the same could be due to the interruption of B-site ordering in BZT due to the presence of Cr^{3+} ions in the lattice. It has been observed that increase in percentage of Cr_2O_3 (upto 2 mol. %) has deteriorated the quality factor and no increase in Qxf values has been seen with increase in annealing time. The soaking time during conventional sintering of the samples was kept constant for 2 hours. When the 0.5 mol.% Cr_2O_3 containing BZT is sintered conventionally at 1500 °C/6hours and subsequently annealed at 1350 °C/12 hours, a quality factor of 98000 GHz was achieved and it is in accordance with the results obtained by M. R. Varma et al [4].

Table 6.1 Dielectric constant and τ_f values of BZT – xCr_2O_3 (x = 0 to 2 mol. %) samples sintered at 1450 °C

BZT-x mol% Cr_2O_3	**ε_r**	**τ_f**
0.5	28.5	-1.89
1	28.2	-2.7
2	27.9	-3.2

The dielectric constant and τ_f values of BZT – xCr_2O_3 (x = 0 to 2 mol. %) samples sintered at 1450 °C are tabulated in Table 6.1. There is a marginal decrease in the dielectric constant value with increasing concentration of Cr_2O_3 and this could be attributed to low dielectric polarizability of Cr_2O_3 (1.45). τ_f values increase in the negative side with increasing concentration of Cr_2O_3. It is already reported that prolonged annealing of BZT samples improves the quality factor and this improvement is attributed to the ordering of B site ions (Zn and Ta) in 1:2 order.

Increasing trend of Q×f values in BZT-0.5Cr_2O_3 samples could be attributed to the fact that the effect of Cr_2O_3 addition to BZT has not been predominantly pronounced on the dielectric properties for the samples sintered using microwaves. Marginal increase in Q×f of samples with 1 mol. % was observed after annealing for 6 hours. Further increase in Cr_2O_3 diminished the quality factor.

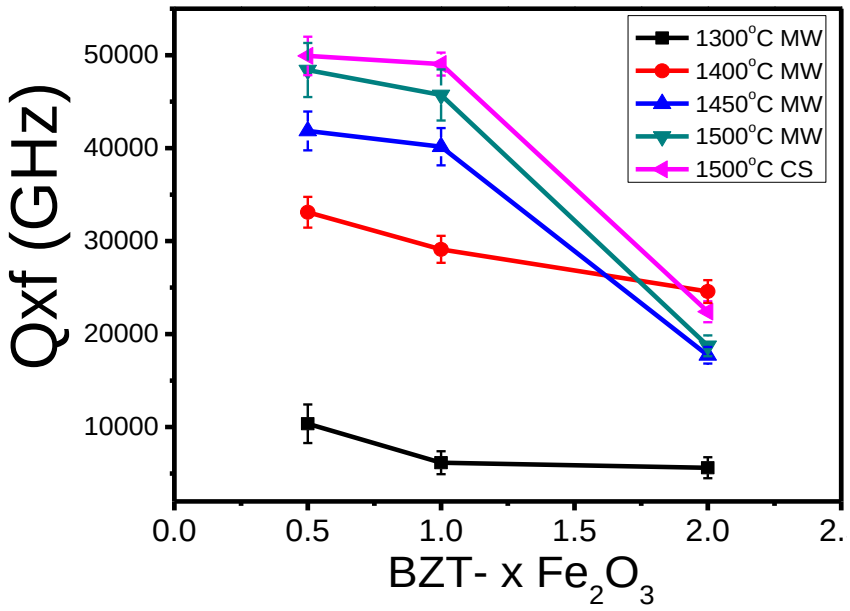

Fig 6.18 Effect of sintering temperature on Quality factor (Q×f) of BZT – xFe_2O_3 (x = 0 to 2 mol. %) samples microwave sintered at 1300 °C - 1500 °C and conventionally sintered at 1500 °C

Figure 6.18 shows the effect of sintering temperature on Quality factor (Q×f) of BZT – xFe_2O_3 (x = 0 to 2 mol. %) samples sintered in microwave furnace. For BZT – xFe_2O_3 (x = 0.5mol. %, 1 mol.%) samples, quality factor values tends to increase with increasing sintering temperature. Maximum quality factor of 48000 GHz has been achieved for sample with 0.5mol% Fe_2O_3 sintered at 1500 °C. In case of sample containing 1 mol% Fe_2O_3, quality factor decreases to a value of 45700 GHz. For BZT – xFe_2O_3 (x = 2 mol.%) samples, quality factor values tends to increase with increasing sintering temperature upto 1400 °C and decreases with further increase in temperature. Samples sintered conventionally at 1500 °C, maximum quality factor (~49900 GHz) was achieved for samples with

0.5mol% Fe_2O_3. There was a marginal decrease in quality factor values for sample with 1 mol% Fe_2O_3 and with further addition of oxide to 2 mol%, quality factor drastically decreased to 22400 GHz. In both microwave and conventional sintered samples, addition of Fe_2O_3 did not improve the quality factor values despite improvement in density.

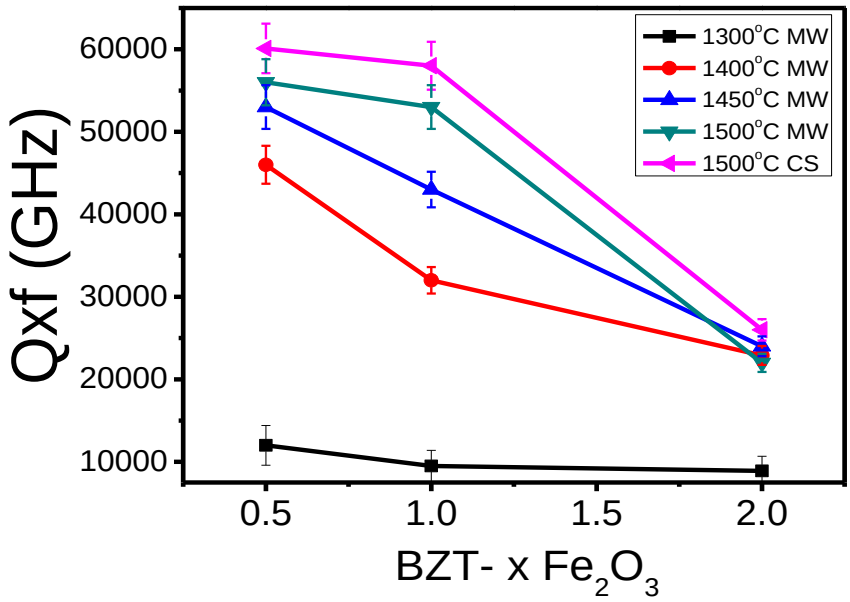

Fig 6.19 Effect of annealing on Quality factor (Q×f) of BZT – xFe_2O_3 (x = 0 to 2 mol. %) samples microwave sintered at 1300 °C - 1500 °C and conventionally sintered at 1500 °C

Figure 6.19 shows the effect of annealing on Quality factor (Q×f) of BZT – xFe_2O_3 (x = 0 to 2 mol. %) samples sintered in microwave furnace. Annealing of the samples did not improve the quality factor to a greater extent. Even after annealing, the quality factor of samples followed the same trend with increasing concentration of Fe_2O_3. Highest quality factor (~56000 GHz) was achieved for sample with 0.5 mol% Fe_2O_3 sintered at 1500 °C and annealed for 8 hours. The quality factor values after annealing the samples containing 0.5 mol% and 1 mol% of Cr_2O_3/ Fe_2O_3 remain almost same. The decrease in quality factor values with further increase in concentration of additives is drastic for samples containing Fe_2O_3 in comparison with sample containing Cr_2O_3. The dielectric constant and τ_f values of BZT – xFe_2O_3 (x = 0 to 2 mol. %) samples sintered at 1450 °C are tabulated in Table 6.2.

Table 6.2 Dielectric constant and τ_f values of BZT – xFe_2O_3 (x = 0 to 2 mol. %) samples sintered at 1450 °C

BZT-x mol% Fe_2O_3	**ε_r**	**τ_f**
0.5	29.3	-1.1
1	29.1	-1.5
2	28.7	-2.3

Dielectric constant value decreases with increasing concentration of Fe_2O_3. But the values are marginally higher than that of samples containing Cr_2O_3 and this can be attributed to higher ionic polarizability of Fe^{3+} ions. τ_f values increase in the negative side with increasing concentration of Fe_2O_3 and the trend is same as that of samples containing Cr_2O_3.

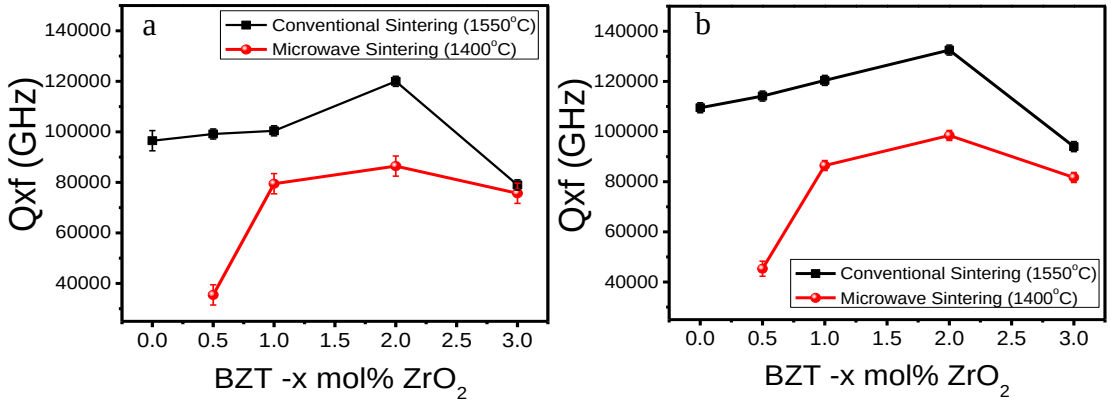

Fig 6.20 Variation of Quality factor (Q×f) of BZT – $xZrO_2$ (x = 0 to 3 mol. %) samples microwave sintered at 1400 °C and conventionally sintered at 1550 °C (a) before annealing (b) after annealing

Figure 6.18 (a) shows the effect of microwave sintering and conventional sintering on quality factor values of BZT – $xZrO_2$ (x = 0 to 3 mol. %) samples. It can be clearly seen from the graph that the conventional sintered samples possessed better Qxf values than the samples sintered in microwave furnace. BZT – 0.5 mol% ZrO_2 sample sintered in microwave furnace had the least Q×f value of 35400 GHz. Sintered density of the sample increases rapidly with 1 mol% addition and Q×f values is

almost doubled (~79400 GHz) for sample with 1 mol% ZrO_2 in comparison with the sample with 0.5 mol% ZrO_2. The values increase to 86400 GHz for BZT - 2mol% ZrO_2 and further addition of ZrO_2 (upto 3 mol%) led to decrease in quality factor values. Since conventional sintered samples had better density in comparison with the samples sintered in microwave furnace, the quality factor values were high even for lower concentrations of ZrO_2. The variation in values with increasing concentration of ZrO_2 remains same for samples sintered conventionally as well as for samples sintered in microwave furnace. Maximum quality factor is achieved for BZT – 2 mol% ZrO_2 sample sintered at 1550 °C and the value drastically decreases with further addition of ZrO_2.

Figure 6.20 (b) shows the effect of annealing on quality factor values of BZT – $xZrO_2$ (x = 0 to 3 mol. %) samples sintered using microwave furnace and conventional furnace. Annealing of BZT – 0.5 mol% ZrO_2 samples sintered using microwave furnace did not improve the quality factor values to a greater extent. The reason for such low value could be attributed to low sintered density of the sample. The quality factor value tends to be maximum (~ 98500GHz) for sample with 2 mol% additive after annealing. In case of conventional sintered samples, the values were higher than the samples sintered using microwave. Annealing of samples did not change the trend in variation of quality factor with increasing concentration of ZrO_2 content. Maximum Q×f value of 137000GHz has been achieved for after annealing BZT – 2 mol% ZrO_2 samples.

Table 6.3 Dielectric constant and τ_f values of BZT – $xZrO_2$ (x = 0 to 3 mol. %) samples sintered at 1450 °C

BZT-x mol% ZrO_2	**ε_r**	**τ_f**
0.5	29.5	1.3
1	29.8	2.7
2	29.7	3.5
3	29.1	4.7

The dielectric properties of BZT – $xZrO_2$ (x = 0 to 3 mol. %) samples were summarized in Table 6.3. The dielectric constant values tend to increase with increase in concentration of ZrO_2 upto 2 mol% concentration of additive. Zirconium ions have higher ionic polarizability in comparison with Fe^{3+} and Cr^{3+} ions. It is generally seen that the value of the dielectric constant increases only when the polarizability of the ions in the additive oxide is higher than the average ionic polarizability. Also the presence of extra phases influences the value of dielectric constant. The temperature coefficient of resonant frequency increases with increasing concentration of ZrO_2.

6.3.4 Crystal structure and ordering:

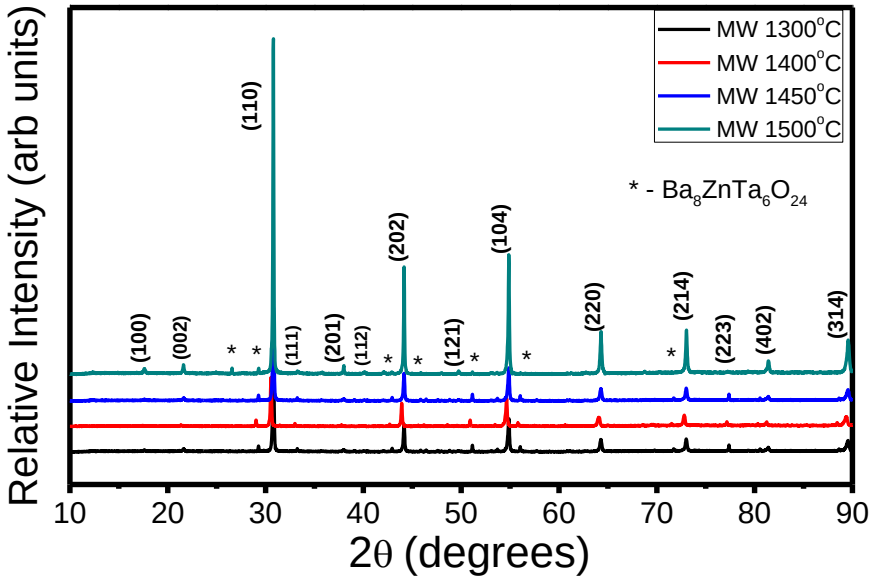

Fig 6.21 X-ray diffraction pattern of BZT – 0.5 mol% Cr_2O_3 microwave sintered samples at various sintering temperature from 1300 °C - 1500 °C

The quality factor of perovskite microwave ceramics is known to depend on crystal structure and ordering of B-site ions in the lattice. The crystal structure and ordering in BZT – xCr_2O_3 was studied using X-ray diffraction. Figure 6.21 shows the X-ray diffraction pattern of BZT containing 0.5mol. % Cr_2O_3 and sintered at 1300 °C - 1500 °C in microwave sintering furnace. BZT samples were reported to possess various zinc deficient phases on the surface after sintering which led to inconsistencies in structure-property correlation [9-12]. Sintered samples were

polished to remove the skin layer and then subjected to microwave dielectric measurements and crystal structure analysis. BZT ceramics possess $Ba_8ZnTa_6O_{24}$ as a secondary phase which is formed due to volatilization of zinc from the system. This zinc deficient phase is seen in all samples that were sintered using microwaves.

Literature on single phase Zn-deficient hexagonal perovskite, $Ba_8ZnTa_6O_{24}$ reports excellent sintering characteristics and very good microwave properties [10]. Hence it is not expected to deteriorate the dielectric properties. The existence of (100) super lattice reflection confirmed that 1:2 ordering in the samples with Cr^{3+} ions. The degree of ordering in the system is estimated by the order parameter which is defined as below,

$$S = \sqrt{\frac{[I_{100}/I_{110,012}]_{obs}}{[I_{100}/I_{110,012}]_{cal}}} \quad - \qquad (1)$$

where $[I_{100}/I_{110,\,012}]_{obs}$ is the ratio of observed intensity of the super lattice reflection to that of the fundamental reflection. $[I_{100}/I_{110,\,012}]_{cal}$ is the calculated intensity ratio for completely ordered ideal sample and the value is 0.037 [12].

Table 6.4 Order parameter values of BZT - 0.5Cr_2O_3 sample sintered at 1300 °C - 1500 °C in microwave sintering furnace

Sintering temperature (^oC)	**BZT - 0.5Cr_2O_3**	
	Order parameter	FWHM $A_{1g}(O)$
1300	0.67	33.5
1400	0.68	31.5
1450	0.73	29.3
1500	0.79	27.8

Table 6.4 shows the order parameter values of BZT - 0.5Cr_2O_3 sample sintered at 1300 °C - 1500 °C in microwave sintering furnace. The value of the order parameter was found to increase with increase in sintering temperature. Low quality factors of the sample sintered at 1400 °C using microwaves, in spite of high density,

can be attributed to the poor ordering in the system. Increase in annealing time of the samples did not improve the order parameter resulting in almost unaffected Qxf values of the system after annealing [13]. Literatures report that addition of dopants to the BZT system generally reduces the ordering [4].

Table 6.5 Order parameter for BZT - x Cr_2O_3 (x = 0 to 2 mol. %) samples sintered at 1450 °C in microwave sintering furnace

BZT-xCr_2O_3	**Microwave sintering (1450 °C)**
	Order parameter
0.5	0.74
1	0.68
2	0.67

Table 6.5 shows the order parameter for BZT- x Cr_2O_3 (x = 0 to 2 mol. %) samples sintered at 1450 °C in microwave sintering furnace. It has been observed that addition of Cr_2O_3 to BZT decreased the ordering in the system. Ordering in BZT is also reflected by lattice distortions in the unit cell. Completely ordered hexagonal structure will have c/a ratio > 1.2247. Hence the lattice parameter values are calculated to study the lattice distortions due to ordering in system.

Table 6.6 Lattice parameters for BZT - x Cr_2O_3 (x = 0 to 2 mol. %) samples sintered at 1450 °C in microwave sintering furnace

BZT-xCr_2O_3	**Lattice parameters**		
	a (Å)	**c (Å)**	**c/a**
0	5.779	7.074	1.223
0.5	5.785	7.071	1.222
1	5.789	7.062	1.219
2	5.791	7.044	1.216

The lattice parameter values and c/a ratio of BZT- x Cr_2O_3 (x = 0 to 2 mol. %) samples were summarized in Table 6.6. It can be seen that the c/a values decrease with increasing concentration of Cr_2O_3 indicating the disruption of ordering in the system. The average crystallite size and strain in BZT- x Cr_2O_3 (x = 0.5 mol%) samples were given in Table 6.7. It can be clearly seen that the average crystallite size of samples increases with increasing sintering temperature.

Table 6.7 Crystalline size and strain values for BZT - 0.5mol% Cr_2O_3 samples microwave sintered at 1300 °C - 1500 °C and conventionally sintered at 1500 °C

Sintering temperature (^oC)	**BZT-0.5Cr_2O_3**	
	Crystallite Size (nm)	**Strain**
1300 ^oC MW	35.14	0.002
1400 ^oC MW	43.27	0.001
1450 ^oC MW	43.61	0.0004
1500 ^oC MW	54.73	0.0010
1500 ^oC CS	84.6	0.0011

Maximum average crystallite size of 54.7 nm was seen in sample sintered at 1500 °C in microwave furnace. The crystallite size of conventionally sintered sample was higher than the sample sintered using microwave furnace at the same temperature. The strain values of samples sintered using microwave furnace were similar to sample sintered conventionally at 1500 °C. The superior quality factor values of conventional sintered samples in comparison with the microwave sintered samples could be attributed to the higher crystallite size of the conventional sintered samples.

Figure 6.22 shows the X-ray diffraction pattern of BZT containing 0.5mol. % Fe_2O_3 and sintered at 1300 °C - 1500 °C in microwave sintering furnace. It can be seen from the x-ray diffraction pattern that the zinc deficient secondary phase existed

in samples and the intensity of this phase increased with increasing sintering temperature.

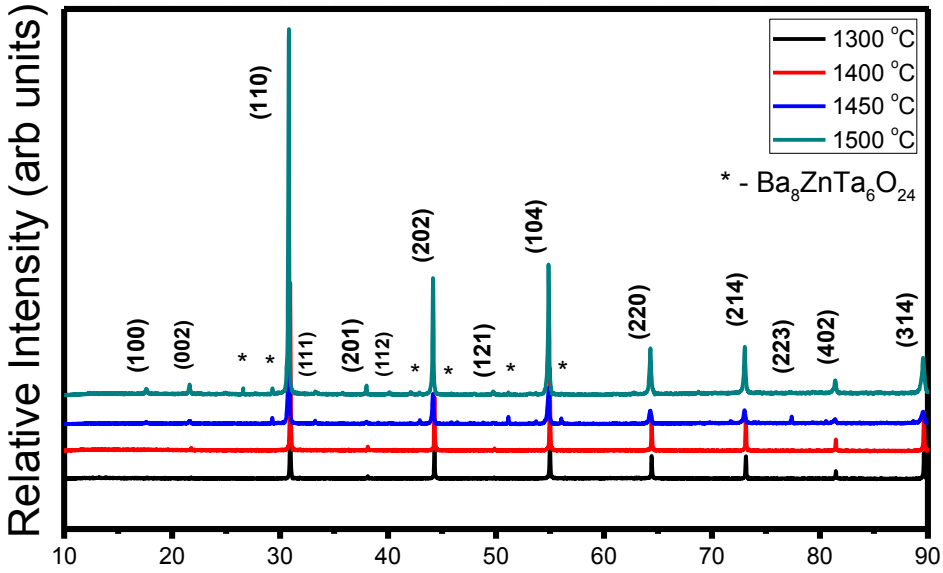

Fig 6.22 X-ray diffraction pattern of BZT – 0.5 mol% Fe_2O_3 microwave sintered samples at various sintering temperature from 1300 °C - 1500 °C

Table 6.8 Order parameter values of BZT - 0.5Fe_2O_3 microwave sintered samples at 1300 °C - 1500 °C

Sintering Temperature	**Order parameter**	**FWHM**
1300 °C	0.67	38.7
1400 °C	0.78	36.7
1450 °C	0.79	35.6
1500 °C	0.82	34.5

Table 6.8 shows the order parameter values of BZT - 0.5Fe_2O_3 sample sintered at 1300 °C - 1500 °C in microwave sintering furnace. The 'S' parameter value increases with increase in sintering temperature. The values are comparable with BZT - x Cr_2O_3 system and the variation of S parameter with respect to different sintering temperature follows same trend in both the systems. The order parameter values for BZT - x Fe_2O_3

(x = 0 to 2 mol. %) samples sintered at 1450 °C in microwave sintering furnace were presented in Table 6.9.

Table 6.9 Order parameter values for BZT - x Fe_2O_3 (x = 0 to 2 mol. %) samples microwave sintered at 1450 °C

BZT-xFe_2O_3	**Microwave sintering (1450 °C)**	
	Order parameter	FWHM
0.5	0.79	38.3
1	0.76	30.2
2	---	43.85

For samples containing 0.5 mol% and 1 mol% of Fe_2O_3, S parameter values were close to 0.79 and 0.76 respectively. Superstructure reflection corresponding to (100) was completely absent for sample containing 2mol% Fe_2O_3 indicating the complete disruption of ordering in the system due to Fe^{3+} ions in B site. The lattice parameter values presented in Table 6.10 indicate the absence of lattice distortion with increasing concentration of Fe_2O_3 additive. The crystallite size and strain values of BZT- x Fe_2O_3 (x = 0.5 mol%) samples were given in Table 6.11.

Table 6.10 Lattice parameters for BZT - x Fe_2O_3 (x = 0 to 2 mol. %) samples sintered at 1450 °C in microwave sintering furnace

BZT-xFe_2O_3	**Lattice parameters**		
	a (Å)	c (Å)	c/a
0	5.779	7.0742	1.2239
0.5	5.785	7.079	1.2236
1	5.791	7.077	1.2220
2	5.813	7.022	1.2079

Table 6.11 Order parameter values of BZT - 0.5Fe_2O_3 sample sintered at 1300 °C - 1500 °C in microwave sintering furnace.

Sintering temperature °C	**BZT - 0.5Fe_2O_3**	
	Crystallite Size (nm)	Strain
1300 °C MW	29.01	0.0006
1400 °C MW	42.14	0.0009
1500 °C MW	59.69	0.0006
1500 °C CS	100.94	0.0005

The crystallite size values increase with increase in sintering temperature. Maximum crystallite size of 59 nm was seen in sample sintered at 1500 °C in microwave furnace and the value is similar to BZT- x Cr_2O_3 sample. Conventional sintered sample had much higher crystallite size (~100nm) than the sample sintered using microwave furnace.

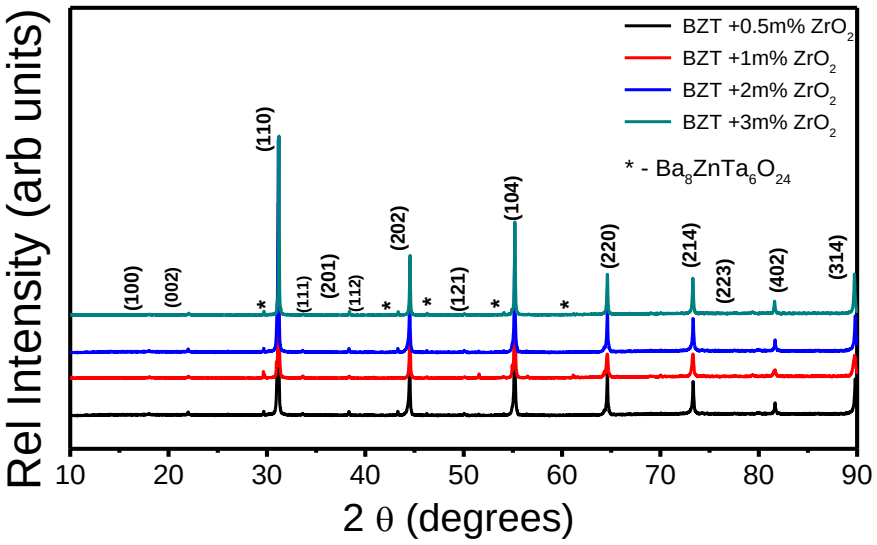

Fig 6.23 X-ray diffraction pattern of BZT – x ZrO_2 (x = 0.5 to 3 mol%) microwave sintered samples at 1550 °C

Figure 6.23 shows the X-ray diffraction pattern of BZT - x ZrO_2 (x = 0 to 3 mol%) sintered in microwave furnace. $Ba_5Ta_4O_{15}$ and $Ba_8ZnTa_6O_{24}$ were

present as zinc deficient secondary phases. The results were in accordance with the microstructural analysis. Presence of bar shaped grains in BZT- x ZrO_2 (x > 2 mol%) could be attributed to $Ba_5Ta_4O_{15}$ phase. The lattice parameter values, crystallite size and order parameter values were given in Table 6.12. From the lattice parameter values, it is clearly seen that c/a values decrease with increase in ZrO_2 concentration. The order parameter values were low for BZT- x ZrO_2 (x < 2 mol%) and ordering is completely lost for samples with ZrO_2 > 2mol%.

Crystallite size of conventionally sintered samples was higher than the microwave sintered samples. The reason for lower values of quality factor for microwave sintered samples could be attributed to smaller crystallite size in comparison with conventional sintered samples.

Table 6.12 *Lattice parameters, order parameter and crystallite size values for BZT - x ZrO_2 (x = 0 to 3 mol. %) samples microwave sintered at 1400 °C and conventionally sintered at 1550 °C*

BZT-x ZrO_2	**Lattice parameters**			**Order parameter**	**Crystallite size**	
	a (Å)	c (Å)	c/a		MW 1400 °C	CS 1550 °C
0.5	5.779	7.072	1.223	0.76	26	55
1	5.788	7.082	1.223	0.69	39	68
2	5.79	7.076	1.222	--	56	103
3	5.833	7.03	1.205	--	43	83

It has been already seen in conventionally sintered BZT - $BaZrO_3$ and BZT - ZrO_2 systems that quality factor is high despite lower annealing times and apparently disordered structure. The reason for high quality factor is attributed to stabilization of domain boundaries by Zr ions in the lattice. The results obtained due to addition of ZrO_2 in microwave sintering also show superior properties which are in accordance with the results obtained in previous literatures.

6.3.5 Raman Spectroscopic studies:

Lattice vibrational modes and ordering in the system is studied using Raman spectroscopy. The position of the A_{1g}(O) mode and FWHM of the peak is generally correlated with the dielectric properties of the samples [8, 14-17]. High Q samples generally possess narrow peak at higher wavenumber of A_{1g}(O) mode.

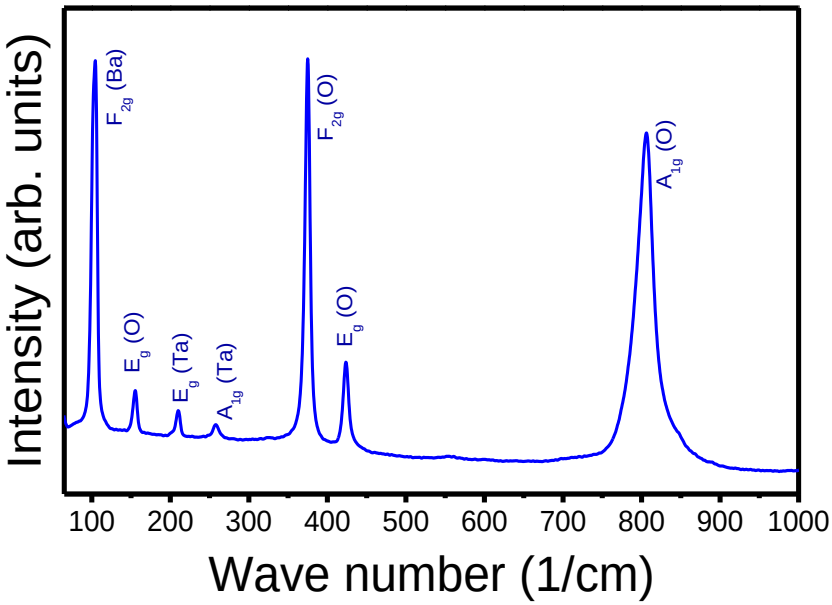

Fig 6.24 Raman spectrum of pure BZT sample sintered at 1550 °C and annealed at 1350 °C.

Figure 6.24 shows the Raman spectrum of pure BZT sample sintered at 1550 °C and annealed at 1350 °C. BZT after calcination exists in ideal cubic perovskite structure with the space group of Pm3m symmetry which has no Raman active modes. After annealing the sintered samples, B site ions adopt 1:2 ordering with the space group of $P\bar{3}m1$ symmetry which has nine active Raman modes. Localized 1:1 ordered structures exhibit a space group of Fm3m symmetry which shows four Raman active modes. The peaks were indexed based on ref [13]. F_{2g}(Ba) occurs at lowest energy near 104 cm^{-1}. The three lines near 158, 212, and 262 cm^{-1} correspond strongly to the existence of 1:2 ordering in the samples. Modes of vibration of O atoms occur at 375 cm^{-1} and 424 cm^{-1}. A_{1g}(O) mode at 806 cm^{-1} corresponds to the stretching mode of the oxygen octahedron.

Raman spectra of BZT samples containing 0.5 mol.% Cr_2O_3 sintered at 1300 °C - 1500 °C in microwave furnace is given in Figure 6.25. Variation of FWHM of $A_{1g}(O)$ mode for BZT - $0.5Cr_2O_3$ samples, sintered at 1300 °C - 1500 °C, is shown in the inset of figure 6.22. The peaks corresponding to 1:2 ordering is not that predominant, which is in accordance with that of the order parameter calculations. Peak corresponding to $A_{1g}(O)$ mode of the sample sintered at 1300 °C is broad indicating poor ordering in the system. FWHM of this peak decreases with the increase in sintering temperature indicating enhanced cation ordering in the system, which is also reflected in the increase in order parameter. A small peak, appearing as a shoulder to the $A_{1g}(O)$ mode peak corresponds to $Ba_8ZnTa_6O_{24}$ phase [15], which correlates well with the XRD results.

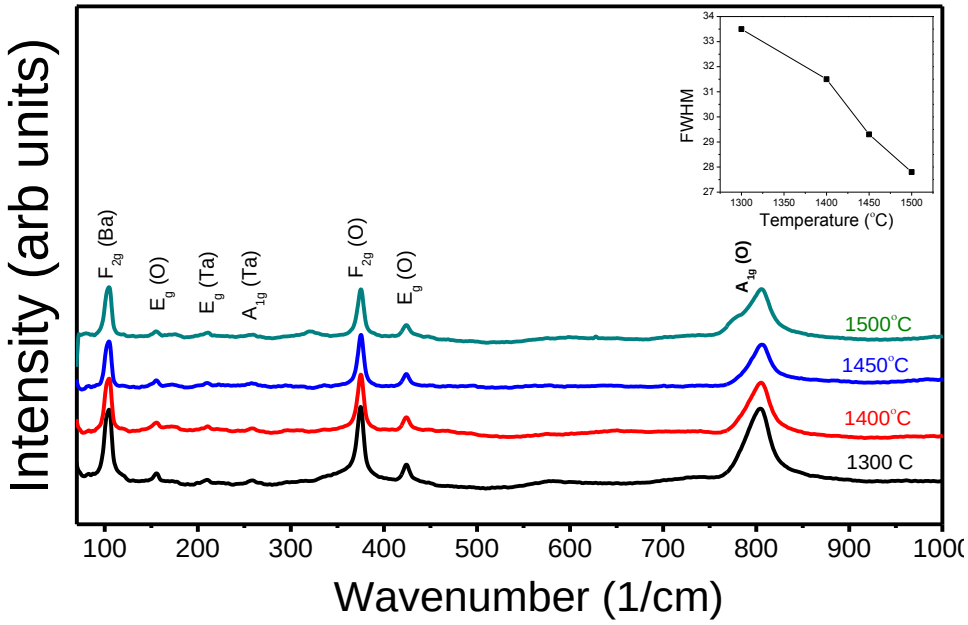

Fig 6.25 Raman spectra of BZT samples containing 0.5 mol.% Cr_2O_3 sintered at 1300 °C - 1500 °C in microwave furnace

Figure 6.26 shows Raman spectra of BZT - x Fe_2O_3 (x = 0 to 2 mol. %) samples sintered at 1450 °C in microwave sintering furnace. The peaks corresponding to 1:2 ordering decrease in intensity with increasing Fe_2O_3 content, which is in accordance with order parameter calculations.

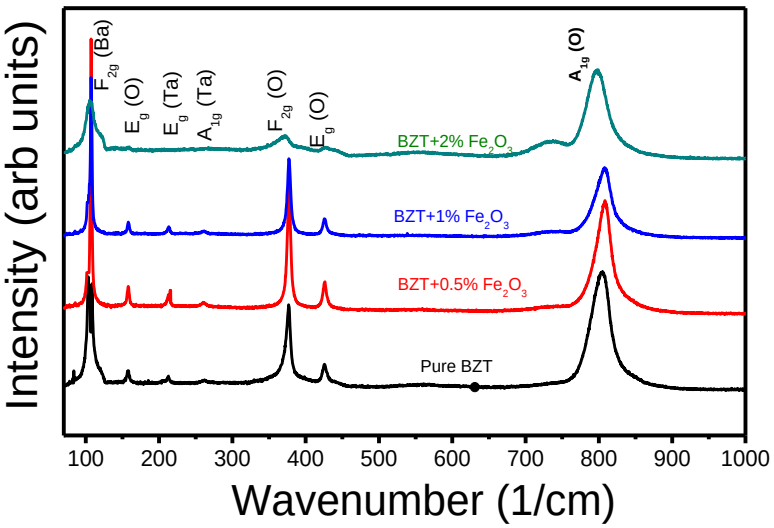

Fig 6.26 Raman spectra of BZT samples containing 0 to 2 mol.% Fe_2O_3 sintered at 1450 °C in microwave furnace

Ordering is completely disrupted by the presence of Fe^{2+} ions in BZT lattice when x = 2 mol% and hence peaks corresponding to ordering were not seen in XRD and Raman spectra. Improvement in ordering with increasing sintering temperature is also reflected in FWHM of A_{1g}(O) mode peak in BZT- x Fe_2O_3 (x = 0.5mol%) sintered in microwave furnace at 1450 °C (as shown in Table 6.8).

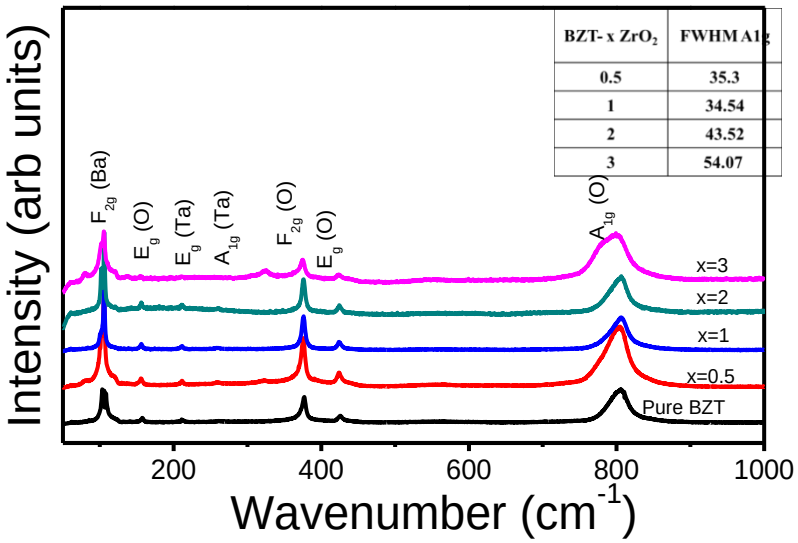

BZT- x ZrO_2	FWHM A1g
0.5	35.3
1	34.54
2	43.52
3	54.07

Fig 6.27 Raman spectra of BZT - x ZrO_2 (x = 0 to 3 mol. %) sintered at 1400 °C in microwave furnace

Figure 6.27 shows raman spectra of BZT- x ZrO_2 (x = 0 to 3 mol. %) samples sintered at 1400 °C in microwave sintering furnace. The BZT- x ZrO_2 (x = 0 to 2 mol. %) samples showed signatures of 1:2 ordering in raman spectra. For BZT - 3mol% ZrO_2, the peaks corresponding to ordering was not seen as per results from XRD. Also the FWHM of A_{1g}(O) mode was high for BZT- x ZrO_2 (x > 1 mol. %) samples indicating the formation of disordered structure.

6.4 Summary

Chromium oxide (Cr_2O_3), iron oxide (Fe_2O_3) and zirconium oxide (ZrO_2) which is known to couple effectively with microwaves, is added as an additive to BZT. Addition of oxide dopants has enhanced the densification and led to higher sintering density of ~97% of TD at a lower sintering temperature of 1400 °C using microwave sintering. Processing time to develop a highly dense ceramic has been drastically reduced by microwave sintering. Microstructural analysis of the microwave sintered samples were in accordance with the densification behavior of microwave sintered BZT. Dielectric properties of microwave sintered samples were not superior to samples processed by conventional sintering. Lattice vibrational modes and ordering in the system is studied using Raman spectroscopy and correlated with the order parameter calculated from XRD analysis.

6.5 REFERENCES

[1] S. A. Nightingale, H.K. Worner, D.P. Dunne, J. Am. Ceram. Soc., 80, 394–400 (2005).

[2] P.D. Ramesh, D. Brandon, L. Schächter, Mater. Sci. Eng. A. 266, 211–220 (1999).

[3] M.N. Rahaman. Densification Process Variables and Densification Practice. Ceram. Process. Sinter., Marcel Dekker, Inc., 2003, p. 779–841.

[4] M.R. Varma, N.D. Kataria, J. Mater. Sci. Mater. Electron. 18, 441–446(2007).

[5] M.R. Varma, S. Biju, M.T. Sebastian, J. Eur. Ceram. Soc. 26, 1903–1907 (2006).

[6] J.-I. Yang, S. Nahm, S.-J. Yoon, H.-M. Park, H.-J. Lee, Jpn. J. Appl. Phys. 43, 211–214 (2004).

[7] J.S. Kim, J.-W. Kim, C.I. Cheon, Y.-S. Kim, S. Nahm, J.D. Byun, J. Eur. Ceram. Soc. 21, 2599–2604 (2001).

[8] S.J. Webb, J. Breeze, R.I. Scott, D.S. Cannell, et al., J. Am. Ceram. Soc. 85, 1753-56 (2002).

[9] V. Tolmer, G. Desgardin, J. Am. Ceram. Soc. 80, 1981–1991 (1997).

[10] Thirumal, P.K. Davies, J. Am. Ceram. Soc. 88, 2126–2128 (2005).

[11] S. Kawashima, M. Nishida, I. Ueda, J. Am. Ceram.Soc. 66, 421–423(1983).

[12] M. Bieringer, S. Moussa, L.D. Noailles, A.Burrows, C.J. Kiely et al., Chem Mater, 5, 586–597 (2003).

[13] S. Marinel, F. Roulland, S. d'Astorg, A. Chaouchi, J. Eur. Ceram. Soc., 27, 3605–3608 (2007).

[14] I.G. Siny, R. Tao, R.S. Katiyar, R. Guo, A.S. Bhalla, J. Phys. Chem. Solids. 59, 181–195 (1998).

[15] M.I. Ioachim, L. Toacsan, L. Nedelcu, Mihut, High- Q BZT Ceramics for Microwave Applications. *6th WSEAS International Conference On Applied Electromagnetics, Wireless And Optical Communications*. 72–77(2008).

[16] P.-F. Ning, L.-X. Li, P. Zhang, W.-S. Xia, Ceram. Int. 38, 1391–1398 (2012).

[17] R.L. Moreira, F.M. Matinaga, A. Dias, Appl. Phys. Lett. 78, 428 (2001).

Chapter – 7

Synthesis, Characterization and Microwave dielectric properties of BLZTG

CHAPTER 7

SYNTHESIS, CHARACTERIZATION AND MICROWAVE DIELECTRIC PROPERTIES OF BLZTG

7.1 Introduction

The rapid growth of telecommunication industry across the globe in the last few decades has created an incessant demand for new devices. These technological advancements have in turn created an opportunity for researchers to develop new materials which are more stable and compact. Microwave dielectric materials with tunable dielectric properties are one such material mostly used in several wireless communication devices which utilizes microwave frequencies [1]. The dielectric properties are generally tuned by different approaches – additive/dopant [2], altering the stoichiometry [3], formation of solid solution [4], texturing [5], mechanical compensation technique [6], surface coating [7], etc.,

Since $Ba(Zn_{1/3}Ta_{2/3})O_3$ (BZT) is one such complex perovskite ceramic which exhibit excellent dielectric properties at microwave frequencies, researchers have shown keen interest to develop such complex perovskite like BZT after its emergence owing to its low loss at microwave frequencies.

Several advance sintering techniques like liquid phase sintering by addition of new glassy phases and also by addition of different dopants have been researched to address the issues elaborated in Chapter 2. In this present work, efforts have been made to tune the microwave dielectric properties of BZT by doping with suitable oxides at low sintering temperatures. The structure-property correlations of BZT by investigating the relationship between stoichiometry and dielectric loss of BZT have been carried out here. Substitution of donor ion (La^{3+}) in the A site of BZT lattice is expected to compensate the local charges and hence influence the degree of ordering [8]. Ga ions in the B site of BZT lattice is known to improve the sinterability and

quality factor of BZT [9]. Modifications in degree of ordering and sinterability of the system is known to be related to high Q. Substitution of smaller ions (La in A site and Ga in B site) may lead non-linear changes in the dielectric constant and τ_f due to alio-valent substitution. In this study BLZTG [$Ba_{1-x}La_x(Zn_{(1+x-2y)/3}Ta_{(2-x-y)/3}Ga_y)O_3$] (x,y-0, 0.01, 0.025, 0.05, 0.075, 0.1) were synthesized by solid state reaction. The microstructure and microwave dielectric properties have been studied and their structure property relationships have been correlated here.

7.2 Experimental procedure for processing of BLZTG:

$Ba_{1-x}La_x(Zn_{(1+x-2y)/3}Ta_{(2-x-y)/3}Ga_y)O_3$ ceramics were prepared using conventional mixed oxide processing method. The raw materials $BaCO_3$, La_2O_3, ZnO, Ga_2O_3 (Sigma Aldrich, USA) and Ta_2O_5 (NFC, Hyderabad) powders with > 99% purity were taken according to stoichiometric quantities. The mixed oxide powders were taken in zirconia (ZrO_2) vials and yttria stabilized zirconia was used as milling media along with isopropyl alcohol as medium. The powders were ball milled in a planetary ball mill (Fritsch Pulverisette 7) for 8 hrs and later dried in an oven at 80 °C for 12 hrs for the evaporation of the alcohol. The ball milled and dried powders were subjected to calcination at 1200 °C for 6 hours and subsequently ball milled to obtain finer sized particles. The obtained reduced particle sized powders were mixed with 1% wt polyvinyl alcohol (PVA) binder and compacted into cylindrical pellets. The green pellets were sintered at different sintering temperatures to study its densification behavior. The sintered pellets were then annealed at 1300 °C for 6 hours to remove the thermal stress. The sintered samples were polished on both sides to remove the secondary phases and thermally etched to study the microstructure. X-ray diffraction pattern has been used to analyze the crystal structure of BZT and modifications due to the presence of La and Ga ions in the BZT lattice. Surface morphology and the grain size analysis of sintered BZT, BLZTG pellets were analyzed using a SEM. Raman spectra was used to study the lattice vibrational modes and FWHM / position of the modes were correlated with ordering and dielectric properties of BLZTG system.

7.3 Results and discussion:

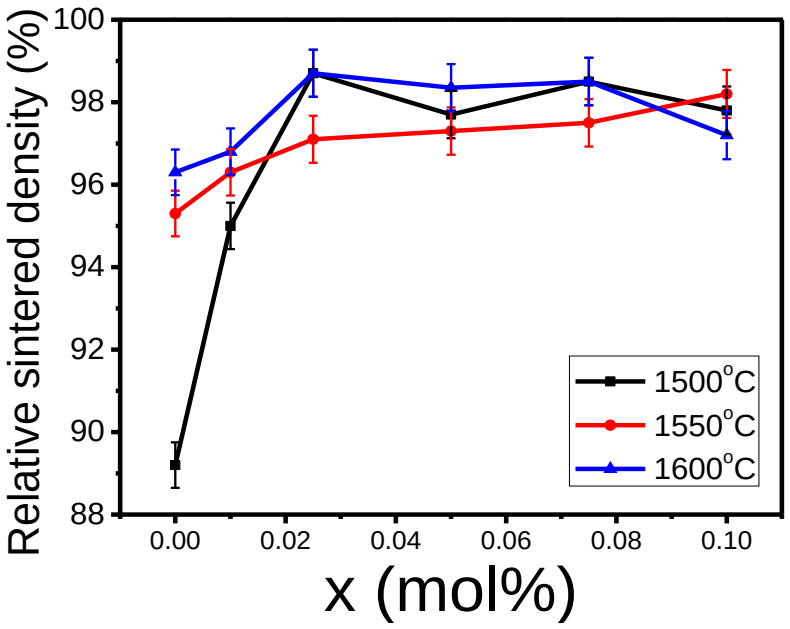

Fig 7.1 Variation of relative sintered density as a function of composition in $Ba_{1-x}La_x(Zn_{(1+x-2y)/3}Ta_{(2-x-y)/3}\ Ga_y)O_3$

Rate of densification of BZT is improved by the presence of La and Ga ions even at a lower temperature of 1500 °C. Fig 7.1 shows the effect of La and Ga ions in the lattice on the densification behavior of BZT for different sintering temperatures. At lower sintering temperature (1500 °C), pure BZT gets densified upto 89% of TD. When x = 0.01, densification rapidly increases and a maximum of 95% of TD has been achieved. 98% of TD has been achieved when x = 0.025 and density almost remains constant with further addition of La and Ga. The variation in density is marginal with increase in sintering temperature. Addition of Ga_2O_3 to BZT has enhanced the relative density and a maximum density of 96% of TD has been achieved after sintering at 1600 °C by J.-I. Yang et al [9]. Improved densification in BZT + xGa_2O_3 has been attributed to the grain growth due to presence of Ga ions. Higher rate of densification at lower temperature (1500 °C) in BLZTG could be attributed to the increased ionic mobility due to the presence of La ions in the 'A' site of perovskite lattice and enhanced grain growth due to Ga ions in the B site.

Dielectric loss properties depend on several factors such as density, microstructure, secondary phase, cation ordering, etc. Hence microstructure of BLZTG ceramics has been studied to investigate the variation in density with increasing concentration of La and Ga ions. Fig 2 (a-f) shows the microstructure of $Ba_{1-x}La_x(Zn_{(1+x-2y)/3}Ta_{(2-x-y)/3}\ Ga_y)O_3$ (x, y= 0, 0.01, 0.025, 0.05, 0.075, 0.1) sintered at 1550 °C. In pure BZT, elongated grains with an average grain size of 4.5 µm have been seen. When x, y= 0.01, elongated grains (average grain size of 13 µm) and small equiaxed grains (average grain size of 2 µm) coexisted. With further increase in concentration, morphology of the grains gradually changes and when x, y = 0.075 cuboidal grains with an average grain size of 11 µm has been observed. Grain morphology and size remains almost the same when x, y = 0.1. It can be clearly seen from the microstructures that grain growth is enhanced which in accordance with the increase in density with La and Ga addition. Grain growth phenomenon has also been observed by J.-I. Yang et al[9] in BZT with Ga_2O_3 as additive and a maximum average grain size of 10 µm has been seen in samples with 1mol% addition of Ga_2O_3. Pure BZT without any hexagonal superstructure is reported to have a homogenous microstructure [10].High temperature sintering and annealing of BZT leads to formation of zinc deficient secondary phases which is reflected by the presence of anisotropic grains in pure BZT. This is in accordance with the microstructure obtained by [11] Tolmer and Desgardin in which the presence of hexagonal zinc deficient perovskite leads to formation of anisotropic grains.

The changes in the grain morphology with increasing concentration of dopants could be attributed either to the presence of secondary phases or change in the crystal structure. Since the changes in grain morphology in pure BZT and in BLZTG systems were found to be closely related to the presence of secondary phase and the crystal structure, the samples were characterized by XRD. Substitution of La ion in the A site of ABO_3 lattice is known to create changes in the ordering of B site ions. [8]

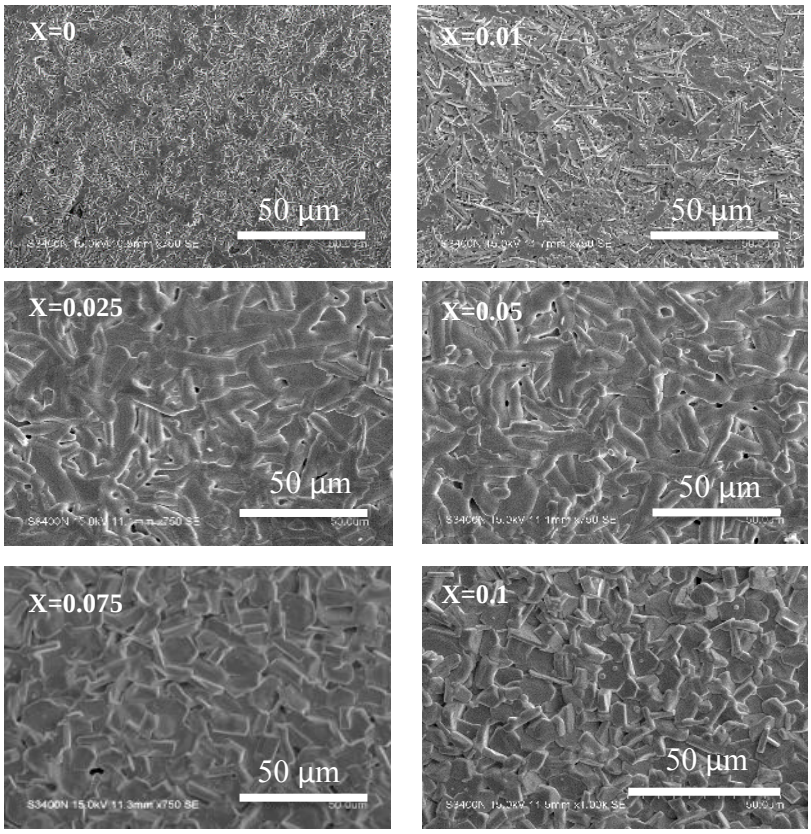

Fig 7.2 Microstructure of BLZTG (x = 0 to 0.1 mol.%) samples sintered at 1550 °C

Crystal structure and changes in ordering as examined by X-ray diffraction pattern (as shown in Fig 3) reveal that the intensities and peak positions of fundamental reflections in BZT and BLZTG systems remain identical whereas there is a change in superlattice reflections. The variation in lattice parameter and order parameter with increasing concentrations of La and Ga is shown in Table (2) and Fig 3(b) respectively. The lattice parameter values of pure BZT were well in agreement with the values reported in literature [12]. Increasing concentration of La and Ga in BLZTG system leads to change in crystal structure from hexagonal to cubic and hence for x>0.025, the lattice parameters were given for cubic system. The expansion of c-axis in hexagonal structure of BZT is associated with ordering of B-site ions. Pure BZT and BLZTG (x, y = 0.01,0.025) were indexed based on hexagonal unit cell. Presence of Ga ions in B-site did not permit the expansion in c-axis thus hindering the ordering of Zn-Ta-Ta ions in BLZTG system. Super lattice reflections

corresponding to B site ordering in pure BZT ($(100)_h$ and $(101)_h$)begins to disappear with the addition of La, Ga ions. When x = 0.05, new set of super lattice reflections corresponding to 1:1 ordering begins to evolve and the unit cell is indexed based on cubic system.

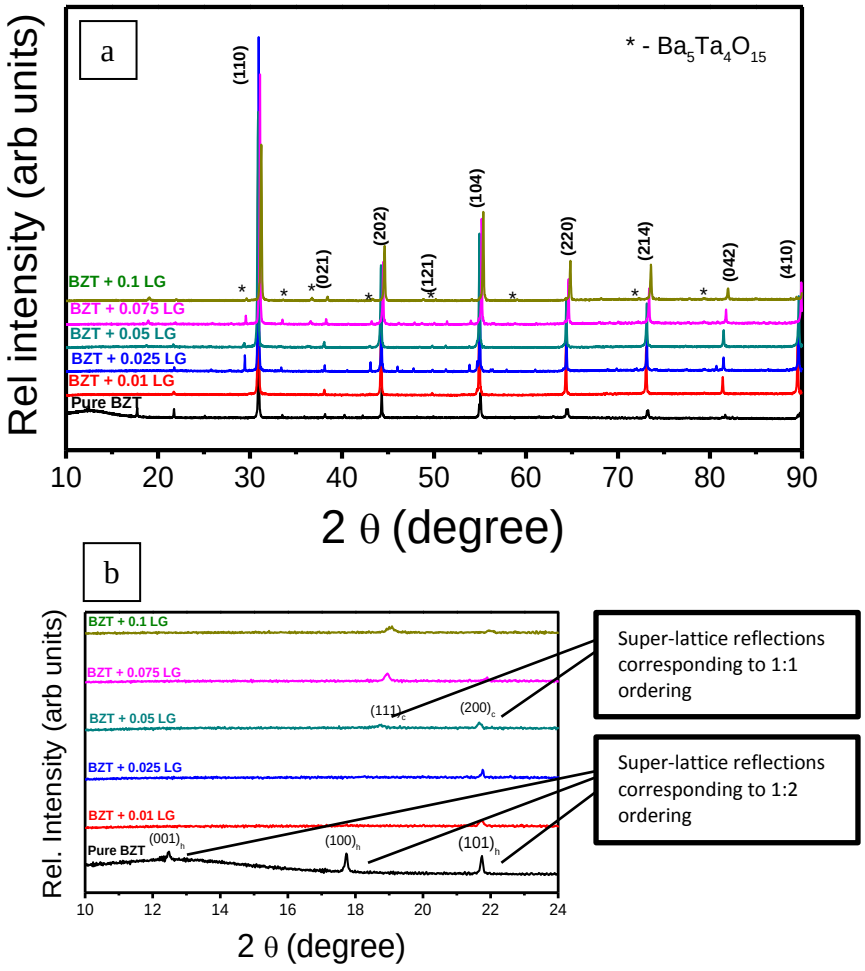

Fig7.3(a) X-ray diffraction pattern of BLZTG (x = 0 to 0.1 mol.%) samples sintered at 1550 °C (b) X-ray diffraction pattern indicating super lattice reflection of BLZTG (x = 0 to 0.1 mol.%) samples sintered at 1550 °C

The degree of ordering in the 1:2 ordered system is estimated by the order parameter which is defined as below,

$$S = \sqrt{\frac{[I_{100}/I_{110,012}]_{obs}}{[I_{100}/I_{110,012}]_{cal}}} \quad - \qquad (1)$$

where $[I_{100}/I_{110,\,012}]_{obs}$ is the ratio of observed intensity of the super lattice reflection to that of the fundamental reflection[13].

Table 7.1 Summary of the lattice parameters of BLZTG for various compositions

x (mol%)	a (Å)	c (Å)
0	5.7805	7.0783
0.01	5.7821	7.0751
0.025	5.7754	7.0694
0.05	4.7269	--
0.075	4.6784	--
0.1	4.6452	--

The ordering parameter corresponding to 1:1 ordering is calculated based on the integrated intensity ratio of I_{111}/I_{220} [8]. The 1:1 ordering gets evolved at x=0.05 but there is a marginal increase in the order parameter value for higher concentrations of La and Ga. It has been observed that 1:2 ordering in BLZT is gradually replaced by 1:1 ordering and a maximum order parameter (corresponding to 1:1 ordering) value of 0.84 has been observed. In a certain composition range of BLZT, there exists a co-existence of 1:1 and 1:2 ordering and order parameter tends to increase with increasing concentration of La in BLZT ceramics [8]. But in case of BLZTG ceramics, the marginal increase in order parameter value with increasing concentrations of La and Ga could be attributed to the presence of Ga ions in the B site. Ordering is favored in compound with higher valency difference in B site ions involved. Ga^{3+} ions in B site prevents the growth of 1:1 ordered domains formed due to presence of La^{3+} in A site.

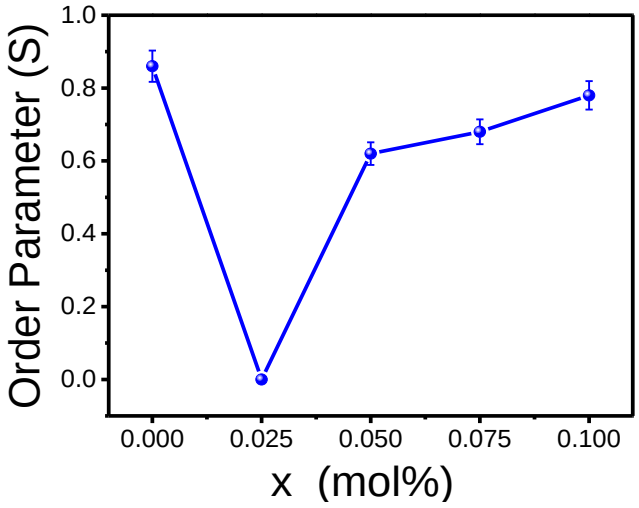

Fig7. 4 Variation of order parameter in BLZTG as a function of composition

The influence of La and Ga ions in the local structure of BZT is studied using Raman spectroscopy. The peaks were indexed based on ref [14]. The peaks corresponding to the torsional modes of vibration of B site atoms (375 cm^{-1} and 424 cm^{-1}) broadens and shifts with increasing concentration of La and Ga. Peak at 375 cm^{-1} tends to broaden and gradually shifts to 347.5 cm^{-1} for x = 0.1. Peak at 424 cm^{-1} mode tends to broaden till x=0.025 and for x≥0.05, the peak shifts to 418 cm^{-1} and then sharpens again.

FWHM of peak at 424 cm^{-1} remains minimum for pure BZT due to the presence of 1:2 ordering. The broadening of peak (as reflected by increase in FWHM) for x = 0.025 could be attributed to the loss in B site ordering which is accordance with the x-ray diffraction pattern. FWHM tends to decrease for x = 0.05 which could be due to the onset of 1:1 ordering. There is a marginal variation in FWHM with further increase in La and Ga concentration. The results are in agreement with order parameter calculated from x-ray diffraction pattern. This broadening and shifting behavior of BLZTG ceramics are in accordance with the results obtained by Cheng-Chang Lee et al. La substitution in A site also influences the local structure leading to changes in the torsional modes of vibration of B site atoms. E_g (O) mode in BLZT originally broadens for the composition range where in the B site ordering is

completely lost. With increasing concentration (as 1:1 ordering evolves) the peak shifts from 424 cm^{-1} to 414 cm^{-1}.

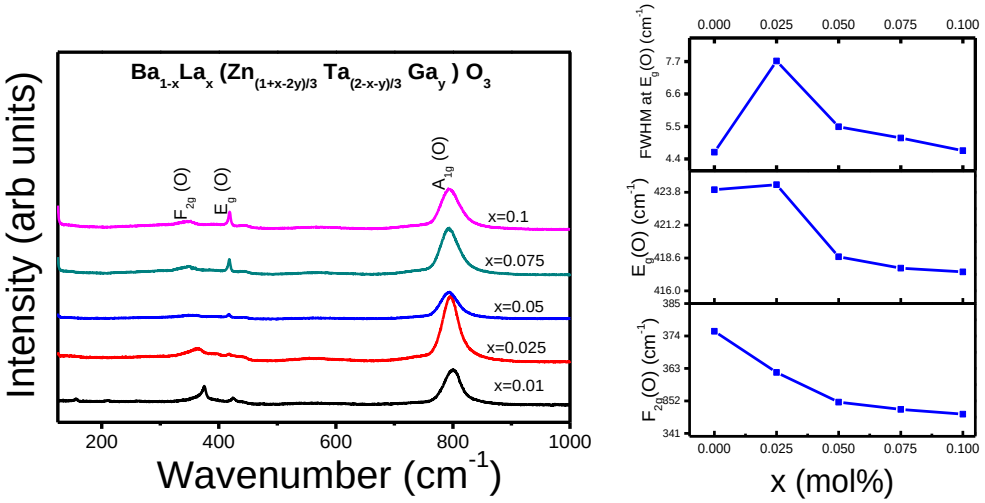

Fig 7.5 (a) Raman spectrum of BLZTG (x = 0 to 0.1 mol.%) sample sintered at 1550 °C (b) Variation of Raman modes of BLZTG (x = 0 to 0.1 mol.%) as a function of composition

The dielectric properties of BLZTG system was evaluated to study its influence on changes in ordering of the system. Quality factor values for samples sintered at 1500 °C and 1550 °C tend to increase with increasing x upto a concentration of x = 0.025. The values decrease with increasing concentration of La and Ga. For samples sintered at 1600 °C, pure BZT samples tend to show maximum value. Q×f values decrease for x = 0.01 and then increase for x=0.025. With further increase in concentration (upto x = 0.1), quality factor value decreases.

Relative density of pure BZT samples sintered at 1500 °C and 1550 °C for 2 hours were poor in comparison with sample containing La and Ga. Hence low Q×f values of pure BZT could be attributed to poor densification.

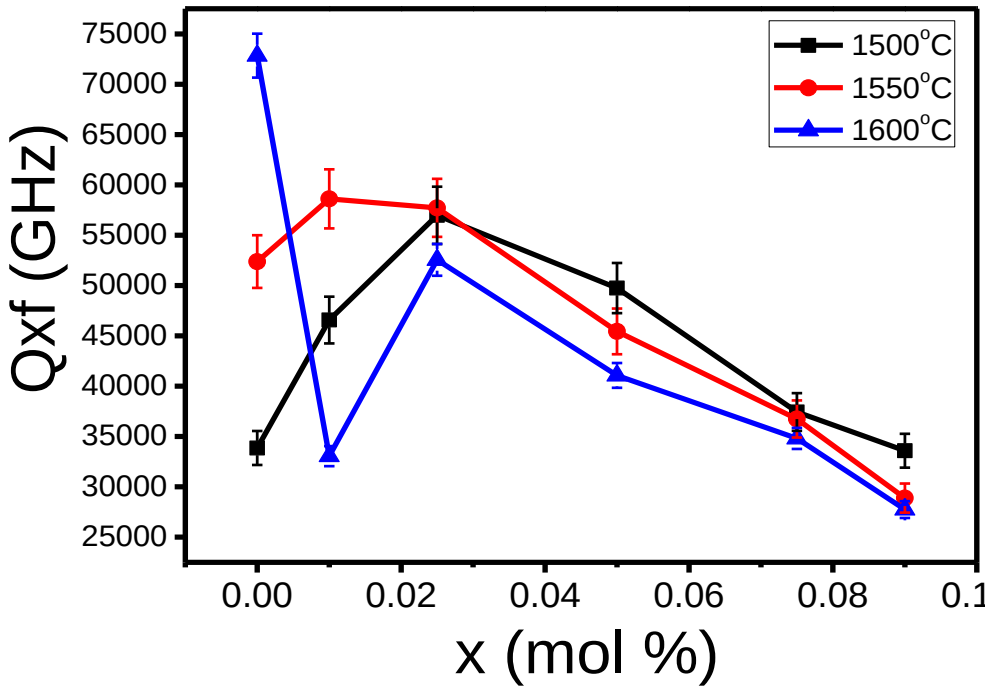

Fig 7.6(a) Variation of Quality factor (Q×f) as a function of composition in BLZTG samples for different sintering temperatures

The increase in values (for x = 0.01 and 0.025) of Q×f inspite of decrease in ordering in the system could be attributed to better densification and grain growth in comparison with pure BZT. Pure BZT sample shows a maximum Q×f value of ~75000GHz when sintered at 1600 °C. The Q×f values of pure BZT reported here was less due to the fact that no precautions were taken to minimize zinc volatilization during sintering. Zinc volatilization tends to increase with increasing sintering temperature [13]. The value suddenly drops to ~35000GHz for x = 0.01 which could be due to the disruption of ordering in the system. The Q×f value for x = 0.025 increases inspite of disruption in ordering. The reason could be attributed to increase in concentration of Ga ions in the B site. For $x \geq 0.05$, Q×f values decrease for samples sintered at all temperatures. The reason for decrease in the values could be ascribed to the presence of 1:1 ordering.

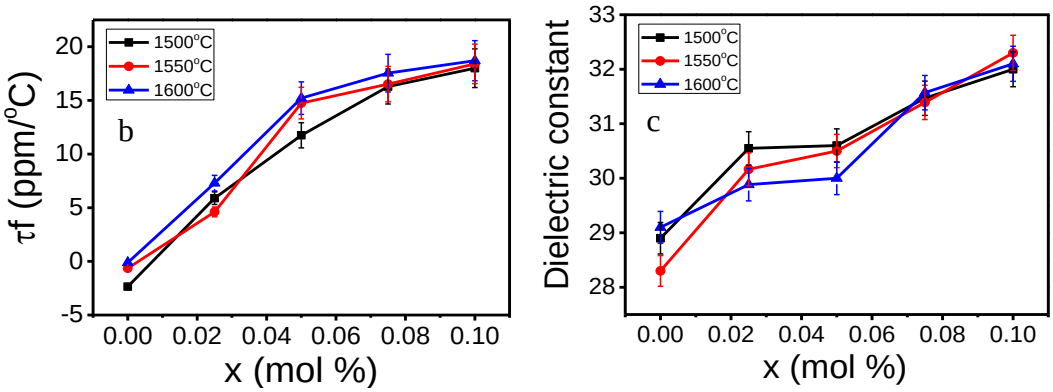

Fig 7.6 (b) Variation of τ_f as a function of composition of BLZTG (x = 0 to 0.1 mol.%) samples for different sintering temperatures (c) Variation of dielectric constant as a function of composition of BLZTG (x = 0 to 0.1 mol.%) samples for different sintering temperatures

τ_f of dielectric mainly depends on τ_ε which is influenced by ordering, octahedral tilting and ionic polarizability. Since there is a change in ordering as well as the dielectric permittivity, τ_f of BLZTG increases with increasing concentration of dopants (as shown in Fig 7.6 b).

The dielectric constant value of BLZTG system tends to increase with increasing concentration of dopants (as shown in Fig 7.6 c). Non-linear change of ε_r vs. composition was observed for the BLZTG complex perovskites. Increase in the dielectric constant could be attributed to higher ionic polarizability of La cation. ε_r of $A(B'B'')O_3$ - $A'(B_1'B_1'')O_3$ shows a linear change with changes in composition when the A-site ions are the same (A = A'). Since the A-site ions are different (A = Ba, A'= La), ε_r change nonlinearly with composition. [15]

7.4 Summary

Sinterability of BZT improved upon addition of LG and ~98% true density was achieved at a relatively lower temperature ~1500 °C. Presence of La in the A-site induces 1:1 ordering in BLZTG as evidenced by a shift in the super-lattice peak in the x-ray diffraction spectra. La and Ga substitution in BZT increased the dielectric constant as well as the temperature coefficient of resonant frequency. The effect of

ordering and size of the ordered domains with increasing x and the corresponding influence on their microwave dielectric properties was investigated.

7.5 References

[1] Reaney and Iddles J. Am. Ceram. Soc., 89 [7] 2063–2072 (2006)

[2] H. Tamura, D.A. Sagala, K. Wakino, Jpn. J. Appl. Phys., 25, 787-791 (1986).

[3] K. P. Surendran, M. T. Sebastian, P. Mohanan, R. L. Moreira, A. Dias Chem. Mater., 17, 1,142–151 (2005)

[4] F. Roulland, G. Allainmat, M. Pollet, S. Marinel, J. Eur. Ceram. Soc., 25, 2763–2768(2005).

[5] K. Wada, Y. Fukami, K. Kakimoto, H. Ohsato Jpn. J. Appl. Phys., 44, 1, 9B, (2002).

[6] Temperature compensated sapphire resonator for ultrastable oscillator operating at temperatures near 77° Kelvin United States Patent 5909160

[7] N.McN.Alford, J.Breeze, S.J.Penn, M.Poole, IEE Proc-Sci. Meas. Technol., 147, 6, November. 2000

[8] C-C. Lee, C-C. Chou, D-S Tsai, J. Am. Ceram. Soc., 80, 11, 2885–90 (1997).

[9] J-I Yang, S. Nahm, C-H. Choi, H-J. Lee, J-C. Kim and H-M. Park, Jpn. J. Appl. Phys., 41, 702–706 (2002)

[10] E. Koga, Y. Yamagishi, H. Moriwake, K. Kakimoto, H. Ohsato, J. Eur. Ceram. Soc. 26, 1961–1964 (2006).

[11] V. Tolmer, G. Desgardin J. Am. Ceram. Soc., 80, 8, 1981–91 (1997).

[12] F.S. Galasso: Structure, Properties and Preparation of Perovskite type Compounds (Pergamon Press, Oxford, U.K., 1969).

[13] M. Bieringer, S. Moussa, L.D. Noailles, A.Burrows, C.J. Kiely et al., Chem. Mater., 5, 586–597 (2003).

[14] S. Marinel, F. Roulland, S. d'Astorg, A. Chaouchi, J. Eur. Ceram. Soc., 27, 3605–3608 (2007).

[15] S. Normura, Ferroelectks, 49, 61-70 (1983).

Chapter – 8

Summary and Conclusions

CHAPTER 8

SUMMARY AND CONCLUSIONS

8.1 Synthesis and sintering studies on pure BZT

BZT ceramics were successfully prepared by conventional solid state reaction and sintering at temperatures 1550 °C and 1600 °C resulted in a maximum of 95% and 96% of the theoretical density respectively. The effect of starting particle size and its distribution on final sintered density has been studied. A low melting flux (B_2O_3) was added to BZT and 97% of the theoretical density was achieved for the samples containing 0.5 wt% B_2O_3 when sintered at a lower temperature of 1500 °C. In spite of higher density and good microwave dielectric properties exhibited by the B_2O_3 containing samples, these samples were unable to withstand the polishing action required to generate a smooth surface finish for subsequent metallization. Sintering parameters such as peak temperature, dwell time, heating rate and sintering atmosphere have been optimized to achieve better density and good microwave dielectric properties.

8.2 Colloidal processing studies on BZT

In the present investigation, the effect of shaping technique on density and dielectric properties has been successfully studied. Suitable dispersant and its concentration, viscosity and solid loading have been systematically optimized to obtain a stable suspension. Slip casting using POP molds has resulted in relative sintered density of 96%. Eco-friendly binder (EW) has been used for gelation studies on BZT and its effect on density, microstructure and dielectric properties has been established. The gelation behavior of the slurry was studied by measuring storage modulus (G′) in order to optimize monomer, cross-linker and initiator concentrations in conventional gel casting technique. Maximum quality factor of 93700 GHz and

dielectric constant of 29.5 have been achieved for sample with maximum solid loading containing optimum concentrations of monomer, cross linker and initiator.

8.3 Microwave sintering of BZT

Pure BZT did not effectively couple with microwaves and maximum relative sintered density of 84% TD has been seen even after sintering at 1500 °C using microwave power. Hence, oxide additives which can couple effectively with microwaves have been added to BZT. The effect of Cr_2O_3 / Fe_2O_3 / ZrO_2 addition on the densification behavior, microstructure development of Ba $(Zn_{1/3}Ta_{2/3})O_3$ (BZT) ceramics and their subsequent effect on the dielectric properties has been studied using two different sintering techniques, microwave sintering and conventional sintering. Addition of oxides during microwave sintering enhanced densification and higher sintered density of ~97% TD at a lower sintering temperature of 1400 °C using microwave sintering. Though the dielectric properties of BZT processed by microwave sintering were not superior to the samples processed through conventional sintering, the processing time to achieve high density was extremely less compared to conventional sintering. FWHM of the vibrational modes of oxygen were in accordance with the changes in ordering in system containing additives.

8.3 Studies on BLZTG

Sinterability of BZT improved upon addition of LG and ~98% true density was achieved at a relatively lower temperature ~1500°C. Presence of La in the A-site induces 1:1 ordering in BLZTG as evidenced by a shift in the super-lattice peak in the x-ray diffraction spectra. Grain growth and changes in grain morphology have been observed with increasing concentration of Ga and La in BLZTG system. La and Ga substitution in BZT increased the dielectric constant as well as the temperature coefficient of resonant frequency. The effect of ordering and size of the ordered domains with increasing x and the corresponding influence on their microwave dielectric properties was investigated.

8.4 Conclusions

- ***Processing of pure BZT***
    - Volatilization of Zn is minimized and densification is improved (98% of TD) by suitably optimizing the process parameters followed by reaction bed sintering.
    - Superior dielectric properties have been achieved without annealing.

- ***Colloidal Processing***
    - Issues during scaling up to large rectangular bars were addressed by processing BZT by colloidal method (slip casting, gelation using egg albumin and conventional gel casting). Linear shrinkage and volume shrinkage of samples remains least for conventional gel casting and maximum for slip casting. Maximum densification has been achieved for samples processed by conventional gel casting

- ***Microwave sintering***
    - Addition of oxide dopants has enhanced the densification and led to higher sintering density of ~97% of TD at a lower sintering temperature of 1400 °C using microwave sintering.
    - Processing time to develop a highly dense ceramic has been drastically reduced by microwave sintering

- ***BLZTG system***
    - BZT-LG system shows better densification at a lower temperature of 1500 °C. The atomic arrangement of BLZTG system is more accurately represented by a cubic unit cell for compositions with $x > 0.05$. Microstructural analysis of BLZTG system reveal the presence of equi-axed grains with increase in concentration in accordance with the change in the crystal structure

Fig 8.1 BZT samples prepared in different dimensions using various processing conditions

8.5 Scope of future work

- BZT ceramics will be subsequently vacuum brazed with Ti6Al4V alloy under high vacuum for RF window application which is given in detail in the section 8.6.1
- Fabricated RF window will be subjected to qualification tests
    - Visual inspection - cracks, deformation or for any gross leaks
    - Helium leak detector (HLD) test is carried out to establish its UHV compatibility
    - RF performance – Insertion loss and return loss
- Effect of different additives on thermal conductivity on BZT can be studied to enhance the thermal conductivity

8.6.1 Fabrication of RF window

Active alloy brazing is considered to be the most economical and efficient technique in joining metal and ceramic. In case of RF window, fabrication of metal - ceramic joint is the most critical process as the window is expected to act as a

vacuum barrier and hence has to be UHV compatible. In this brazing procedure, the active metal in the filler gets migrated to the surface of ceramic and forms intermetallic compounds to establish metal - ceramic interface. The feasibility of active alloy brazing BZT with Ti6Al4V alloy using different filler materials has been investigated and primary leak test results of brazed joints have been reported as a part of scope of future work. The details of the tests carried out are as follows:

Ag - Cu alloy with a few percent of Ti (Cusil - ABA) is one of the widely used filler due to ability to impart good wettability at appropriate temperature with degrading Ti6Al4V alloy. The composition of BZT, Ti6Al4V and Cusil ABA are given in Table 8.1. The composition of alternate filler materials used for brazing BZT with Ti6Al4V alloy are tabulated in Table 8.1(c).

Table 8.1(a) Compositional analysis of BZT

Elements	**Barium**	**Zinc**	**Tantalum**	**Niobium**	**Tungsten**	**Oxygen**
Wt.%	39.98	7.07	37.29	0.17	0.21	15.28

Table 8.1(b) Compositional analysis of Ti6Al4V alloy

Element	**Titanium**	**Aluminum**	**Vanadium**	**Carbon**	**Iron**	**Oxygen**	**Nitrogen**	**Hydrogen**
Wt.%	89.707	6	4	0.03	0.1	0.15	0.01	0.003

Table 8.1(c) Compositional analysis of various fillers

Brazing filler alloy	**copper%**	**silver%**	**titanium%**	**palladium%**	**nickel%**
Cusil-ABA	35.25	63	1.75%	-	-
Palladium based filler alloy	31.5	58.5	-	10	-
TiCuNi alloy	15	-	70	-	15

The filler material is placed in the form of foil between the ceramic and Ti6Al4V frame (as shown in Fig 8.2 a). A gap of 50µm is maintained during brazing and the entire assembly is placed in vacuum furnace and heat treated at various

temperatures based on the melting point of the filler alloys. The heating schedule followed during brazing with CuSil ABA is shown in Fig 8.2b. The brazed samples are then be subjected to visible leak test using iso propyl alcohol and leak test under pressure using He (1 bar gauge pressure) to check the integrity of the joint. The results of the leak test were summarized in Table 8.2.(a)

Table 8.2 (a) Leak test results of brazing using CuSil ABA filler alloy

FILLER	SAMPLE DIMENSIONS	CHARACTERIZATION	REMARKS
CuSil ABA	Circular disc (25mm dia) – 1 Circular disc (10mm dia) – 1 Square (15mm X 15mm)-1	Visible leak test using IPA	Pass
		Leak test using He (1 bar gauge pressure)	Fail

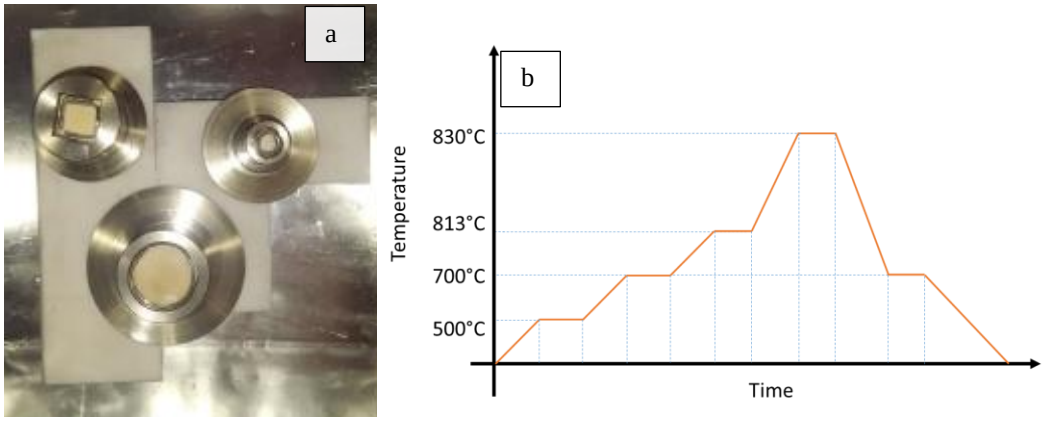

Figure 8.2(a) Ceramic and Ti6Al4V assembly with Cusil ABA filler alloy (b) Heating Schedule for brazing BZT-Ti6Al4V with Cusil ABA filler alloy

Palladium based filler alloy is taken in the form of wire and an allowance of 50µm is maintained during brazing. The alloy had a melting temperature of 850 °C the samples upon brazing at 890 °C showed small cracks at the peripheries and so samples failed during leak test under pressure even at less than 1 bar pressure range. TiCuNi filler alloy in the form of foil (50µm thick) is used for brazing BZT with Ti6Al4V frame. The samples could not pass the leak test under pressure of 1 bar.

Table 8.2(b) Leak test results of brazing using Palladium based filler alloy

FILLER	SAMPLE DIMENSIONS	CHARACTERIZATION	REMARKS
Ag-58.5%, Cu 31.5%, Pd-10% in wire form (T – 850 °C)	Circular disc (25mm dia) – 1 Circular disc (10mm dia) – 1 Square (15mm X 15mm)-1	Visible leak test using IPA	Fail
		Leak test using He (1 bar gauge pressure)	Fail

In order to improve the integrity of the joints, the samples were re-brazed using CuSil ABA alloy. Components were pressurized at 1 bar pressure using helium gas. Main leakage was found at edges and also on broad side where clearance was large around 0.2 mm approximately (before re-brazing).

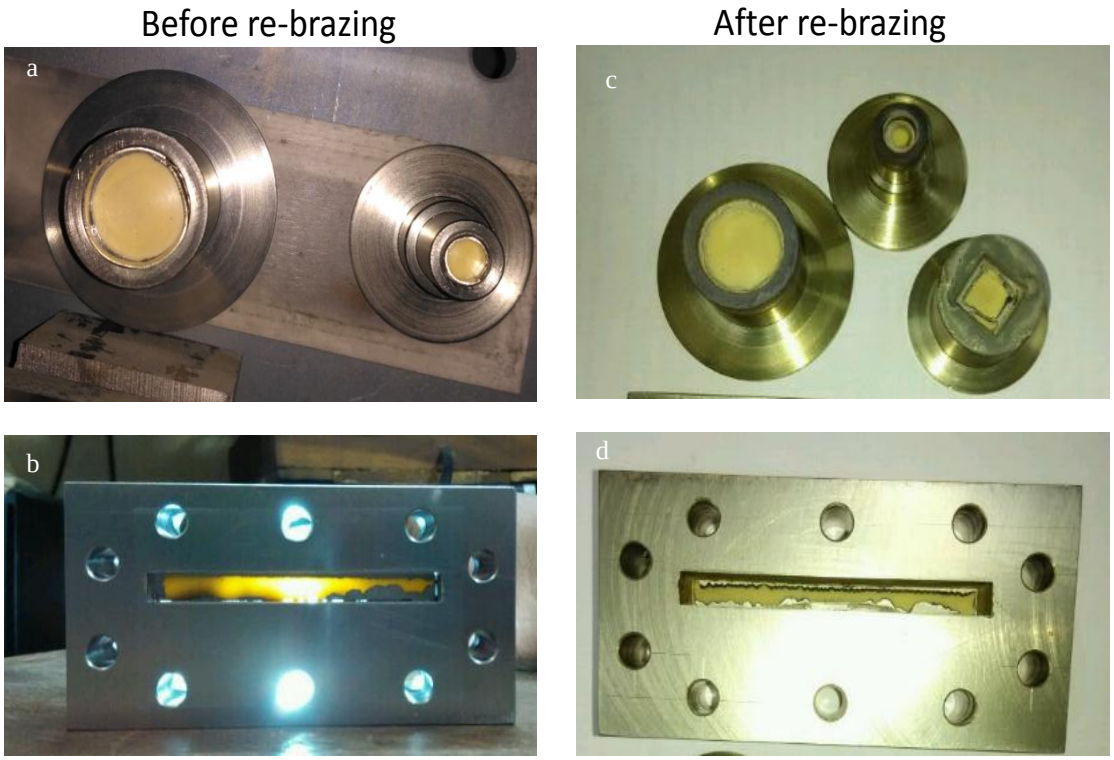

Fig 8.3 BZT samples (a,b) before re-brazing and (c,d) after re-brazing

Re-brazing the samples improved the integrity at the ceramic –joint interface. Leak at the edges could be addressed by fabricating ceramic and frame slots with rounded corners. This also enables easy fitting of braze filler alloy at the joints. Studies on brazing using other filler alloys and metallization followed by brazing can be done to improve the quality of brazed joint.

8.6.2 Thermal conductivity of BZT samples:

Thermal conductivity is one of the important properties for successful functioning of RF window. The heat generated during the interaction of microwaves with ceramics has to be effectively conducted. Failure of the window is mainly due to cracks developed due to thermal gradients in the sample.

Thermal diffusivity measurements were done of sintered samples having a dimension of 10mm × 10mm × 2mm. Measurements have been done at room temperature, 100, 200, 300 and 400 °C. Thermal conductivity values were calculated using the formula

$$k=Cp*d*r \quad (1)$$

where, k is thermal conductivity,

Cp is the specific heat,

d is the thermal diffusivity and

r is the density of the material

The effect of compositional variation on thermal conductivity of BZT samples in the temperature range of RT-400 °C has been shown in Fig 8.4

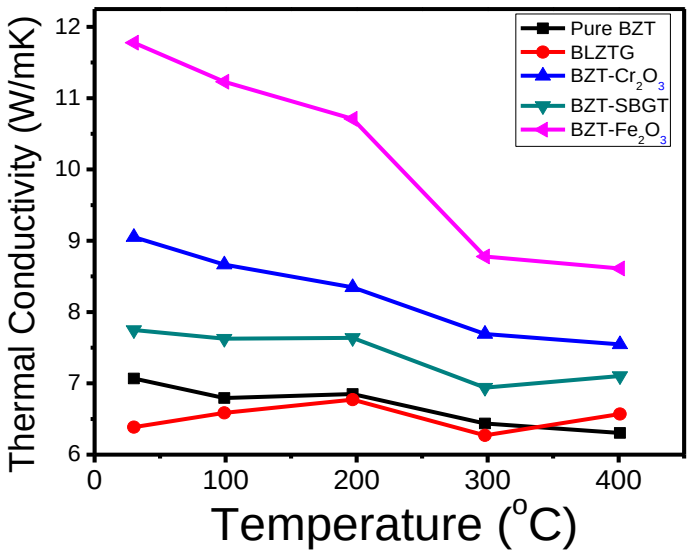

Fig 8.4 Effect of compositional variation on thermal conductivity of BZT samples in the temperature range of RT - 400°C

Thermal conductivity in dielectric ceramics is mainly governed by thermal vibrations of lattice. Presence of imperfections and inhomogeneity in the lattice leads to scattering of phonons thereby decreasing the thermal conductivity. Thermal conductivity of all BZT samples decrease with increase in temperature due to increase in lattice vibrations which hinder the flow of phonons. Pure BZT samples exhibited TC value close to 7 W/mK. Formation of solid solution with SBGT improved the thermal conductivity of BZT to 7.7 W/mK. Ga ions in B – site promotes grain growth and presence of iso-valent Sr ion in A-site aids in ordering of BZT lattice.

Zn vacancies formed during heat treatment (calcination, sintering, annealing) of BZT synthesis leads to imperfections in the lattice. Dopant (Cr_2O_3 and Fe_2O_3) atoms which are known to have ionic radius close to B site ions in the lattice replace the Zn vacancies formed during processing of BZT. Increase in TC values in BZT- Cr_2O_3 and BZT- Fe_2O_3 could be attributed to the replacement of vacancies by dopant atoms. Simultaneous substitution of La in A site and Ga in B site of BZT is accompanied by changes in ordering of the system. Micro-domains with different ordering exist in BLZTG system thus hampering the propagation of phonons. Presence of such domains can be attributed to deterioration in TC values in comparison with pure BZT.

The effect of various other additives on thermal conductivity of BZT can be studied and further improved to design RF window with better thermal stability and dielectric performance.